DISSERTATION

DEVELOPMENT OF REDOX-RECYCLABLE ION EXCHANGE MATERIALS FOR THE REMOVAL AND RECOVERY OF HEAVY METAL CONTAMINANTS FROM AQUEOUS MEDIA

Submitted by

Lisa Dysleski

Department of Chemistry

In partial fulfillment of the requirements

for the Degree of Doctor of Philosophy

Colorado State University

Fort Collins, CO

Spring 2003

COLORADO STATE UNIVERSITY

January 28, 2003

WE HEREBY RECOMMEND THAT THE DISSERTATION PREPARED UNDER OUR SUPERVISION BY LISA DYSLESKI ENTITLED *DEVELOPMENT OF REDOX-RECYCLABLE ION EXCHANGE MATERIALS FOR THE REMOVAL AND RECOVERY OF HEAVY METAL CONTAMINANTS FROM AQUEOUS MEDIA* BE ACCEPTED AS FULFILLING IN PART REQUIREMENTS FOR THE DEGREE OF DOCTOR OF PHILOSOPHY.

Committee on Graduate Work

N.E. Levinger

F.R. Stermitz

K.F. Reardon

P.K. Dorhout/Co-advisor

S.H. Strauss/Co-advisor

C.M. Elliott/Department Head

ABSTRACT OF DISSERTATION

DEVELOPMENT OF REDOX-RECYCLABLE ION EXCHANGE MATERIALS FOR THE REMOVAL AND RECOVERY OF HEAVY METAL CONTAMINANTS FROM AQUEOUS MEDIA

Alkali metal or proton intercalated molybdenum disulfides, A_xMoS_2 (where A = H^+, Na^+, or K^+ and x < 1.3) were investigated as redox-recyclable ion exchange extractants for the soft, aqueous metal ions Hg^{2+}, Pb^{2+} and Ag^+. The charge on the MoS_2^{x-} layers was successfully decreased from its initial value of 1.3– to 0.80– by contacting $Li_{1.3}MoS_2$ with an aqueous solution of ANO_3. The residual charge on the layers of the resulting solid was determined by hydrogen (H_2) gas evolution and mass balance studies. The charge compensating cations were a combination of Li^+ (from the original solid) and A^+ from the reaction solution, depending on the initial reaction conditions. All of the molybdenum disulfide intercalates were found to have varying degrees of hydration. Upon drying under dynamic vacuum, however, only the Na^+ and K^+ analogs retained their hydration spheres. This resulted in a larger interlayer spacing, *d*, into which ion exchange with various heavy metal cations was facile.

Proton intercalated MoS_2 was found to decompose at approximately 100 °C, to form H_2(g) and MoS_2. The sodium and potassium analogs were stable to

elevated temperatures (to 500 °C), however decomposed in acidic, aqueous solution to form H_xMoS_2. All of the above-mentioned extractants were found to be inappropriate for use at low pH.

The thiospinels $Cu_2MSn_3S_8$ (M = Fe, Mn) were also investigated as effective and stable ion exchange extractants for heavy metal cations. Metal ion extraction reactions were investigated using mass balance experiments and indicated exchange of both copper and transition metal ions out of the solid for soft heavy metal cations in solution. This ion exchange reaction was found to be both slow as well as incomplete with low ion removal over time periods up to 6 days, even in the presence of excess extractant. In addition, these extractants were shown to perform poorly in aqueous acid.

In order to increase the thermodynamic driving force and decrease the kinetic barrier to ion exchange, it was desirable to introduce alkali metal cations such as lithium or sodium into the parent structures. In order to do this, cations were extracted from or inserted into the parent solids using chemical oxidation and reduction reactions. These reactions were typically limited to the surface of the powders, however, resulting in little oxidation or reduction of the bulk material. Therefore, direct synthetic methods were used to prepare the following new thiospinels: $CuMnSn_3S_8$; $Cu_2Sn_3S_8$; $CuFeSn_3S_8$; $Li_2FeSn_3S_8$; and $LiCuFeSn_3S_8$. The compounds $Na_2FeSn_3S_8$ and $NaCuFeSn_3S_8$ were also synthesized, however these two solids did not crystallize with a spinel structure.

Finally, new proton-activated thiospinels were also synthesized as potential metal ion extractants. Stoichiometries of the synthesized proton-activated iron compounds ranged from $H_{0.10}Cu_{1.96}Fe_{0.97}Sn_3S_8$ to $H_{0.18}Cu_{1.90}Fe_{0.96}Sn_3S_8$ depending on reaction conditions. In the case of the manganese analog, a material with a stoichiometry of $H_{0.37}Cu_{1.9}Mn_{0.82}Sn_3S_8$

was synthesized. The degree of protonation depended on the contact time between the parent solid and an acidic solution. The type of acid used had little effect.

In all cases, the alkali metal and proton intercalated thiospinels out-performed the parent spinel compounds in terms of total metal ion extracted as well as extraction time. Using mass balance experiments, the mechanism of metal ion removal with the proton activated thiospinels was shown to be ion exchange. The mechanism of ion extraction by alkali metal intercalates is, however, still unclear. Metal ion recovery from various spinels investigated showed that heating to 500 °C resulted in the release and recovery of reduced metal.

Lisa Dysleski
Department of Chemistry
Colorado State University
Fort Collins, CO 80523
Spring 2003

TABLE OF CONTENTS

List of Figures

List of Tables

Chapter I

Introduction: Heavy Metal Cations in the Environment and Current Remediation Technologies

Commercial Use of Heavy Metals and Environmental Contamination

Heavy metals such as mercury, lead and cadmium are of environmental concern due to extensive use, prevalence, and toxicity to humans and natural wildlife. Common uses of each of these metals are wide ranging and include both industrial and consumer applications. Although a greater understanding of the magnitude of their toxicity and environmental cycling is slowly being realized, and regulations set forth by agencies such as the Environmental Protection Agency (EPA) are reducing the quantity of metal discharged annually to the environment, their discontinued use in common applications is not complete. Cadmium is the least commonly used of the three metals. Nevertheless, the consumption of cadmium in the United States in 2001 was 1,440 metric tons.[1] The most common use of cadmium, accounting for approximately 75 percent of total consumption, is as an electrode material in rechargeable nickel-cadmium batteries. Most of the remaining cadmium, as

cadmium sulfide, is used as a pigment in paints and plastics[2] or as a photoconductive detector in infrared instrumentation.[3]

Lead, on the other hand, is the most commonly used of the three metals. Over 1.6 million metric tons of lead were produced in the United States in 2001.[2] Similar to cadmium, lead is commonly used as a pigment in paint because of the stability and insolubility of many lead salts. Lead chromate ($PbCrO_4$) is the yellow pigment used to color school buses and road stripes; lead oxide (Pb_3O_4) has a bright red color; and lead carbonate hydroxide ($Pb_3(CO_3)_2(OH)_2$) is used as a pigment in white paint. Prior to 1978, lead salts were commonly used as pigments for indoor paints. It was found, by the late 1970s, that the ingestion of this paint resulted in elevated blood levels of between three and four million children. As a result, the use of lead pigments in indoor paint was discontinued and the number of lead-contaminated children dropped to approximately 900,000 by 1990.[4] In fact, federal law now mandates that individuals (renters or buyers) be advised through a formal disclosure form by an owner about the threat of lead-based paint in houses constructed prior to 1978. Although lead is no longer used in indoor paint, it is still commonly used in outdoor paint and is the cause of environmental contamination as the paint chips off and lead slowly leaches into surrounding soil and groundwater. In a similar application, lead oxide is used as a pigment on pottery to provide a yellow tint and a glazed appearance. This practice has been used since ancient Egyptian times and is still used today.

Lead has also been used for centuries as a structural building material as well as a containment material (such as lead piping) due to its low melting point and ease of manipulation. It is also used as a solder material to make connections between pieces of metal in these types of applications. Because of increased environmental awareness and elevated blood levels in urban citizens

(especially children), many products using lead were discontinued in the early 1980s. These included: leaded gasoline, to which tetramethyl- or tetraethyllead were added to prevent engine knocking; leaded pipes and copper pipes connected with lead solder, from which dissolved lead entered public drinking water; and, as mentioned, lead salts in indoor paints. In addition to the regulation of lead in consumer products, recycling efforts have increased the amount of post-consumer lead used in production to approximately 67 percent. Of that, 91 percent is recovered from recycled batteries, which might otherwise have been disposed of in landfills.[2]

Both personal and industrial uses of mercury are also common and widespread. Mercuric oxide (HgO), used as a cathode material in alkali batteries until the 1980s, was the single largest source of mercury in municipal solid waste as estimated by the EPA in 1989.[5] Metallic mercury was also used in devices such as thermometers and sphygmometers. For years, methylmercury fungicides were used and discharged directly into natural waters through natural run-off.[6] Fortunately, this direct discharge is currently regulated by improved environmental laws. Mercury is used in fluorescent lamps and in automobile headlights due to its emission in the visible region. In addition, each dentist in the United States uses, on average, over one kilogram of mercury-containing fillings each year. Finally, large quantities of mercury are still used in industrial processes such as the chlor-alkali process and the mining of soft metals such as gold.

Environmental contamination due to mercury has recently received considerable media attention due to the global implications that this contaminant presents. In 1997, the United States EPA released "Mercury Study Report to Congress" detailing the environmental and health impacts of mercury.[7] Alarmingly, this report indicated that the global contribution of

mercury from natural sources rivals that of anthropogenic sources. Naturally occurring mercury is released into the atmosphere from volcanoes, faults in bedrock, and erosion of mineral soils. These sources contribute approximately 2,500 tons of mercury annually into the atmosphere.[8] Anthropogenic sources, releasing mercury directly into the environment, are now estimated at 3,000 tons per year. Although it is impossible to distinguish between mercury contributed by natural sources and mercury contributed by anthropogenic sources when considering the total global mercury repository, it is believed that the overall concentration of mercury in the environment has increased since the onset of the industrial age.

Mercury Cycling in the Environment

It is the physical characteristics of the element mercury that set it apart from all other heavy metal contaminants and make its distribution in the environment unique. Mercury is the only metal that is a liquid at room temperature. It is because of this physical property and mercury's silver appearance that the chemical symbol for mercury is Hg, which is derived from the Latin word *hydrargyrum* meaning liquid silver. The vapor pressure of mercury is 2.6×10^{-4} kPa at 25 °C[9] and, as can be seen in Table 1.1, is significantly higher than that of other metals. This volatility increases global distribution and contamination.

In the 1980s, ecological research discovered elevated levels of mercury in certain US watersheds. Interestingly, the waterways sampled were far from any potential point source of contamination. This indicated that the contamination stemmed initially from air pollution that was subsequently deposited from the atmosphere into the aquatic system.[10]

Table 1.1 Vapor pressures and melting points of some common substances.[9]

Material	Vapor Pressure/kPa	Melting Point/°C
Hg (l)	2.6×10^{-4}	-38.87
Cd (s)	3.1×10^{-12}	320.9
Au (s)	2.5×10^{-56}	1064.43
Fe (s)	2.1×10^{-63}	1535
H_2O (l)	3.2	0.0

Atmospheric contamination in the United States is known to originate from a variety of sources, some of which are listed in Table 1.2. From this table, it can be seen that the largest source, contributing approximately 87 percent of the overall emissions in 1997, is combustion from incinerators and power plants. It is believed that stack emissions include both gaseous and particulate mercury in which mercury is present in both oxidized (Hg^{2+}) and elemental (Hg^0) forms.[7] The estimated lifetime of oxidized mercury in the atmosphere ranges from a few hours to a few of months, meaning that most Hg^{2+} released deposits locally. Elemental mercury, on the other hand, can reside in the atmosphere for periods of up to one year.[7]

During that time, Hg^0 is carried for miles from the point of emission. Because of this transport, mercury is able to deposit even in remote regions. Upon deposition, mercury becomes part of a complex and not completely understood cycle. A depiction of parts of this cycle, including some of the pathways mercury is believed to take part in is shown in Figure 1.1. Inorganic mercury deposits from either a gaseous or a particulate form. This deposition can also be either terrestrial or aquatic. Due to its volatility, elemental mercury, on the other hand, does not deposit directly. Instead, it is believed to undergo a series of reactions through which it is oxidized to Hg^{2+}. One possible pathway is oxidation by ozone as shown in Equations 1.1 and 1.2.[7] This form of mercury enters the environment through wet precipitation or through evaporation onto a dust particle and subsequent dry deposition.

$$Hg^0(g) \longrightarrow Hg^0(aq) \qquad (1.1)$$

$$Hg^0(aq) + O_3(aq) \longrightarrow Hg^{2+}(aq) \qquad (1.2)$$

Table 1.2 Annual mercury emissions from various anthropogenic sources.[7]

Combustion Sources - Total	137.9
Electric utilities	
Oil- and Gas-fired	0.2
Coal-fired	51.6
Incinerators	
Municipal waste combustors	29.6
Medical waste incinerators	16.0
Commercial/Industrial boilers	28.4
Other combustion sources	11.9
Chlor-alkali production	7.1
Primary lead smelting	0.1
Primary copper smelting	0.06
Other sources	13.3
Total	158.26

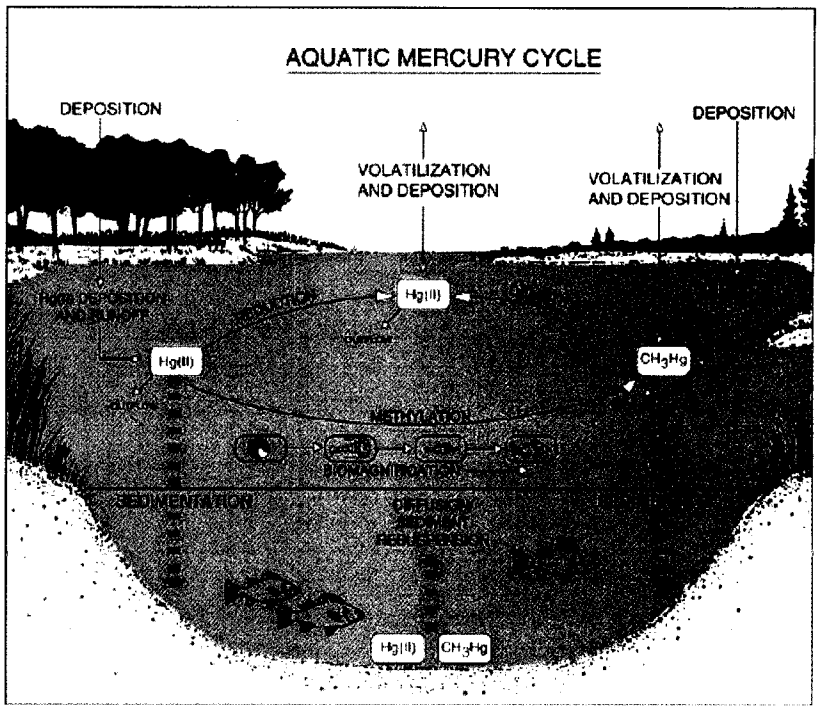

Figure 1.1 Cycling of mercury in the environment.[11]

Once in the aquatic environment, mercury is converted by bacteria to the methylmercury cation, CH_3Hg^+. The methylmercury-containing bacteria are then consumed by organisms one level higher on the food chain. It is the longer half-life of methylmercury in the tissue of these organisms that causes the bioaccumulation of methylmercury in the tissue of aquatic life.[7] Bioaccumulation is typically more pronounced in organisms with longer life spans, meaning that the concentration of methylmercury in an organism will incrementally increase up the food chain through a process termed biomagnification.[10] Bioaccumulation and biomagnification become detrimental to humans when fish with high levels of mercury are consumed. This is also true for other fish eating mammals and birds, including Florida panthers, otters, bald eagles and loons.[12]

Heavy Metal Toxicity and Effect on Humans

There are several cases of large-scale heavy metal poisoning that are well known and documented. The most serious contamination due to cadmium that affected humans is known from the Jintsu River Valley region of Japan where rice fields were irrigated with water that had been contaminated with cadmium by a zinc mining operation. Individuals that consumed this rice complained of severe joint pain that resulted in the naming of the condition *itai-itai* or 'ouch-ouch'. It appears as though this disease resulted from the substitution of Ca^{2+} ions in bones by Cd^{2+}.[13]

Lead has also been found to substitute for calcium in bones, which produces a detrimental effect as the contaminated person ages and the bones dissolve, re-introducing lead into the blood stream. Commonly, however, lead is a contaminant that is known to deleteriously affect children under the age of

seven years. Contamination can occur through the placenta or post-natally through breast milk. As discussed above, lead contamination in young children can come from ingestion of solids contaminated with lead or through drinking water. The main health affect associated with high levels of lead in the body is slow neurological development. This includes impairment of behavior, attentiveness and possibly IQ.[14]

Mercury vapor is the only metal discussed to this point that is toxic in elemental form when inhaled. In addition, it is extremely toxic when alkylated by short chain organic groups. Alkylation increases the solubility and transport of mercury through biological tissue. Because of its great affinity for sulfur, mercury binds to enzymes in the body that contain sulfhydryl groups. This binding affects the normal function of the enzyme, and the metabolic reactions that the enzyme catalyzes are compromised.

There are two well known cases of large scale mercury contamination, the first occurring in 1956 in Minimata Bay, Japan, where an industrial release of methylmercury contaminated local fish supplies and caused either death or neurological damage in 111 people. The second incidence occurred in Iraq in 1971, where wheat initially intended to be used as seed was treated with a methylmercury fungicide and then used to make bread. As a result, approximately 500 people died and more than 6,500 were hospitalized with neurological effects. Contamination was due to methylmercury in both cases.[13]

The half-life of methylmercury in the human body is much longer than that of inorganic mercury. As a result, methylmercury can build up to toxic levels more quickly. In addition, methylmercury can cross the blood-brain or blood-placental barrier, causing severe neurological and developmental damage. The most common symptoms associated with severe methylmercury poisoning

are impairment of speech, vision, and coordination that makes walking and chewing difficult.[10]

Solid State Ion Exchange Extractants for Heavy Metal Ion Remediation

There is an interest in the development of remediation systems to decrease the concentrations of the three above-mentioned contaminants from natural waters. Implementation of the Resource Conservation and Recovery Act (RCRA)[15] and the Safe Water Drinking Act (SWDA)[16] required the regulation and safe management of toxic pollutants and chemical waste. As a result, new systems targeting the selective sequestration of these toxic elements became necessary in order to fulfill requirements set forth by the EPA.

The current industry standard for the removal of mercury ions from aqueous solution is activated carbon. Unfortunately, the capacity of activated carbon for mercury is low, only 1 mg of Hg/g of activated carbon at pH four.[17] Therefore, research devoted to the design of systems to separate ionic pollutants from aqueous systems is focused on the improvement of extractant capacity, but is also focused on other factors such as selectivity and stability. Cost is also an obvious concern when designing a practical extraction system.

Liu and co-workers at Pacific Northwest National Laboratory have developed a functionalized mesoporous silica in an attempt to remove Hg^{2+} from aqueous solution.[18] The mesoporous silica (average pore size, 55 Å) was functionalized with a monolayer of mercaptosilylpropyl groups. Mesoporous silica was the chosen support because of its high surface area (900 m^2g^{-1}) and ease of functionalization, and thiol functional groups were chosen because of their affinity for binding soft heavy metal ions. With 25 percent of the silica surface functionalized, this material was shown to remove up to 505 mg of Hg^{2+}

per gram of material, and also removed other soft heavy metal ions such as silver and lead. This is an example of an effective, selective extraction system.

The extracted heavy metal ions were recovered from the loaded extractant and the extractant was recycled by contacting it with a solution of 12 M hydrochloric acid for four hours. One of the shortcomings of this system is that a large volume of highly acidic secondary waste was generated in the recovery of the target metal ions. In addition, the capacity of this recycled material for mercury decreased by 50 percent after just one cycle. Acid recovery demonstrates that the material will not extract metal ions from acidic solutions ($pH \leq 1$).

At Colorado State University, the Dorhout and Strauss research groups have also been developing solid state materials as ion-exchange extractants for the removal and recovery of soft heavy metal cations from aqueous waste streams.[19-25] The requirements for an ideal extractant are: selectivity for soft metal cations (such as Hg^{2+}, Pb^{2+}, and Cd^{2+}) over hard ones (such as Na^{+}, Li^{+}, Mg^{2+}, and Cr^{3+}); recovery of the target element in a minimal volume of secondary waste; and ability of the deactivated extractant to undergo multiple extraction cycles to ensure that the extractant is recyclable and cost efficient. Finally, the extraction process should not require the use or discharge of any harmful or dangerous chemicals.

A new approach to the design of extraction systems that fulfill these requirements is that of redox-recyclable extraction and recovery (R^2ER).[23] A generic depiction of this approach for a solid state extractant is shown in Figure 1.2. Depending on its redox state, an R^2ER extractant will reversibly bind metal ions. The activation, use, and deactivation of the extractant can be achieved in three general steps. If the target ion is a cation, the first step

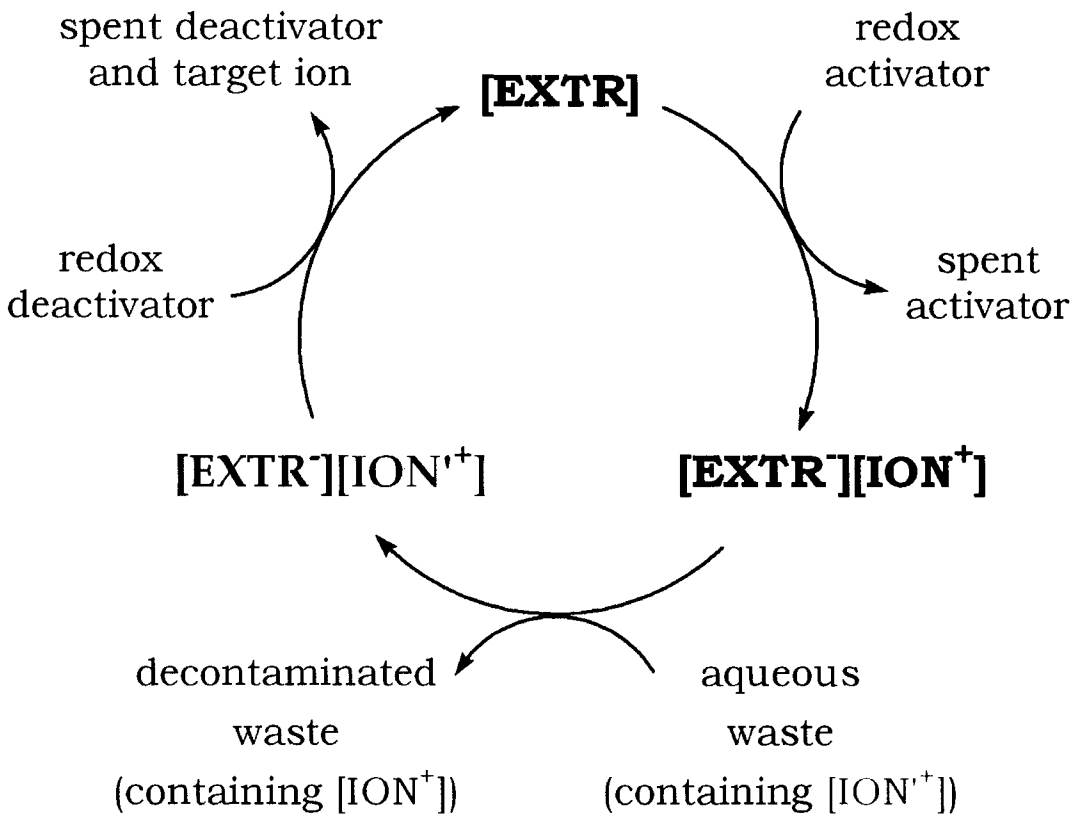

Figure 1.2 Generic representation of a redox-recyclable extraction and recovery (R^2ER) cycle for extractant [EXTR]. [$EXTR^-$] represents the reduced form of the extractant and [ION^+] and [ION'^+] represent the initial and contaminant cations, respectively.

involves reduction of the material to impart a net negative charge on the extractant. In order to maintain charge neutrality, this reduction necessitates the inclusion of a cation to form an ion pair complex, or a charge neutral solid, depicted $[EXTR^-][ION^+]$. In the second step, the reduced extractant is contacted with a waste solution and an ion exchange reaction occurs whereby the target ion, $[ION'^+]$ is removed from the contaminated waste stream and the cation initially paired with the extractant, $[ION^+]$, moves into the now decontaminated waste stream. The new complex is referred to as the loaded form of the extractant. Finally, after the $[EXTR^-][ION'^+]$ solid complex has been separated by filtration from the decontaminated waste stream, the extractant is oxidized to a deactivated form. In this step, the target metal ion is released from the extractant and both the contaminant and the deactivated extractant are separated and recovered.

A variety of different materials have been investigated as R^2ER ion exchange extractants. These materials have two structural similarities. The first is the presence of an open or flexible framework, so that ion exchange is facile and able to withstand repeated ion-exchange cycles. The second structural characteristic is the presence of sulfide-rich surfaces along with one or more exchangeable cations. A current hypothesis is that materials providing a sulfide rich environment will preferentially exchange hard cations initially held within the solid for soft cations in solution, according to Lewis hard-soft acid-base theory.[26]

I. Lithium Intercalated Molybdenum Disulfide – $Li_{1.3}MoS_2$

The naturally-occurring layered compound, MoS_2 was employed as a redox active ion exchange extractant in the R^2ER of numerous heavy metal

ions.[21] A rendering of the structure of the neutral form of MoS_2 (denoted 2H-MoS_2) is shown in Figure 1.3. The activated form of the extractant, $[MoS_2^{1.3-}][Li^+]_{1.3}$, was prepared using the known reductive intercalation reaction between MoS_2 and *n*-butyllithium.[27] In this reaction, *n*-butyllithium donates 1.3 electrons to MoS_2, imparting a net negative charge on the layers as shown in Equation 1.3.

$$MoS_2(s) + 1.3\ CH_3(CH_2)_3Li \longrightarrow Li_{1.3}MoS_2(s) + \text{products} \qquad (1.3)$$

The intercalation of charge compensating lithium cations into the interlayer spaces, occurred simultaneously with reduction and was possible because the flexible nature of the structure as a result of weak van der Waals forces between the layers. The chemical formula of the activated compound is $Li_{1.3}MoS_2$.

When contacted with an aqueous waste simulant, a portion of the 1.3 reducing equivalents of $Li_{1.3}MoS_2$ reduced water to form hydrogen gas. The production of hydrogen gas in the interlayer space caused the MoS_2 layers to exfoliate into negatively-charged $[MoS_2]^{n-}$ slabs ($n < 1.3$). After exfoliation, the extraction mixture contained a suspension of negatively charged $[MoS_2]^{n-}$ slabs, lithium ions, the contaminant metal ion $[ION'^+]$, and its charge compensating anion. The cations present in solution attract the negatively charged single layers, reforming a three dimensional solid in a process called flocculation. As a result of this process, cations are included in the interlayer spaces of the restacked material. The preferential inclusion of soft heavy metal cations between the MoS_2 layers in the flocculated product is a result of the greater affinity of sulfide anions, which are soft Lewis bases for soft Lewis acid heavy metal cations. A schematic of the exfoliation and flocculation mechanism is

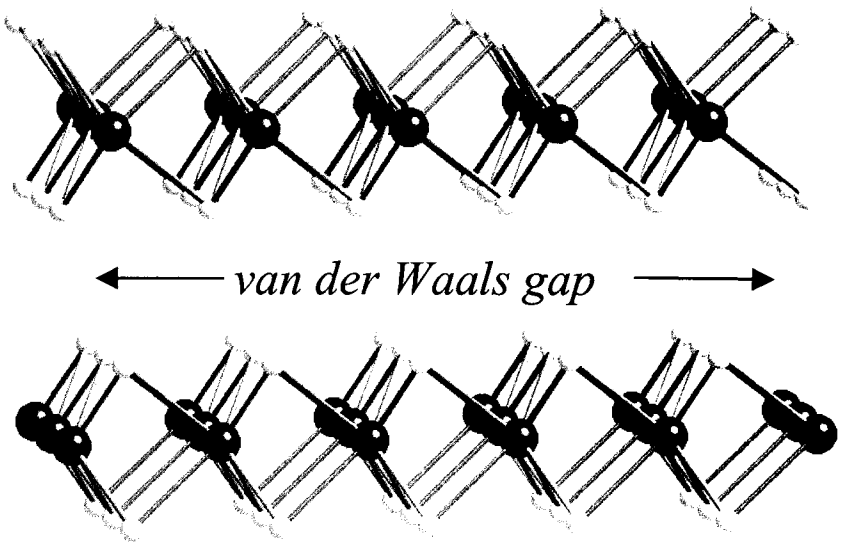

Figure 1.3 Ball and stick structural representation of 2H-MoS_2.

shown in Figure 1.4. The resulting material had the chemical formula M_xMoS_2.[28] Examples of heavy metal ions that were reported to undergo this type of reaction are Hg^{2+}, Pb^{2+}, Ag^+, and Cd^{2+}.[20]

This extraction system is unique because the metal cations can be recovered from the loaded extractant simply through heating. Mercury was removed from Hg_xMoS_2 by heating the solid under vacuum at 425 °C for two hours. The heating process induced an entropy-driven internal redox reaction in which the $[MoS_2]^{n-}$ layers reduced Hg^{2+} to Hg^0. During heating, the MoS_2^{n-} were oxidized to neutral MoS_2. The Hg^0 that was released from the solid was collected in a cold trap in near quantitative yield.[20] This recovery step is attractive in that essentially mercury-free MoS_2 was recovered and mercury was collected in the smallest volume of secondary waste possible – elemental mercury. The MoS_2 recovered after deactivation was also reactivated multiple times with *n*-butyllithium. The maximum reported capacity of this material for mercury was found to be 580 mg of Hg^{2+} per gram of $Li_{1.9}MoS_2$. This behavior was also seen with Ag^+ as the target metal ion, but Ag^0 had to be isolated from the extractant in a second step. The complete R^2ER cycle specific to MoS_2 is shown in Figure 1.5.

$Li_{1.3}MoS_2$ was proven effective on a laboratory scale, but there were limitations that made it impractical for use in a large-scale remediation project. One major problem with this system was the use of *n*-butyllithium as a redox activator for MoS_2. Butyllithium is a pyrophoric chemical and air-sensitive chemical handling techniques were required for the synthesis and handling of $Li_{1.3}MoS_2$. Furthermore, $Li_{1.3}MoS_2$ was oxidized by atmospheric water, indicating that stringent procedures had to be followed to ensure that no contact with air occurred before contact with a waste solution in order for the full capacity of the extractant to be realized. These characteristics represent an

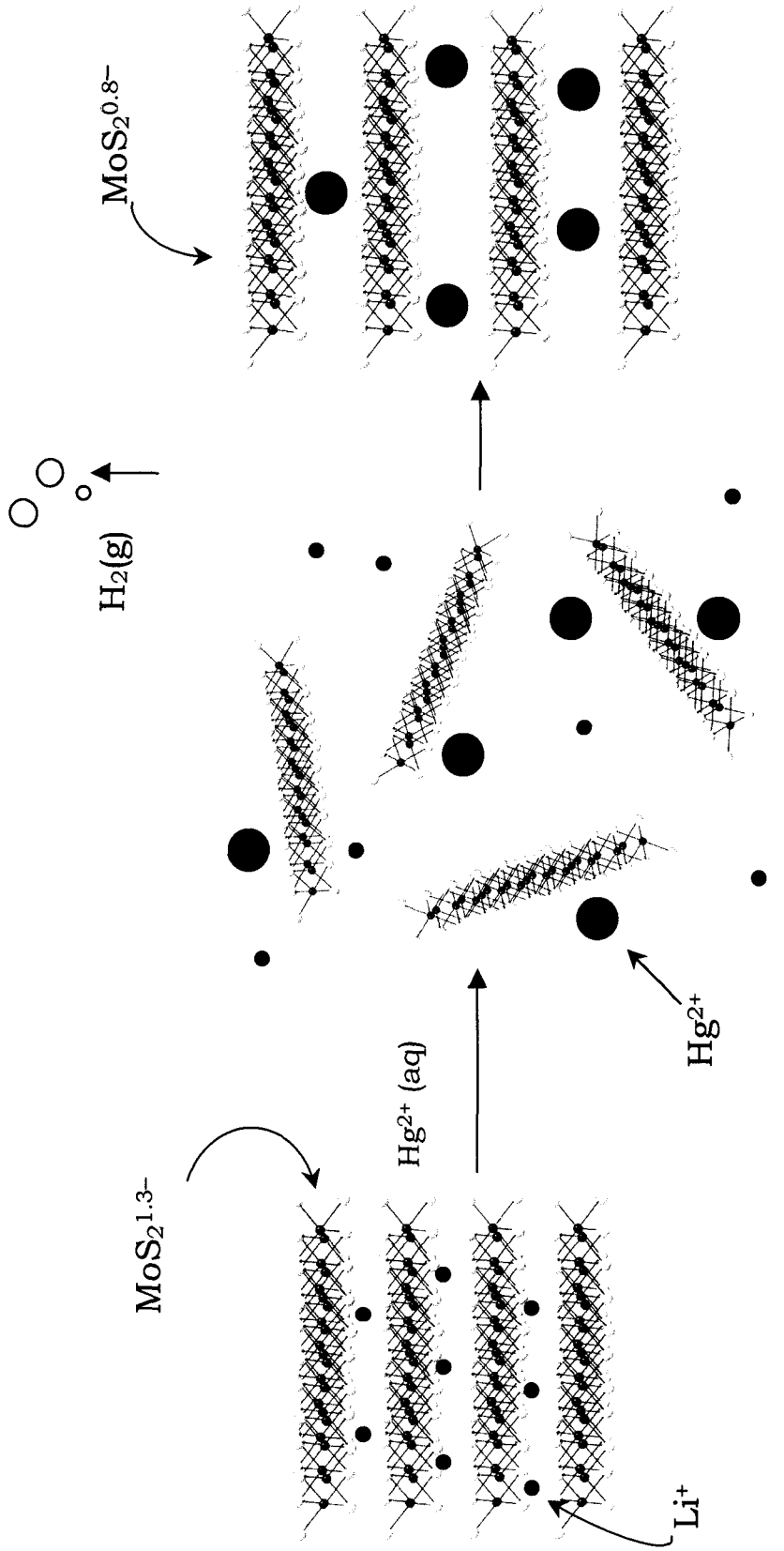

Figure 1.4 Schematic for exfoliation/flocculation mechanism of $Li_{1.3}MoS_2$ in an aqueous solution of Hg^{2+}.

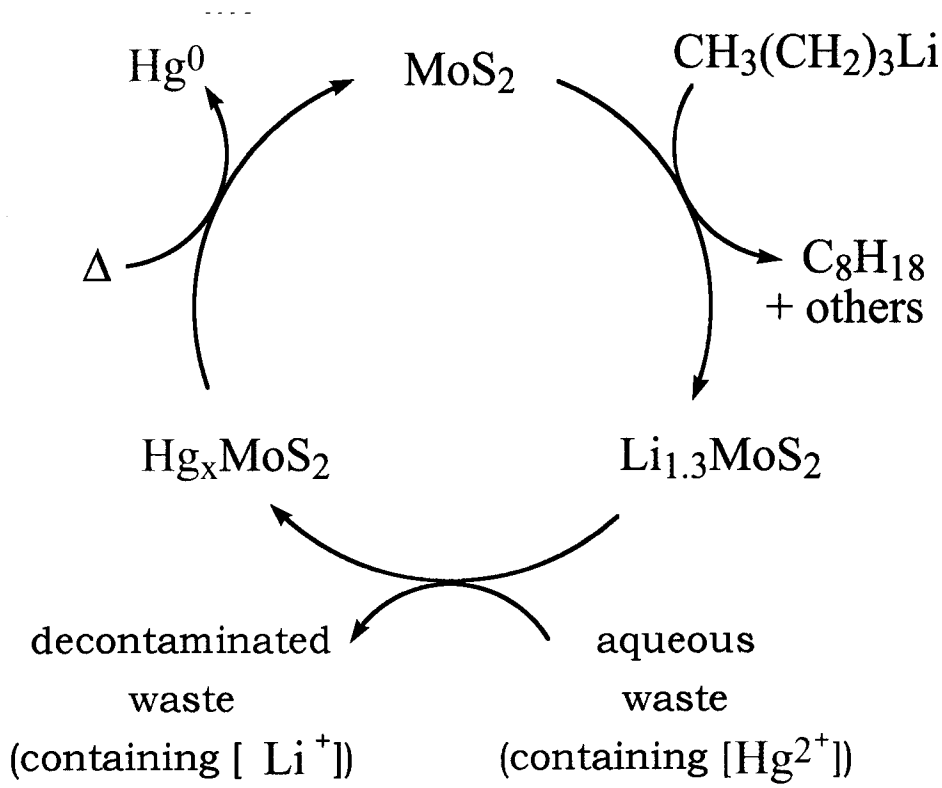

Figure 1.5 R^2ER cycle for MoS_2.

increased cost for remediation due to the need for special equipment and safety precautions.

A second drawback was that one of the by-products of the extraction reaction was hydrogen gas. In a practical sense, any material used on the kilogram scale is not appropriate if it generates large amounts of flammable gas at a cleanup site. Therefore, although $Li_{1.3}MoS_2$ is an effective R^2ER extractant, it is not practical for use on a large scale. Modifications to the synthesis of the extractant and to the mechanism by which the material removes heavy metal ions from solution must be achieved.

II. Zirconium Monothiophosphate

A second material investigated as an ion exchange extractant (although not redox active) was zirconium monothiophosphate, $H_2Zr(PO_3S)_2$.[21, 22] The structure of $H_2Zr(PO_3S)_2$ is shown in Figure 1.6 and is related to the family of layered phosphates initially developed by Clearfield.[29-33] Through vibrational spectroscopy and structural analysis, it was shown that the protonated monothiophosphate unit, $(HPO_3S)^{2-}$ oriented in the lattice so that the SH groups pointed into the interlayer spaces of the compound. After loss of a proton, this structural characteristic provided a soft, anionic Lewis basic environment that was attractive to soft Lewis acid cations in solution. It was shown that this material removed metal cations from solution according to the ion exchange reaction shown in Equation 1.4.

$$H_2Zr(PO_3S)_2(s) + yM^{n+}(aq) \rightleftharpoons H_{2-nx}M_xZr(PO_3S)_2(s) + nxH^+(aq) + (y-x)M^{n+}(aq) \quad (1.4)$$

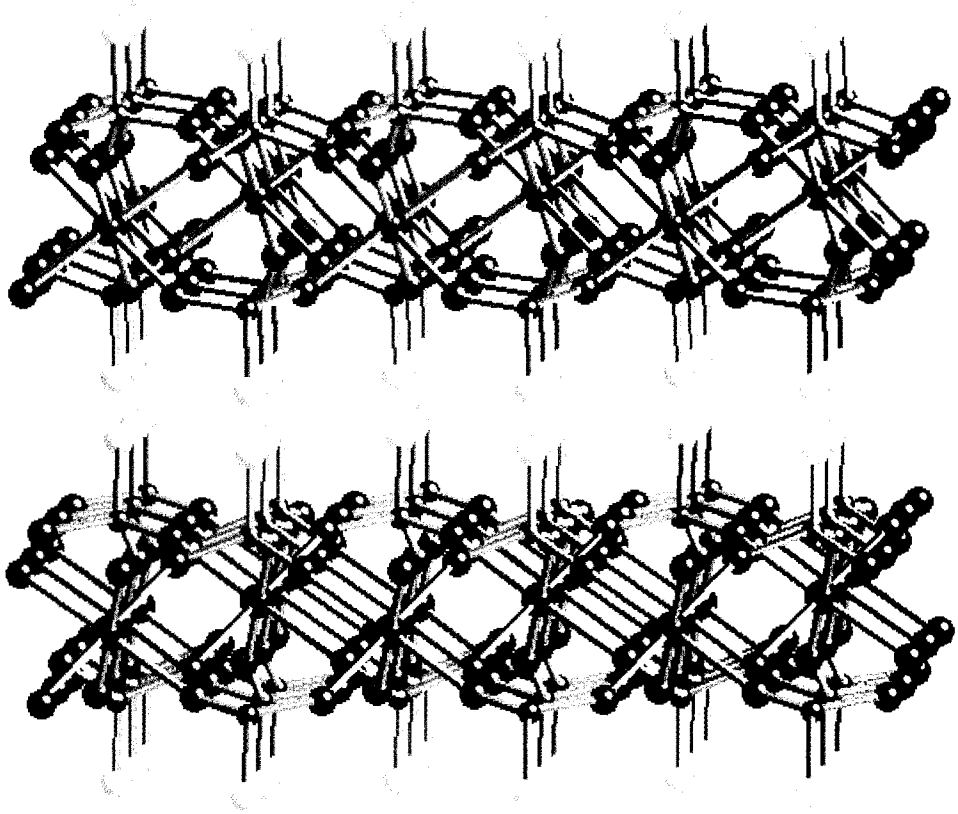

Figure 1.6 Structure of $H_2Zr(PO_3S)_2$. Protons (which reside in the interlayer space of the solid) have been omitted for clarity.

As is consistent with this equilibrium, there was a pH dependence on the ion-exchange ability; at lower pH values, the value of x in $H_{2-nx}M_xZr(SO_3S)_2$ decreased.

Using this same concept, however, the complexed metal ion was recovered from the solid through treatment with 3M HCl. In this recovery reaction, the equilibrium in Equation 1.4 was reversed, resulting in the re-formation of $H_2Zr(PO_3S)_2$ and a solution containing dissolved M^{n+}. Although the recyclability of this material was convenient, it was somewhat inefficient, producing an acidic secondary waste stream that had a volume potentially equal to or greater than that of the initial waste stream. The disposal of large volumes of acidic secondary waste can be costly. Therefore, in terms of recyclability, $H_2Zr(PO_3S)_2$ is not an attractive extractant system.

In the presence of either Hg^{2+} or Pb^{2+} and water, $H_2Zr(PO_3S)_2$ decomposed over time to form HgS and PbS, evidenced by powder X-ray diffraction. This decomposition was evaluated in two ways. On one hand, the formation of transition metal sulfides was detrimental in that decomposition of the extractant meant that it was not recyclable in the presence of either mercury or lead. Therefore, if a goal was to reuse the extractant, this system failed. On the other hand, HgS is an extremely stable form of mercury (K_{sp} = 5 x 10^{-54})[34] and might be an appropriate storage form if neither the metal ion nor the extractant was to be recycled.

As is the case with many sulfide-based materials, it is believed that $H_2Zr(PO_3S)_2$ is susceptible to hydrolysis by atmospheric water over the time frame of months.[35] Therefore, special considerations would be required if this extractant were used in large quantities in an actual remediation situation. Specifically, the extractant would need to be synthesized and used within a short time frame in order to avoid decomposition and maintain extractant

efficiency. On a large scale, and with an actual remediation situation, this is not always possible. In addition, this property would limit the number of extraction cycles the material would be able to complete before needing to be replaced.

Goals of This Research

The problems associated with the current extractants have been described above. There is an interest in modifying these systems, or developing new ones based on the current understanding of efficient and effective ion exchange. Research has indicated that sulfide based materials, which provide a soft Lewis basic environment, are appropriate for selectively removing toxic, soft heavy metal ions such as Hg^{2+} from aqueous solution. In addition, solids with a flexible or open structure are expected to be more efficient in a process where the mechanism of ion extraction is exchange of cations from the solid for cations in solution. These materials should also satisfy the following requirements: toxic precursors or byproducts should be reduced or eliminated from the synthesis or from the extraction step of the R^2ER cycle; the extraction process should be complete on a short time scale (hours to a few days); the materials should be stable in air and appropriate to use under a variety of conditions (as part of a batch process, packed in a column, on an electrode, etc.); and, environmentally benign cations should be used as exchangeable cations out of the solid, so as to produce a decontaminated waste stream that is as environmentally sound as possible.

Scope of This Dissertation

This dissertation will describe research based on the optimization of two different classes of sulfide-based materials as selective extractants for soft heavy metal cations from aqueous waste streams. Chapter II compares a variety of alkali metal and proton intercalated MoS_2 compounds. The different synthetic methods used to prepare these materials, as well as their relative extraction abilities are reported. Most importantly, this research presents the use of alkali-intercalated molybdenum disulfide analogs that do not produce hydrogen gas upon contact with aqueous waste streams. The stoichiometry of the cations included in the MoS_2^{n-} layers was examined and found to depend on the preparative reaction conditions. The mechanism of extraction/ion exchange with these materials was found to be markedly different from that of $Li_{1.3}MoS_2$ in that it did not involve exfoliation or flocculation. This mechanistic difference was examined through the use of timed extractions as well as through a comparison of the extraction abilities using different metal cations.

Chapters III and IV examine the development of a different and new extraction system based on a class of transition metal tin sulfide-based materials with the spinel structure. These materials have the general formula $Cu_2MSn_3S_8$, where M is either Fe or Mn. Chapter III discusses the synthesis and characterization of the parent thiospinels as well as novel analogs to this spinel family. The goal of this research was the synthesis of spinel compounds with alkali metal cations or protons present in the structure to act as ion exchange cations. Different synthetic techniques were employed, including both chemical and solid state approaches. Synthetic routes that took advantage of the redox properties inherent in these materials were investigated. This involved the initial oxidation of the material, through direct synthesis or

chemical oxidation and then reduction with a chemical reducing agents. Novel materials with the spinel structure were also synthesized with the direct incorporation of an alkali metal cation into the spinel structure to form compounds such as $Li_2FeSn_3S_8$ and $LiCuFeSn_3S_8$.

Finally, aqueous intercalation of the parent compounds with protons to form compounds with chemical formulas such as $H_{0.37}Cu_{1.98}Mn_{0.82}Sn_3S_8$ was also successful. Structural characterization using powder X-ray diffraction analysis and X-ray photoelectron spectroscopy is presented.

Chapter IV presents a comparison of the extraction capabilities of the different transition metal spinels for various contaminant heavy metal ions, including Hg^{2+}, Pb^{2+}, and Ag^{+}. It describes the mechanism of heavy metal ion removal through an examination of structural changes as well as mass balance comparisons. It is evident that these materials are all ion exchange extractants for the removal of heavy metal ions. In most cases, the alkali metal intercalated spinels extracted soft heavy metal ions from solution more efficiently and more rapidly than the parent compounds. The mechanisms of ion removal with the new extractants were investigated through detailed structural comparisons and mass balance considerations.

References

1. http://minerals.usgs.gov/minerals/pubs/commodity/cadmium/140302.pdf.
2. *Mineral Commodity Summaries 2002.* 2002, U.S. Geological Survey: Washington.
3. Skoog, D.A.; Leary, J.J. *Principles of Instrumental Analysis.* 4th Edition; Harcourt Brace College Publishers: Philadelphia, 1992.
4. http://www.epa.gov/opptintr/lead/index.html.
5. Holton, W.C. *Environmental Health Perspectives* **1998**, *106(2)*, A74-A76.
6. Hanisch, C. *Environ. Sci. Tech.* **1998,** *32,* 176A-179A.
7. *Mercury Study Report to Congress, Volume III: Fate and Transport of Mercury in the Environment.* U.S. Environmental Protection Agency, Office of Air Quality Planning & Standards and Office of Research and Development: Washington, DC., 1997.
8. http://www.eurochlor.org/chlorine/science/risk13.htm.
9. Lide, D.R., Ed. *CRC Handbook of Chemistry and Physics.* 73rd ed.; CRC Press: Ann Arbor, 1992-1993.
10. Krabbenhoft, D.P. and D.A. Rickert, *Mercury Contamination of Aquatic Ecosystems.* U.S. Geological Survey, 1995.
11. Watras, C.J.; Huckabee, J.W., Eds. *Mercury Pollution: Integration and Synthesis*; Lewis Publishers, Inc.: Boca Raton, FL, 1993.
12. http://www.epa.gov/oar/mercover.html.
13. Baird, C., *Environmental Chemistry*; W.H. Freeman and Company,: New York, 1995.
14. Lippmann, M. *Environmental Research* **1990**, *51*, 1-24.
15. http://www.epa.gov/region5/defs/html/rcra.htm, December 19, 2002.

16. http://www.epa.gov/safewater/sdwa/sdwa.html#theact, December 19, 2002.

17. Faust, S.D.; Aly, O.M *Chemistry of Water Treatment.* 2nd Edition.; Ann Arbor Press: Michigan, 1998.

18. Feng, X., et al. *Science*, **1997**, *276*, 923-926.

19. Dorhout, P.K. and S.H. Strauss, *The Design, Synthesis and Characterization of Redox-Recyclable Materials for Efficient Extraction of Heavy Element Ions from Aqueous Waste Streams*, in *ACS Symposium Series: Inorganic Materials Synthesis*, C.E. Winter and D.M. Hoffman, Editors. American Chemical Society: Washington, D.C., 1999, p. 53-68.

20. Gash, A.E., et al. *Environ. Sci. Tech.* **1998,** *32*, 1007-1012.

21. Gash, A.E., *Lithium Intercalated Transition Metal Chalcogenides as Redox-Recyclable Extractants and Synthesis and Characterization of Group IVB Metal Bis(Hydrogen Monothiophosphate) Compounds*, Ph.D. Dissertation. 1999, Colorado State University: Fort Collins.

22. Gash, A.E., et. al. *Inorg. Chem.* **2000**, *39*: 5538-5546.

23. Strauss, S.H., *Redox-Recyclable Extraction of Heavy Metal Ions and Radionuclides from Aqueous Media*, in *ACS Symposium Series: Metal-Ion Separation and Preconcentration Progress and Opportunities*, A.H. Bond, M.L. Dietz, and R.D. Rogers, Editors. American Chemical Society: Washington D.C., 1999, p. 156.

24. Allen, P.G., et al. *Chem. Mat.* **2001**, *13*, 2257-2265.

25. Dysleski, L., et al., *Design and Synthesis of New Materials for Heavy Element Waste Remediation*, in *Interfacial Applications in Environmental Engineering*, M.A. Keane, Editor. Marcel Dekker, Inc.: New York, 2003, p. 111-125.

26. Pearson, R.G., *Survey of Progress in Chemistry*, Scott, A., Ed.; Academic Press: New York, 1969.

27. Dines, M.B., *Mat. Res. Bull.* **1975**, *10*, 287-292.

28. Depending on reaction conditions (the initial ratio of MoS_2:M^{n+}), the negative charge on MoS_2 will also be balanced by protons or lithium cations in solution. In addition, these cations may or may not be hydrated. For the sake of brevity, however, this formula will be used as an abbreviation.

29. Clearfield, A.; Stynes, J.A. *J. Inorg. Nucl. Chem.* **1964**, *26* 117-129.

30. Clearfield, A., et. al. *J. Inorg. Nucl. Chem.* **1968**, *30*, 2249-2258.

31. Clearfield, A., et al., *J. Phys. Chem.* **1969**, *73*, 3424-3430.

32. Clearfield, A.; Medina, A.S. *J. Inorg. Nucl. Chem.* **1970**, *32* 2775-2780.

33. Clearfield, A., *Chem. Rev.* **1988**, *88*, 125-148.

34. Harris, D.C., *Quantitative Chemical Analysis*. 3rd Edition.; W.H. Freeman and Company: New York, 1991

35. Hufford, F.D. Colorado State University, Fort Collins, CO. unpublished work.

Chapter II

Synthesis and Characterization of A_xMoS_2 ($A^+ = H^+, Na^+, K^+$; $x < 1.3$) as Ion-Exchange Extractants for Heavy Metal Cations

Introduction - Metal Ion Extraction Mechanism with $Li_{1.3}MoS_2$

MoS_2 is a member of the family of transition metal dichalcogenides that form layered structures. In its native form, denoted the 2H polymorph, one neutral layer of MoS_2 consists of a hexagonal array of molybdenum atoms, each coordinated to six sulfur atoms in a trigonal prismatic arrangement.[1] The layers of this material are held together by weak van der Waals forces at a distance of 6.14 Å.[2] MoS_2 can be reductively intercalated with lithium ions through a reaction of MoS_2 and *n*-butyllithium.[3] In this reaction, *n*-butyllithium donates electrons into the electronic band structure of MoS_2 imparting a net negative charge on the MoS_2 layers. Lithium ions intercalate into the interlayer space as charge compensating cations. During this reaction, the MoS_2 undergoes a structural phase change to the 1T polymorph in which the molybdenum atoms are octahedrally coordinated to six sulfur atoms.[4] The reduction of MoS_2 and structural phase change necessitates the intercalation of

lithium cations to maintain charge neutrality. Therefore, the compound changes from a binary compound (MoS_2) to a ternary compound (Li_xMoS_2). For the remainder of this dissertation, references to reduced MoS_2 implies a residual negative charge on the MoS_2 layers and the presence of charge compensating cations. A comparison of the structures of the two polymorphs of MoS_2 is shown in Figure 2.1

The ternary compound, Li_xMoS_2, produced in the reaction with *n*-butyllithium is a strong enough reducing agent to reduce water and form hydrogen gas (H_2), as described in Chapter I. The formation of hydrogen gas in the interlayer space causes the layers to exfoliate in aqueous solution forming a suspension of MoS_2 particles.[5] In a solution containing cations, exfoliated MoS_2 will flocculate and form an inclusion compound with cations intercalated between the MoS_2 layers. There is a large body of research devoted to understanding the chemistry of exfoliated MoS_2 because this technique has been used to synthesize a variety of new MoS_2 compounds.

The first reported use of the exfoliation/flocculation technique to synthesize inclusion compounds of MoS_2 was by Gee and co-workers in 1986.[6] In this study, lithium-intercalated MoS_2 was exfoliated in water with initial pHs ranging from 3 to 11. It was postulated that $LiMoS_2$ reduced water to form hydrogen gas and hydroxide anions.[7] The hydrogen gas bubbles in the solid "blew apart" the layers to form a suspension of single layers in solution. Production of hydroxide resulted in a final solution with a basic pH. Because of the high concentration of OH^-, it was believed that the surfaces of the single layers of MoS_2 in the exfoliated solution were covered with hydroxide anions. This surface hydroxylation was also reported by Morrison in 1989.[8]

The metal cations in solution were believed to attract the negatively charged, hydroxylated MoS_2 layers back together.

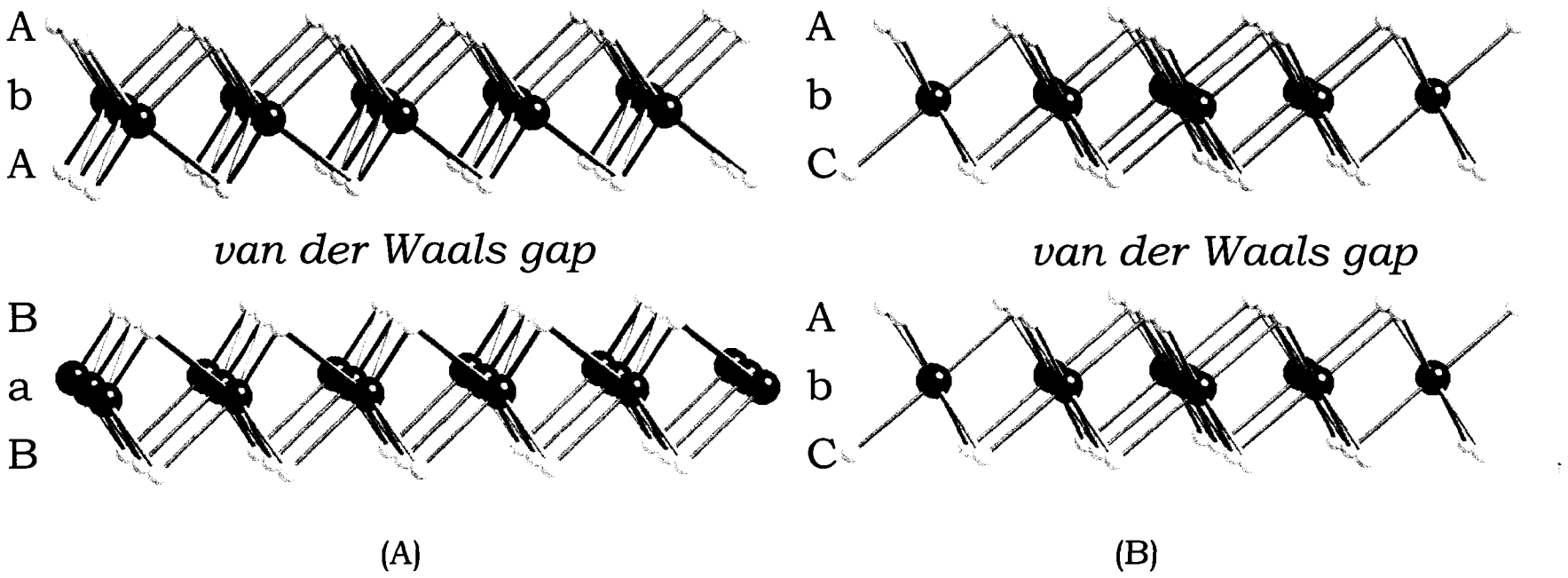

Figure 2.1 Ball and stick structural representation of (A) 2H-MoS_2 (B) 1T-MoS_2. Note the trigonal prismatic MoS_6 units in (A) and the octahedral MoS_6 units in (B).

Furthermore, the metal cations were assumed to be included between the layers of MoS_2 in the form of metal hydroxides. The authors' conclusion that the metal ions were present between the layers with charge compensating anions implied that the MoS_2 layers were neutral. No reference to any negative charge on the MoS_2 layers, or oxidation of MoS_2^{n-} layers was made.

In 1994, Rouxel and co-workers examined the formation of alkyammonium- and transition metal-intercalated MoS_2 using the exfoliation method and were the first to state that the MoS_2 layers after exfoliation were negatively charged.[9] When alkylammonium cations were included (from an aqueous solution of the alkylammonium chloride or bromide), stoichiometries of $(R_4N^+)_x(MoS_2)^{x-}$ were obtained where x ranged from 0.15 to 0.30. No oxygen or halide was detected by elemental analysis and the residual charge on the MoS_2^{n-} layers was therefore assumed to be approximately 0.25. In the case of transition metal included MoS_2, the M^{2+}/Mo ratio of the Fe^{2+}, Co^{2+}, and Ni^{2+} compounds was 0.5. Since the 0.25 equivalents of negative charge on the MoS_2 layers (determined from the alkylammonium experiments) were not sufficient to balance the one equivalent of positive charge from the metal cations in these newly formed compounds, it was assumed that the remaining positive charge was balanced by included hydroxide anions to give an actual product stoichiometry of $(M^{2+})_{0.5}(OH^-)_{1-x}(H_2O)_y(MoS_2)^{x-}$. Hydroxide was formed as the result of reduction of water by MoS_2^-, proposed in Equation 2.1.

$$Li^+MoS_2^- + H_2O \longrightarrow Li^+ + MoS_2^{x-} + (1-x)OH^- + (1-x)/2\ H_2 \qquad (2.1)$$

No further discussion was devoted to direct evidence for the presence of hydroxide anions between the layers, or how water and hydroxide were distinguished from one another using elemental analysis. An aerobic method

was used to synthesize these compounds and the authors noted that aging of the solids in solution resulted in a slow decrease in the value of x, indicating oxidation of the MoS_2^{x-} layers. Since then, other literature reports have determined that the value of x in MoS_2^{x-} that had been exfoliated and flocculated in the presence of different cations under aerobic conditions ranged from 0.1 to 1.[10-12]

The purported binary form of MoS_2 referred to as 'restacked MoS_2' is another compound formed using the exfoliation/flocculation technique. This was first synthesized by Morrison and co-workers in 1991.[13] In this report, $LiMoS_2$ was exfoliated in water and the pH of the solution was then lowered to between 2 and 3. It was postulated that the addition of acid neutralized the surface hydroxides present on the MoS_2 layers, forming a solid that flocculated as MoS_2. Later reports indicated that restacked MoS_2 could be synthesized by exfoliation and subsequent washing with water until the pH of the wash solution decreased to 7.[14-17] These washes were apparently sufficient to remove any surface hydroxides present and allowed for flocculation of the neutral MoS_2 layers. Again, these reactions were performed aerobically and no consideration to the possibility of negative charge on the MoS_2 layers or cation inclusion (to form compounds such as H_xMoS_2 or Li_xMoS_2) was mentioned.

In 1998, the Dorhout and Strauss research groups at Colorado State University used the exfoliation/flocculation technique to target and remove soft heavy metal cation contaminants from acidic, aqueous solution. Using mass balance experiments, the redox and ion exchange reactions that occurred during the anaerobic exfoliation and flocculation in an aqueous, acidic solution of $Hg(NO_3)_2$, was proposed and is shown in Equation 2.2.[18]

$$Li_{1.3}MoS_2(s) + 0.9H_3O^+(aq) + 0.20Hg^{2+}(aq) \longrightarrow$$
$$Hg_{0.20}H_{0.38}MoS_2(s) + 0.26H_2(g) + 1.3Li^+(aq) + 0.9H_2O(aq) \quad (2.2)$$

As can be seen from this equation, 0.26 equivalents of hydrogen gas were evolved and measured in this reaction. This indicated that 0.78 equivalents of negative charge remained on the MoS_2 layers and was compensated for by a combination of 0.40 equivalents of positive charge from mercuric cations and 0.38 equivalents of protons (or hydronium ions) that were shown to be removed from solution.[19] In addition, no lithium cations were detected in the flocculated product. This was the first report to show that the charge remaining on the MoS_2^{n-} layers after exfoliation under anaerobic conditions was 0.78–. It was also the first report to measure the oxidation of $MoS_2^{1.3-}$ under anaerobic conditions and to consider only exfoliation in the oxidation process. All other literature experiments to this point had been performed under aerobic conditions, meaning that oxidation of MoS_2^{n-} could have been the result of a combination of oxidation by both water and atmospheric oxygen. Oxidation by atmospheric oxygen is not commonly discussed in the literature, however this process is, in fact, an important contributor to the oxidation of MoS_2^{n-}. The report by Strauss and Dorhout was also the first to indicate that protons were included in the interlayer space as a result of exfoliation and flocculation in acidic solution.[20]

This research was also the first to measure the affinity of MoS_2 for competing cations in solution (including the lithium cations present from the reactant, $Li_{1.3}MoS_2$). Depending on this affinity, the cation distribution in the final product can vary. Formation of $H_{0.38}Hg_{0.20}MoS_2$, demonstrated that the flocculation process was selective. In the reaction discussed above, there were three cations present in solution after exfoliation: Li^+, H^+ and Hg^{2+}.

Even though H^+ was present in a 100 times excess compared to Hg^{2+} (based on the experimental conditions), the ratio of H^+ to Hg^{2+} in the final product was two to one. This selectivity allowed for greater than 99% removal of soft heavy metal cations from acidic solution. In a similar experiment targeting Na^+ as a 'contaminant' ion in acidic solution, only 5% of the sodium cations were included in the flocculated product, demonstrating the preferential inclusion of H^+ over Na^+.

Based on this work, using the exfoliation/flocculation technique, proton and alkali metal included MoS_2 inclusion compounds were synthesized and studied with the goal of developing an ion exchange extractant that would not evolve hydrogen gas during the extraction step of the R^2ER cycle as was seen with $Li_{1.3}MoS_2$. The first new extractant examined was the product of the exfoliation and flocculation of $Li_{1.3}MoS_2$ in acid, as described in Equation 2.3.

$$Li_{1.3}MoS_2(s) + 1.3H_3O^+(aq) \longrightarrow 0.26H_2(g) + 1.3Li^+(aq) + (H_3O)_{0.78}MoS_2(s) + 0.52H_2O(l) \quad (2.3)$$

Mass balance experiments of this reaction to determine the amount of residual charge on the MoS_2 layers and the cation distribution of the flocculated product were performed to identify the correct stoichiometry of this product.

Contaminant metal ions were then extracted with H_xMoS_2 through a direct ion exchange mechanism, similar to that seen with $H_2Zr(PO_3S)_2$, demonstrated in Equation 2.4. This synthetic modification moves hydrogen gas evolution into the activation step of the R^2ER cycle and out of the extraction step.

$$(H_3O)_{0.78}MoS_2(s) + 0.20Hg^{2+}(aq) \longrightarrow$$
$$(H_3O)_{0.38}Hg_{0.20}MoS_2(s) + 0.40H_3O^{+}(aq) \quad (2.4)$$

In order to synthesize alkali metal intercalated MoS_2 (A_xMoS_2), $Li_{1.3}MoS_2$ was exfoliated and flocculated using an aqueous solution of the alkali metal nitrate salt at pH 5. The negative charge remaining on the MoS_2^{n-} layers after exfoliation necessitated the inclusion of A^+ in order for flocculation to occur. These materials, H_xMoS_2 and A_xMoS_2, with a lower overall negative charge on the MoS_2^{n-} layers than $Li_{1.3}MoS_2$ (and consequently less reducing strength) do not reduce water on contact, and therefore do not produce hydrogen gas, nor do they exfoliate. Exchangeable cations, present in the interlayer space of the material, however are available to ion exchange with soft metal cations in solution. As extractants, they are considered better than $Li_{1.3}MoS_2$ because they do not produce hydrogen gas during metal ion extraction.

The synthesis of $A_{0.8}MoS_2$ was also attempted through a variety of other reactions as well, however the exfoliation/flocculation mechanism in an aqueous solution of the alkali metal nitrate salt was found to be the most effective. The efficiency of each of these new materials to extract soft heavy metals from solution was tested and compared to that of $Li_{1.3}MoS_2$. Since these materials do not produce hydrogen gas when contacted with aqueous solution, their mechanism of extraction is different from that of $Li_{1.3}MoS_2$. Therefore, factors such as extraction time and overall stability are considered.

Experimental

Materials and Reagents. Distilled water was purified and deionized (to 18 MΩ) with a Barnstead NANOPure purification system. Nitric acid

(Mallinckrodt), hydrochloric acid (Mallinckrodt), acetonitrile (Fisher Scientific) and metal nitrate salts were reagent grade or better and were used as received. Reagents for syntheses were used as follows: *n*-butyllithium (2.5 M in hexanes) (Aldrich), MoS_2 powder (<2 mm)(Aldrich). Schlenk, glovebox and high vacuum techniques were employed for some experiments.[21] Purified, anhydrous hexane was prepared by stirring over H_2SO_4 (Mallinckrodt), flowing through activated basic alumina (Aldrich, 150 mesh) and distillation from sodium metal.

Synthetic Methods. The compound $Li_{1.3}MoS_2$ was prepared by a literature procedure.[22] In a typical experiment, 100 mL of *n*-BuLi (250 mmol) was added to a Schlenk flask containing 8.00 g of MoS_2 (50.0 mmol) and a teflon-coated magnetic stir bar. The mixture was stirred at 25 °C for 48 hours under a nitrogen atmosphere. The solid product was recovered by filtration under inert atmosphere and was washed with two 50-mL aliquots of dried hexanes. The recovered solid was stored in a glovebox with a purified nitrogen atmosphere.

A_xMoS_2 was prepared by the reaction of $Li_{1.3}MoS_2$ and an aqueous solution of 0.1M ANO_3 (where A = H, Li, Na, K). In a typical experiment, 1.00 g of $Li_{1.3}MoS_2$ was loaded into a 250 mL Erlenmeyer flask in the inert atmosphere. The flask was then stoppered with a rubber septum and transferred into an inert atmosphere "wet" box. It was then contacted with 200 mL of ANO_3 solution that had been degassed under a purge of flowing nitrogen for at least 30 minutes. The reaction was stirred for 2 hours after which time it was filtered using a medium glass frit. The solid was dried under dynamic vacuum overnight on a Schlenk line at room temperature. The recovered solids were stored under inert atmosphere.

Hydrogen uptake experiments were performed using a hydrogen uptake apparatus with a known internal volume. A known amount of solid (~ 0.2 g) was loaded into the apparatus in the glovebox. The apparatus was sealed to laboratory atmosphere and transferred to a high vacuum manifold (P ~ 10^{-5} torr) where the sample chamber was evacuated. A known pressure of H_2(g) was introduced into the chamber and the pressure was monitored at various time intervals using an electronic manometer.

Extraction Experiments. In a standard extraction, a known mass of solid was contacted with an aqueous solution of metal nitrate salt in a 5:1 extractant to metal ion ratio. For aerobic extractions, a known mass of solid was placed into a 25 mL Erlenmeyer flask in an inert atmosphere glovebox and exposed to laboratory atmosphere immediately before a freshly prepared metal ion solution was added. For anaerobic extractions, the solid was similarly weighed in an inert atmosphere glovebox, sealed with a rubber septum and moved into an oxygen free "wet" box. Then, 20 mL of a metal ion solution that had been degassed under flowing nitrogen was added. Each flask was stirred on a stir plate for an appropriate time after which the loaded extractant was filtered from the decontaminated waste. The filtrate was diluted to a constant volume of 25 mL.

The effect of metal ion intercalation on the structure was monitored qualitatively by powder X-ray diffraction (PXRD) and differential scanning calorimetry (DSC). The stoichiometry of the loaded extractant is quantitated by comparing the initial and final metal ion concentrations in solution by inductively coupled plasma atomic emission spectroscopy (ICP-AES).

Instrumentation. In a typical experiment to measure the amount of hydrogen gas evolved from a particular sample, 20 mL of 0.1M HNO_3 (or a solution of $M(NO_3)_x$ in 0.1M HNO_3) was degassed in the larger compartment of a hydrogen evolution apparatus (shown in Figure 2.2) through three freeze-pump-thaw cycles, to ensure that no dissolved gas was present in the reaction environment prior to the extraction process. The initial vapor pressure of the solution was measured and recorded. The apparatus was brought into an inert atmosphere glovebox, with the area containing the aqueous medium closed, and a known amount of activated extractant was weighed into the smaller of the two compartments. The apparatus was then attached to a high vacuum line, where the compartment containing the solid sample was evacuated. Finally the solid sample was contacted with the aqueous media and placed in a constant temperature bath (20 °C) until temperature equilibration. An electronic manometer was used to measure the evolved pressure. The measured pressure was a result of water vapor in addition to the pressure of the evolved hydrogen gas. The quantity of gas evolved was then calculated using the ideal gas law (PV=nRT).

The concentrations of metal ions in solution were determined by inductively-coupled plasma atomic emission spectrometry (ICP-AES) using a Perkin-Elmer P400 ICP atomic-emission spectrometer equipped with a high salt nebulizer. The emission lines monitored were 670.781 nm for lithium, 589.592 nm for sodium, 202.030 nm for molybdenum, 194.227 nm for mercury, 220.353 nm for lead, 214.438 nm for cadmium, and 328.068 nm for silver. Calibration curves were constructed using known concentrations of metal salts in each particular aqueous solution studied and were linear in concentration over the range 1.00 to 0.0500 mM. Matrix matching was used for all experiments. For each sample, five readings of the ICP-AES intensity were

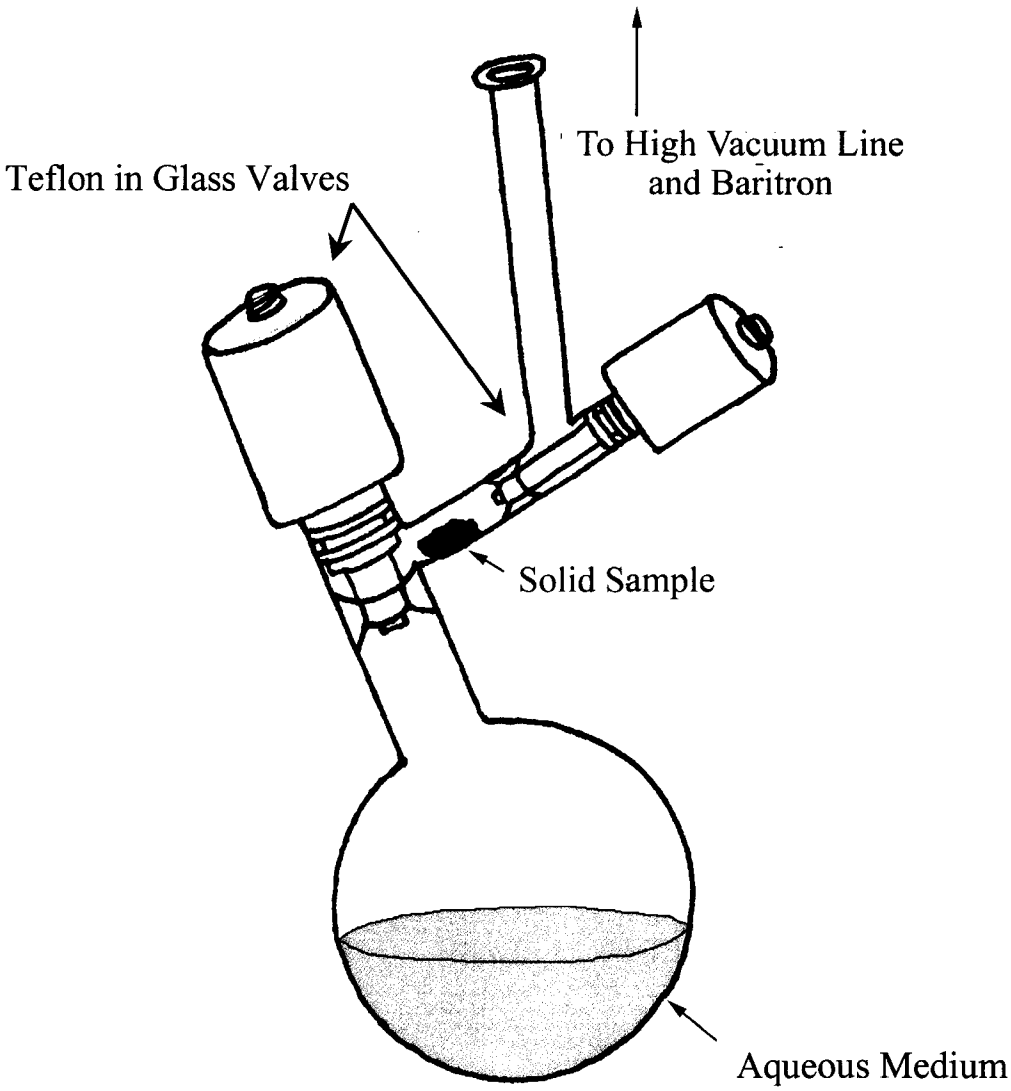

Figure 2.2 Schematic of apparatus used for hydrogen evolution experiments.

recorded and averaged.

Differential scanning calorimetry data was collected on a TA Instruments 2920 Differential Scanning Calorimeter. Powdered samples were sealed in aluminum pans and heated at 10 °C/min under a flow of nitrogen. Thermogravimetric/mass spectroscopic analyses were performed on a TA Instruments 2950 Thermogravimetric Analyzer interfaced with a Balzers Thermostar Mass Spectrometer. The thermal unit was ramped at 10 °C/minute under a constant flow of He carrier gas. Evolved gasses were analyzed using multiple ion detection mode.

Powder X-ray diffraction measurements were recorded with a Philips diffractometer using Cu-Kα radiation. XRD patterns were taken of samples on frosted glass sample holders. XRD patterns of air-sensitive samples were taken by preparing the sample and holder in a nitrogen atmosphere glove box and then placing a piece of transparent tape over the sample. Powder patterns were compared to those in the PDF data base.

Results and Discussion

I. Synthesis and Characterization of New Extractants:
A_xMoS_2 ($A^+ = H^+, Na^+, K^+$; $x < 1.3$)

The exfoliation/flocculation technique was found to be the most effective method for preparing alkali-metal intercalated molybdenum disufide analogs that are stable in aqueous media. Each of the different alkali-metal intercalates were found to behave similarly in terms of structural properties, air stability, thermal stability and reactions with aqueous solution (pH ~ 1 and 5).

The powder diffraction analysis of the four intercalation compounds prior to drying indicated that these compounds have varying degrees of hydration. This is similar to the hydrated form of $Li_{1.3}MoS_2$ that forms upon exposure to air. In the proton intercalated material, as can be seen in Figure 2.3, there are three general stages of hydration that are lost as the material is dried from 12 to 24 hours under dynamic vacuum. The most hydrated form has an interlayer space of 13.1 Å. This is an increase over native MoS_2 (d = 6.14 Å) of approximately 6.96 Å. This material also contains a phase with an interlayer space of 9.4 Å which is 3.26 Å larger than that of native MoS_2. Finally, the most dehydrated form of the material has an interlayer space of 6.24 Å, only slightly larger than that of native MoS_2. In the case of the proton intercalated material, it should be noted that the crystallinity of the material decreases significantly from that of native MoS_2 as the result of the exfoliation and flocculation mechanism.

The sodium and potassium analogs also have varying degrees of hydration, the d-spacings of which can be found in Table 2.1. The most hydrated form of Na_xMoS_2 has an interlayer space of 12.1 Å and is attainable if the compound is filtered in an anaerobic chamber. Upon drying on a Schlenk line overnight, the compound converts to a material with an interlayer spacing of 9.4 Å. The hydration of Na_xMoS_2 is reversible upon exposure to water (under anaerobic conditions), however, when the dry compound is exposed to the laboratory atmosphere, no rehydration takes place.

Assuming that the radius of an octahedral hole in an hexagonally closest-packed system is $0.414r$[23], and the radius, r, of an S^{2-} ion is 1.70 Å[24], then the radius of a hexagonal hole in 1T-MoS_2 is 0.70 Å. The ionic radius of Na^+ (C.N. = 6) is 1.16 Å[24],and should produce a d-spacing increase of ([1.16 Å – 0.70 Å]*2) 0.92 Å. An increase of the interlayer space of ~ 3.3 Å implies that the

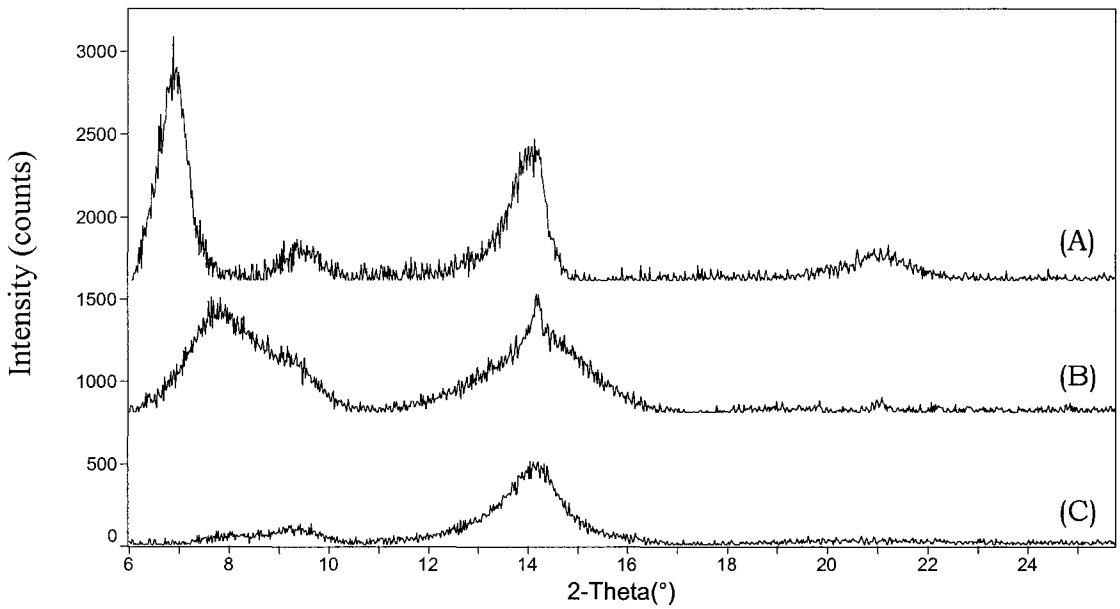

Figure 2.3 Powder X-ray diffraction analysis of H_xMoS_2 with varying degrees of hydration. (A) prior to drying (B) drying for 12 hours under dynamic vacuum (C) drying for 24 hours under dynamic vacuum.

Table 2.1 Interlayer distances for MoS_2 intercalates of varying degrees of hydration.

	Interlayer Distances, d_n (Å)		
Intercalate	d_1	d_2	d_3
H^+	13.1	9.4	6.2
Na^+	12.1	9.4	
K^+	9.3	8.3	

sodium has intercalated in a hydrated form. The interlayer distances found for Na_xMoS_2 correspond well with those previously reported in the literature using other synthetic routes.[25-29] It had been proposed that in $Na_x(H_2O)_yMoS_2$, the sodium cations are hydrated by a bilayer of water molecules surrounding the Na^+ in an octahedral coordination.[20]

Similarly, the interlayer distance of the hydrated $K_x(H_2O)_yMoS_2$ is 9.3 Å and when it is dried under vacuum, the interlayer space decreases to 8.3 Å. Again, the ionic radius of K^+ is 1.52 Å, so the increase in d-spacing should be (2[1.52 Å – 0.70 Å]) 1.64 Å. The actual increase, 2.2 Å was slightly larger than expected for an dehydrated cation. This difference in interlayer space, 0.56 Å, is significantly less than the difference seen in the sodium compound, 2.38 Å. This difference has been attributed to the fact that the potassium cations in $K_x(H_2O)_yMoS_2$ are coordinated by a monolayer of water molecules instead of a bilayer. A depiction of different alkali metal intercalates of MoS_2 with either a monolayer or a bilayer coordination of water, as presented by Weber, can be seen in Figure 2.4.[29]

Aerobic/Thermal Stability

In order to further characterize the partially oxidized materials, their aerobic stability under laboratory conditions (i.e. room temperature and pressure) was monitored as a function of time. The oxidation process in air involved the reduction of atmospheric water to form hydrogen gas. As a result of this reduction, MoS_2^{n-} was oxidized slowly to $[MoS_2]^{0,}$ where the MoS_2 layers are neutral. In addition, the alkali metal cation de-intercalated forming the alkali metal hydroxide, as described in Equation 2.5.

$$A_xMoS_2(s) + H_2O(g) \longrightarrow (x/2)\ H_2(g) + x\ AOH(aq) + MoS_2(s) \qquad (2.5)$$

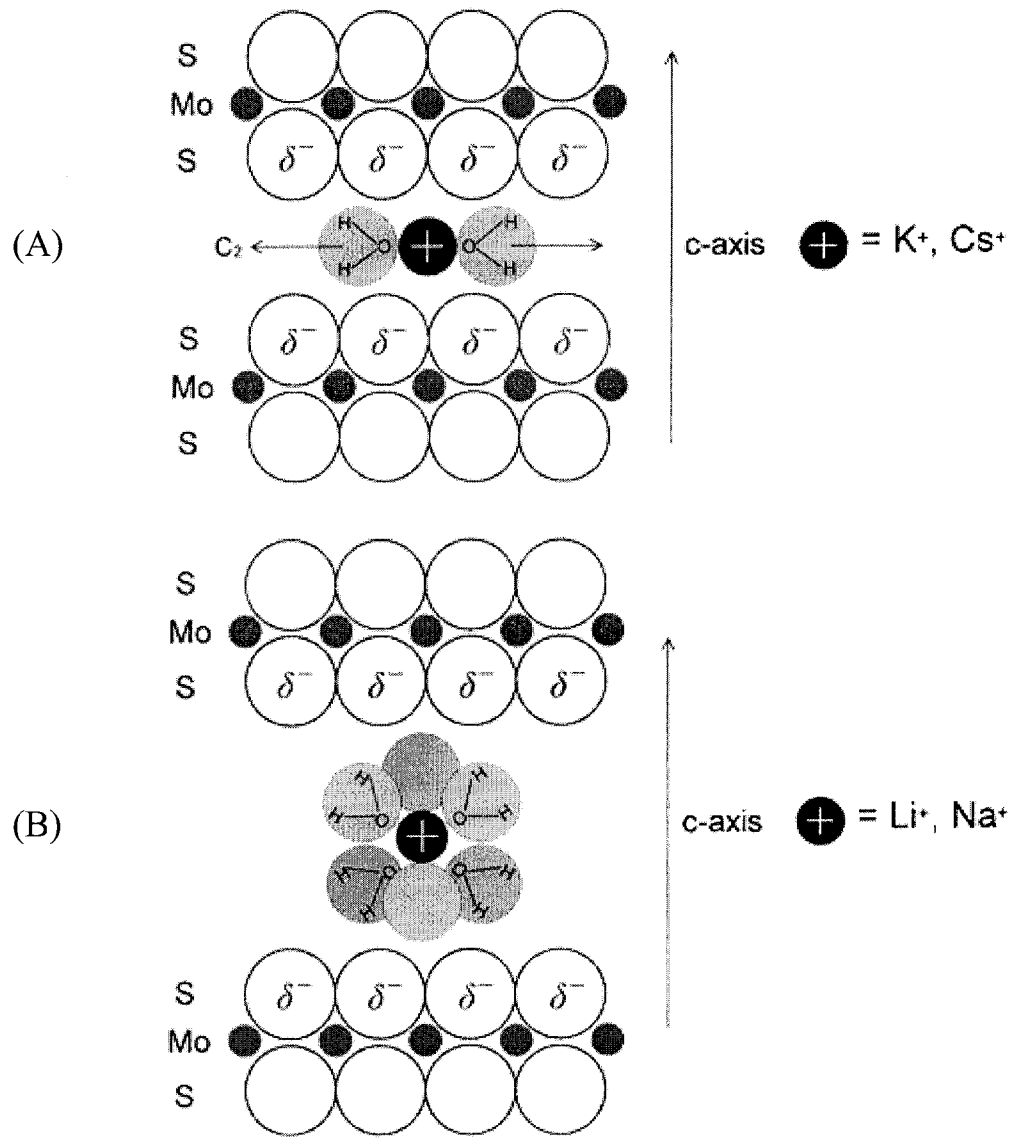

Figure 2.4 Representation of (A) monolayer and (B) bilayer hydration of alkali metal cations in MoS_2. Adapted from 29.

A comparison of the diffraction patterns of A_xMoS_2 exposed to air for different periods of time can be used to monitor the oxidation process. The time dependent X-ray diffraction patterns of a sample of Na_xMoS_2 and K_xMoS_2 exposed to air over time can be seen in Figures 2.5 and 2.6. Over a period of approximately 191 hours, there is complete conversion of Na_xMoS_2 to 2H-MoS_2 and NaOH. The formation of NaOH as a byproduct of the reaction was confirmed by the hygroscopic appearance of the solid (native MoS_2 is hydrophobic) and a basic solution resulting from the washing of the solid with distilled, deionized water. In the case of K_xMoS_2, there was no diffraction evidence for the formation of 2H-MoS_2, however, the compound became amorphous after 88 hours.

Another type of stability that was investigated was thermal stability. When H_xMoS_2, was heated to 500 °C, an exotherm was observed at 103 °C in the thermal scan as seen in Figure 2.7A, prior to the endothermic loss of water. This exotherm is the result of the reduction of $2nH^+$ to $nH_2(g)$ and oxidation of MoS_2^{n-} to MoS_2. A similar behavior was seen with M_xMoS_2 (M = Hg, Pb, Ag...), although the exotherm of the metal loaded materials occurred at higher temperatures.[19] Neither Na_xMoS_2 nor K_xMoS_2 displayed the exothermic 1T to 2H phase transition and internal redox reaction, as shown in Figures 2.7B and 2.7C. In the cases of Na_xMoS_2 and K_xMoS_2, this transition is not present due to the unfavorable reduction potentials of Na^+ and K^+ and improbability of forming Na^0 and K^0. From this, Na_xMoS_2 and K_xMoS_2 were considered to be thermally stable to 500 °C.

Characterization of H_xMoS_2 using Hydrogen Gas (H_2) Evolution

Hydrogen gas evolution experiments were used to obtain information about the degree of oxidation of the MoS_2^{n-} layers. Based on the amount of

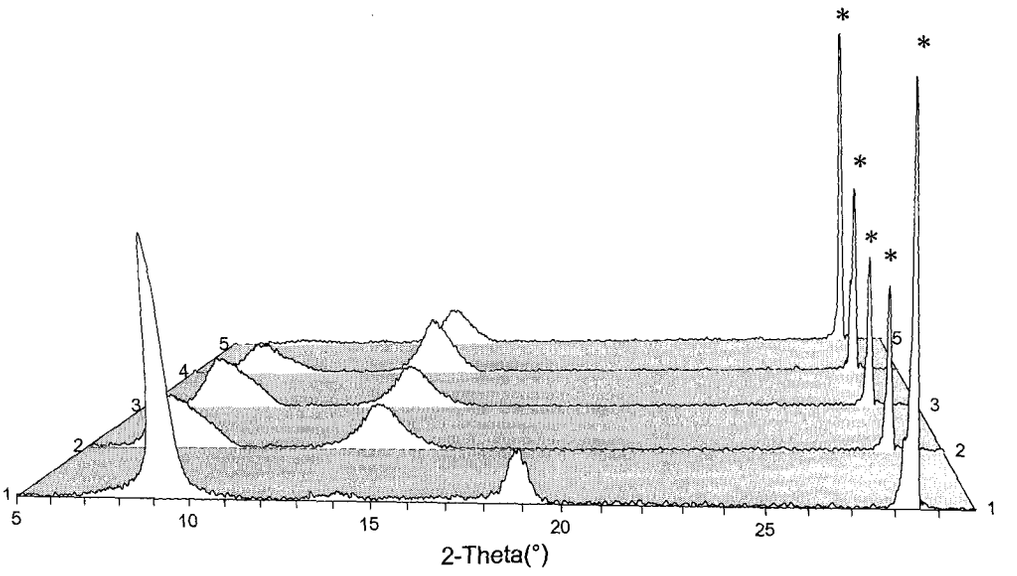

Figure 2.5 Aerobic Decomposition of Na_xMoS_2 Over Time (1) 0 hrs. (2) 24 hrs. (3) 95 hrs. (4) 146 hrs. (5) 191 hrs. Peaks denoted with an asterisk (*) represent an added Si standard.

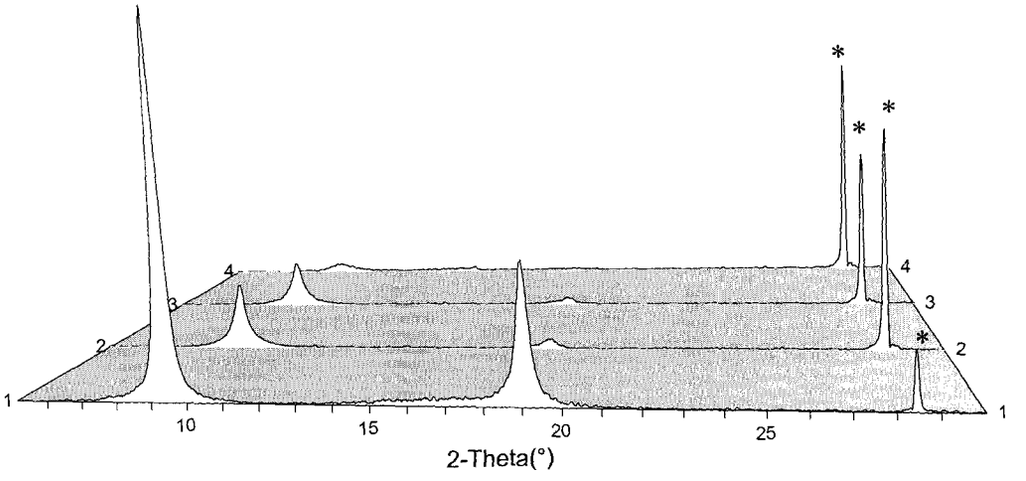

Figure 2.6 Aerobic Decomposition of K_xMoS_2 Over Time (1) 0 hrs. (2) 22 hrs. (3) 48 hrs. (4) 88 hrs. Peaks denoted with an asterisk (*) represent an added Si standard.

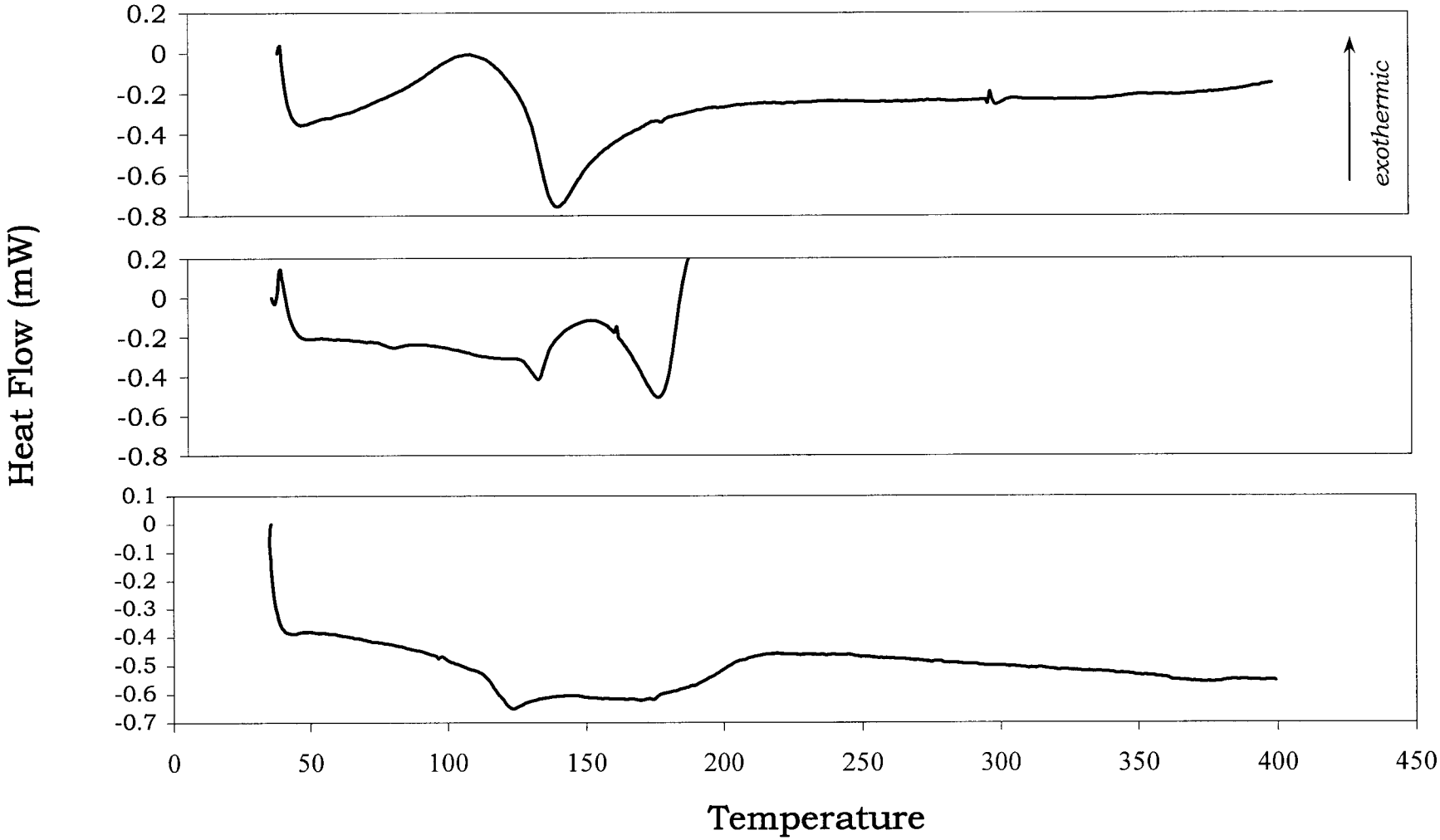

Figure 2.7 Differential scanning calorimetry analysis of (A) H_xMoS_2 (B) Na_xMoS_2 (C) K_xMoS_2.

hydrogen gas evolved, the residual charge on the layers, *n*, is obtained from the relationship shown in Equation 2.6 where *a* represents the number of moles of $Li_{1.3}MoS_2$ used in the experiment and *b* represents the number of moles of H_2(g) generated in the experiment.

$$n = (1.3a - 2b)/a \tag{2.6}$$

Equation 2.6 can be rearranged to obtain Equation 2.7 that relates the number of moles of hydrogen gas evolved (*b*) to the amount of $Li_{1.3}MoS_2$ used (*a*). The slope of the line formed when these two variables are graphically compared is related to the residual charge on the MoS_2^{n-} layers.

$$b = [(1.3 - n)/2]a \tag{2.7}$$

Figure 2.8 shows a series of experiments designed to calculate *n* by examining the amount of H_2(g) evolved (*b*) as a function of $Li_{1.3}MoS_2$ used (*a*). The slope of the line was found to be 0.246 and the residual charge on MoS_2^{n-} was calculated to be 0.808.

The charge remaining on the MoS_2^{n-} layers can alternatively be determined through mass balance experiments in combination with hydrogen evolution data. Mass balance was completed by monitoring the concentration of lithium cations present in the initial and final reaction solutions (using ICP-AES), in combination with monitoring the initial and final pH of the solution (using a strong acid/strong base titration).

Mass balance studies performed during the synthesis of H_xMoS_2 revealed that in a typical synthesis, both protons and lithium cations were incorporated into the flocculated solid and that H_xMoS_2 is an over simplified representation

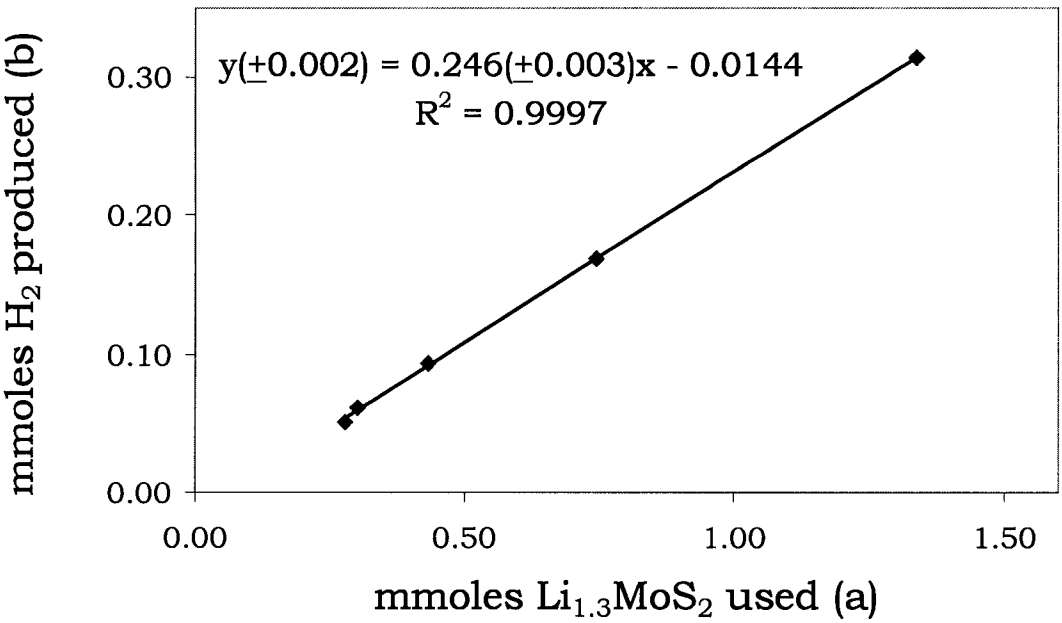

Figure 2.8 A comparison of the amount of hydrogen gas evolved as a function of $Li_{1.3}MoS_2$ used.

of the true stoichiometry of this material. The ratio of H^+ and Li^+ in the product was found to be a function of the ratio of H^+/Li^+ present in the initial reaction solution. For example, when the initial ratio of H^+/Li^+ was one to one, the final product had a stoichiometry of $H_{0.56}Li_{0.19}MoS_2$. When the ratio was increased to five to one, the final product had a stoichiometry of $H_{1.00}Li_{0.09}MoS_2$. The slope analysis method and cation concentration determination of *n*– were found to agree to within $\pm$ 0.1. These experiments provide evidence that there is residual charge on the MoS_2 layers after exfoliation and flocculation in acid and that depending on reaction conditions, the cations included between the $MoS_2^{0.8-}$ layers are a combination of H^+ and Li^+. To this point, no other literature report had shown this.

Synthesis using other methods

The solids that had been exfoliated and flocculated in water, irrespective of the cation distribution, were found to be stable in aqueous solution under anaerobic conditions (i.e. no oxidation, H_2 production, exfoliation). Therefore, other synthetic techniques were attempted to directly prepare a material with the stoichiometry $A_{0.8}MoS_2$. One approach was lowering the number of equivalents of *n*–butyllithium per Mo used in the synthesis of the parent material. This extractant was prepared using the reductive intercalation reaction described previously for the synthesis of $Li_{1.3}MoS_2$, with a ratio of 0.80 *n*-butyllthium to one MoS_2. A portion of the product was digested in an aliquot of *aqua regia* with a known volume. Analysis of lithium and molybdenum in the digest using ICP-AES confirmed that the final product had a stoichiometry of $Li_{0.74}MoS_2$. With a reduced lithium stoichiometry, this material was not expected to produce hydrogen upon contact with aqueous solution. In fact, however, hydrogen evolution experiments and ICP analysis combined to suggest

Equation 2.8 for the reaction between $Li_{0.74}MoS_2$ and aqueous nitric acid:

$$Li_{0.74}MoS_2\ (s) + 0.71\ H_3O^+\ (aq) \longrightarrow$$
$$0.12\ H_2\ (g) + Li_{0.03}H_{0.47}MoS_2\ (s) + 0.71\ Li^+\ (aq) + 0.71\ H_2O \qquad (2.8)$$

This experiment, in addition to X-ray powder diffraction data that showed two distinct interlayer spacings of 6.41 Å ($Li_{1.3}MoS_2$) and 6.15 Å (2H-MoS_2)[19] was further evidence that the $Li_{0.74}MoS_2$ was actually a mixture of phases consisting of 2H-MoS_2 and $Li_{1.3}MoS_2$. From this it appeared that the synthesis of $Li_{0.8}MoS_2$, using a stoichiometric reaction of butyllithium and MoS_2 with a homogeneous distribution of lithium ions, was not possible. One can conclude therefore that Li_xMoS_2, where $x < 1.3$, cannot be prepared using an *n*-butyllithium reaction.

Using a different approach, from literature reports by Schöllhorn, it was know that K_xMoS_2 was synthesized as an intermediate material during the synthesis of 1T-MoS_2.[30] This solid state reaction involved the reduction of K_2MoO_4 with H_2S(g) and H_2(g) as summarized by Equation 2.9.

$$K_2MoO_4 \xrightarrow[400^oC,\ 8\ h.]{H_2S} K_zMoS_4 \xrightarrow[800^oC,\ 72\ h.]{20\%H_2/80\%N_2} KMoS_2 \xrightarrow[r.t.,\ 1h.]{CH_3CN,\ I_2} 1T\text{-}MoS_2 \qquad (2.9)$$

In a two hour extraction, using a five to one ratio of $KMoS_2$ and Hg^{2+}(aq) a material with a final Hg:Mo ratio of 0.19 was formed. Bubbles observed in the reaction flask during the extraction process, however, indicated that H_2(g) was formed as a byproduct of the reaction. Because of this hydrogen evolution, the charge on the MoS_2^{n-} layers must be greater that 0.8. Because of this, K_xMoS_2 does not appear to have any benefits as an extractant over $Li_{1.3}MoS_2$.

II. Metal Ion Extractions with A_xMoS_2

The extraction capability of the less-reduced ion exchange materials were investigated to compare their efficiency to that of $Li_{1.3}MoS_2$. Important factors considered included overall capacity, extraction time and capacity under aerobic vs. anaerobic conditions. No exfoliation was visually apparent during extractions with any of the materials to be discussed. This was confirmed by hydrogen evolution experiments in which no detectable amount of $H_2(g)$ was evolved upon contact of the solid with water. This class of compounds therefore satisfies the requirement that no hydrogen gas be evolved during the metal ion removal step of the extraction cycle.

H_xMoS_2

A comparison of the final stoichiometries of loaded extractants formed during extractions with various metal cations is shown in Table 2.2. From this comparison, it is obvious that H_xMoS_2 is a less-effective extractant for $Hg^{2+}(aq)$, $Pb^{2+}(aq)$, and $Cd^{2+}(aq)$ than the parent compound, $Li_{1.3}MoS_2$. In the case of $Hg^{2+}(aq)$, only half as much mercury is removed from solution with H_xMoS_2 over an equivalent extraction time as compared to $Li_{1.3}MoS_2$. Actually, a material with a stoichiometry of $Hg_{0.17}MoS_2$ can be obtained from a similar solution given a longer contact time (6 hours). In the cases of $Pb^{2+}(aq)$ and $Cd^{2+}(aq)$ however, no appreciable amount of metal was extracted from solution, even after a longer contact time.

The decreased capacity of H_xMoS_2 compared to $Li_{1.3}MoS_2$ in a two hour extraction is probably due to a barrier to ion exchange introduced when exfoliation is no longer a part of the ion exchange mechanism. Exfoliation, during the extraction process with $Li_{1.3}MoS_2$ produced a high surface area

Table 2.2 Extraction analysis of A_xMoS_2 for various cations.

A_xMoS_2	M^{n+} (aq)	Initial Ratio Extr/M^{n+}	pH	Time, hours	M_yMoS_2 recovered	$([M^{n+}(aq)]_i - [M^{n+}(aq)]_f)/[M^{n+}(aq)]_i$
$Li_{1.3}MoS_2$	Hg^{2+}	5	1	2	$Hg_{0.20}MoS_2$	1.00(1)
	Pb^{2+}	5	1	2	$Pb_{0.15}MoS_2$	0.75(1)
	Cd^{2+}	5	1	2	$Cd_{0.08}MoS_2$	0.41(1)
	Ag^{+}	5	1	2	$Ag_{0.20}MoS_2$	1.00(1)
H_xMoS_2	Hg^{2+}	5	1	2	$Hg_{0.09}MoS_2$	0.52(6)
	Pb^{2+}	5	1	4	$Pb_{0.01}MoS_2$	0.046(1)
	Pb^{2+}	5	5	4	$Pb_{0.02}MoS_2$	0.12(1)
	Cd^{2+}	5	5	4	$Cd_{0.01}MoS_2$	0.031(1)

Table 2.2 (cont.)

A_xMoS_2	M^{n+} (aq)	Initial Ratio Extr/M^{n+}	pH	Time, hours	M_yMoS_2 recovered	$([M^{n+}(aq)]_i - [M^{n+}(aq)]_f)/[M^{n+}(aq)]_i$
Na_xMoS_2	Hg^{2+}	5	5	4	$Hg_{0.20}MoS_2$	1.00(1)
	Pb^{2+}	5	1	2	$Pb_{0.15}MoS_2$	0.75(1)
	Cd^{2+}	5	5	4	$Cd_{0.17}MoS_2$	0.85(7)
	Ag^{+}	5	5	4	$Ag_{0.20}MoS_2$	1.00(1)
K_xMoS_2	Pb^{2+}	5	5	4	$Pb_{0.14}MoS_2$	0.70(5)
	Cd^{2+}	5	5	4	$Cd_{0.14}MoS_2$	0.75(4)

colloid that increased the contact between the extractant and cations in solution. For this reason, the extraction of metal ions using $Li_{1.3}MoS_2$ was complete in less than ten minutes.[19] In the absence of exfoliation, however, a slower extraction rate was expected, as ions must diffuse into and out of a structurally limiting material. In addition, the only points of contact between the solid and solution were edges of the material, rather than the surface of a layer. Therefore, the surface area contact was greatly reduced.

The reduction in the rate of ion exchange is examined more closely in Figure 2.9. By monitoring the ion exchange reaction as a function of time, the maximum loading of H_xMoS_2 with Hg^{2+} is actually found to be $Hg_{0.17}MoS_2$, after a six hour contact time. This loading is ultimately comparable to that obtained using $Li_{1.3}MoS_2$ however the slower rate could be considered a potential drawback when evaluating the overall extraction system. Given that metal ion extraction with H_xMoS_2 is slower than with $Li_{1.3}MoS_2$, stirring the solution during extraction is critical in order to achieve good contact between the extractant and heavy metal ions. In experiments in which the extraction mixture was not stirred, maximum mercury loading after four hours was $Hg_{0.05}MoS_2$. This further reduction in extraction rate, when the system is not agitated is important when considering the type of extraction process that will be used in the remediation project. For example, a permeable membrane extraction system will not allow for the stirring of the extractant and will therefore depend on the flow rate of the solution through the solid barrier.

The equilibrium governing this ion exchange reaction will also affect the final loading stoichiometry. This equilibrium is shown in Equation 2.10.

$$H_{0.8}MoS_2(s) + x\ M^{n+}(aq) \rightleftharpoons M_xH_{0.8-nx}MoS_2(s) + nx\ H^+(aq) \qquad (2.10)$$

where $0 < x \leq (0.8/n)$

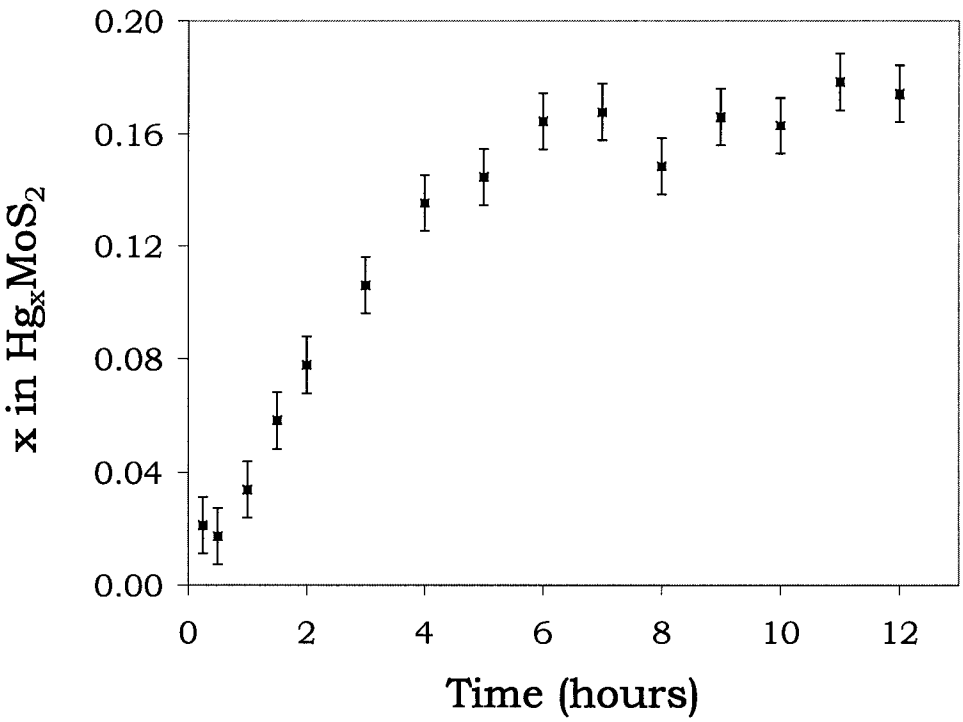

Figure 2.9 Hg^{2+} extraction as a function of time.

At a low pH, metal ion extraction might be low due to the large concentration of protons in solution, pushing the equilibrium to the left. This might also be one explanation for the inability of H_xMoS_2 to extract $Pb^{2+}(aq)$ from a solution at a pH of one. In fact, however, when the extraction was performed in distilled, deionized water (pH ~ 5), the amount of $Pb^{2+}(aq)$ extracted from solution remained negligible. The same was true in the case of $Cd^{2+}(aq)$. Therefore, the capacity of $H_{0.78}MoS_2$ for borderline soft Lewis acids is not significantly increased by the added driving force of a less acidic solution.

The capacity of H_xMoS_2 decreased further under aerobic conditions. Since the MoS_2^{n-} is in a partially reduced state, it is expectedly prone to oxidation by atmospheric oxygen and water. Mercury loading after four hours in an aerobic extraction was $Hg_{0.13}MoS_2$. Exposure of the material to air for 24 hours before contact with the metal ion solution reduced the maximum loading stoichiometry of a four hour extraction to $Hg_{0.08}MoS_2$. Again, this characterization and study of the degradation is important if the extractant is to be used in a permeable barrier type of extraction system that is designed to slowly extract metal ion contaminants as ground water flows through the barrier.

Considering the final stoichiometries for a variety of metal cations, compounded by slow extraction rates and the aerobic decomposition over time, it is obvious that H_xMoS_2 is not as effective an ion exchange material as $Li_{1.3}MoS_2$. This is mostly due to the fact that it does not produce a high surface area colloid and ion movement through the solid (ion exchange) is slow. In the case of some metals, such as $Cd^{2+}(aq)$ and $Pb^{2+}(aq)$, ion exchange is insignificant.

Na_xMoS_2 and K_xMoS_2

Na_xMoS_2 and K_xMoS_2 were examined with the hypothesis that a material with a larger interlayer gallery would better fit the requirements for an ideal extractant. If the hypothesis were true that metal ion removal with H_xMoS_2 was slow due to a kinetic barrier to ion exchange, then incorporating a larger cation in the interlayer gallery should facilitate ion exchange. Furthermore, because both sodium and potassium are present in a hydrated form, the interlayer spaces of Na_xMoS_2 and K_xMoS_2 are considerably larger.

The use of an extractant such as Na_xMoS_2 could also be considered an advantage over H_xMoS_2 in that the secondary waste stream produced would not be acidified by the extraction process. Instead, innocuous sodium cations would act as the exchangeable cations that are substituted for heavy metals.

There are several observations that can be made about the extraction behavior of Na_xMoS_2 and K_xMoS_2. The first is that both Na_xMoS_2 and K_xMoS_2 extract all four of the metal cations investigated; $Hg^{2+}(aq)$, $Pb^{2+}(aq)$, $Cd^{2+}(aq)$ and $Ag^{+}(aq)$. In a comparison of all four extractants, $Li_{1.3}MoS_2$, Na_xMoS_2 and K_xMoS_2 remove more metal ion relative to H_xMoS_2. In the case of $Hg^{2+}(aq)$, $H_{0.78}MoS_2$ is only 75% as efficient as the three other extractants. More importantly, $H_{0.78}MoS_2$ will not extract $Pb^{2+}(aq)$ nor $Cd^{2+}(aq)$ from solution.

Interestingly, Na_xMoS_2 and K_xMoS_2 exchanged more $Cd^{2+}(aq)$ than $Li_{1.3}MoS_2$, extracting almost twice as much metal ion from solution. The $Cd^{2+}(aq)$ extraction with $Li_{1.3}MoS_2$ was done in 0.1M HNO_3 whereas the Na_xMoS_2 and K_xMoS_2 extractions were done in distilled, deionized water. This was indicative of a competition reaction between $Cd^{2+}(aq)$ and $H^{+}(aq)$ for exchangeable equivalents in the initial extractant. In the absence of protons, Cd^{2+} had access to all of the ion exchange sites and the potential exchange is non-competitive.

Na_xMoS_2 removed 85% - 100% of the metal ion from solution when a 5:1 extractant to metal ion ratio was used. When a 1:1 extractant to metal ion ratio was used, a stoichiometry of $Ag_{0.49}MoS_2$ was obtained for both Na_xMoS_2 and K_xMoS_2.[31] When a 1:1 extractant to metal ion ratio is used in a $Pb^{2+}(aq)$ extraction, the maximum stoichiometry was the same as reported when a 5:1 ratio was used. This indicated that the products obtained in a reaction between $Pb^{2+}(aq)$ and $Li_{1.3}MoS_2$, Na_xMoS_2 and K_xMoS_2 were thermodynamic products. This stoichiometry is still less than the theoretical maximum of 0.40 if all of the sodium were exchanged for $M^{2+}(aq)$ ions.

Contrary to the limited rate of ion exchange present with H_xMoS_2, the rates of exchange of Na_xMoS_2 and K_xMoS_2 are comparable to that of the exfoliated $Li_{1.3}MoS_2$ system. Figures 2.10 and 2.11 show the loading stoichiometries of Pb_xMoS_2 as a function of time obtained from the contact of these two ion exchange materials with a solution of $Pb(NO_3)_2$ in water under anaerobic conditions. The one minute extractions were filtered immediately after the solution was contacted with the extractant and the solution had been shaken for 10-15 seconds (no stirring was involved). This included the amount of time that the solution took to completely filter through the frit, in most cases amounting to about thirty seconds.

It can be seen from these experiments that the extraction of $Pb^{2+}(aq)$ was faster than the mercury extractions previously described for H_xMoS_2. In the case of Na_xMoS_2, the extraction is complete within ten minutes. This is comparable to the extraction time reported for $Li_{1.3}MoS_2$, so, although it was originally believed that the ion exchange mechanism without exfoliation would be a drawback for these types of extractants, since the interlayer space is sufficiently large, there is no kinetic barrier to ion exchange or metal ion extraction. The reported stoichiometries were stable in water for at least

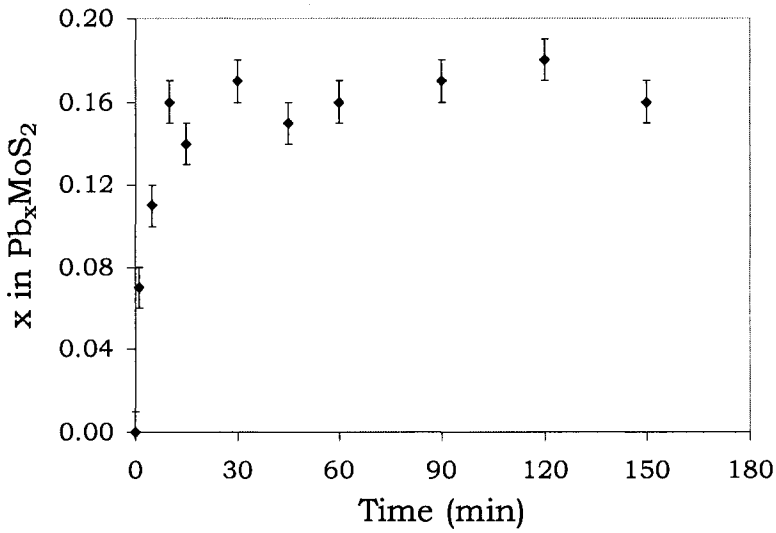

Figure 2.10 Extraction of Pb^{2+} by Na_xMoS_2 as a function of time.

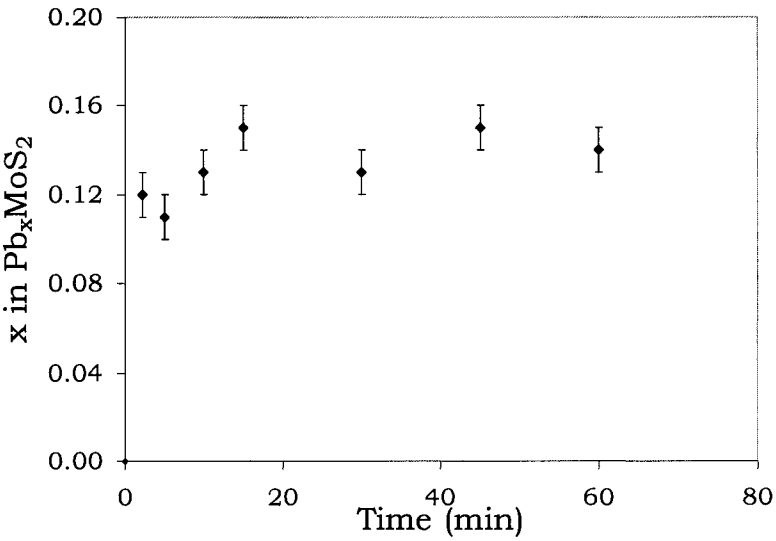

Figure 2.11 Extraction of Pb^{2+} by K_xMoS_2 as a function of time.

24 hours.

With respect to long term stability, it was shown in the previous section that H_xMoS_2 becomes a less effective extractant over time under aerobic conditions. In the case of Na_xMoS_2 and K_xMoS_2, a similar oxidation occurred. Again, the structural transition of the material was monitored as a function of time. Figures 2.12 and 2.13 show the powder diffraction analysis of two aerobic $Pb^{2+}(aq)$ extractions with Na_xMoS_2 and K_xMoS_2 after various exposure times to air. Clearly, these materials consist of two phases; one phase with an interlayer space of 7.2 Å (2θ = 12.2), corresponding to Pb_xMoS_2, and a second phase with an interlayer space of 6.3 Å (2θ = 14.0), corresponding to oxidized, 2H-MoS_2. With increased aerobic exposure times, the relative area of the former peak increases, indicating increased oxidation of the material. In Figure 2.14, however it can be seen that this oxidation leads to no appreciable decrease in the loading of the material.

One troubling aspect relating to the 'decomposition' or relative ineffectiveness of these materials, however, is their behavior in highly acidic solution. In the introduction to this chapter, the concept of the selectivity of MoS_2 for protons over alkali metal cations was suggested and discussed. By eliminating protons from the reaction mixture during the synthesis of Na_xMoS_2, sodium cations were included in the flocculated material. From these synthetic reactions, the understanding of the greater affinity of MoS_2^{n-} for protons than for sodium cations in solution indicated that in highly acidic solutions, Na_xMoS_2 would convert to H_xMoS_2 over time. Because of this, some of the capacity that the initial extractant, Na_xMoS_2, had for metal cations such as $Pb^{2+}(aq)$ and $Cd^{2+}(aq)$ (that are known not to be extracted by H_xMoS_2) would be lost if the extraction were performed under acidic conditions. One experiment

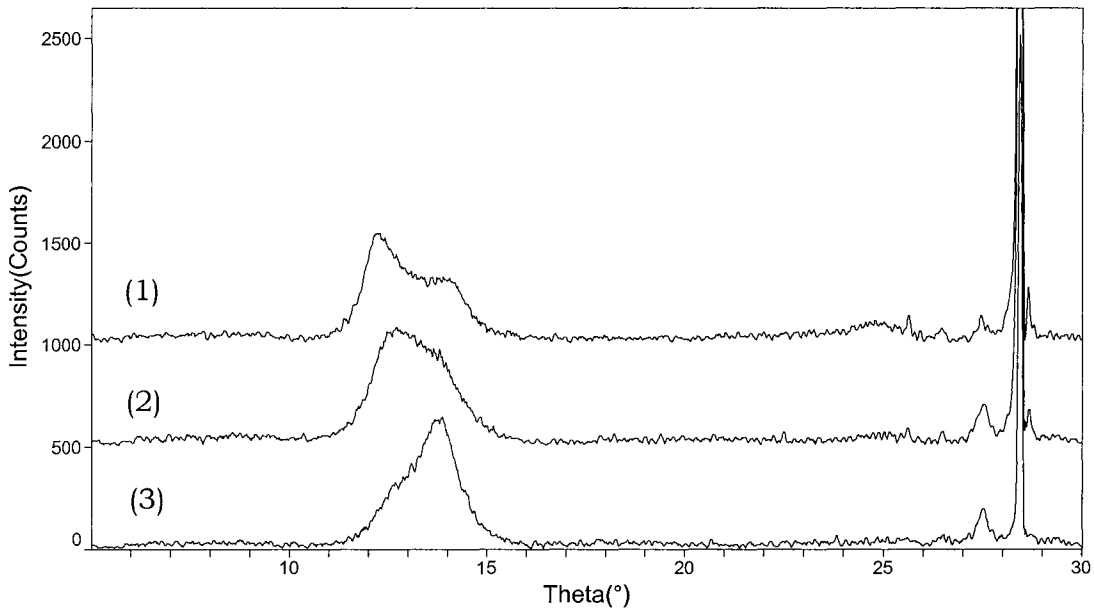

Figure 2.12 Aerobic extractions of Pb^{2+} with Na_xMoS_2 (1) 0 hrs. (2) 24 hrs. (3) 96 hrs. The peak at 28.4 is due to the reflection of an internal standard, Si.

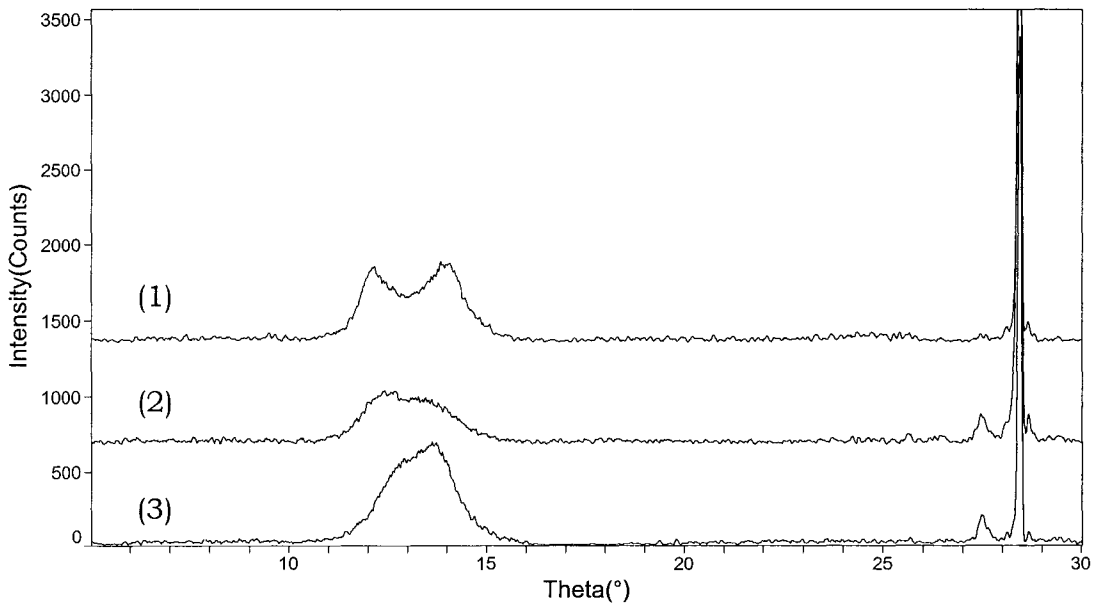

Figure 2.13 Aerobic extractions of Pb^{2+} with K_xMoS_2 (1) 0 hrs. (2) 24 hrs. (3) 96 hrs. The peak at 28.4 is due to the reflection of the internal standard, Si.

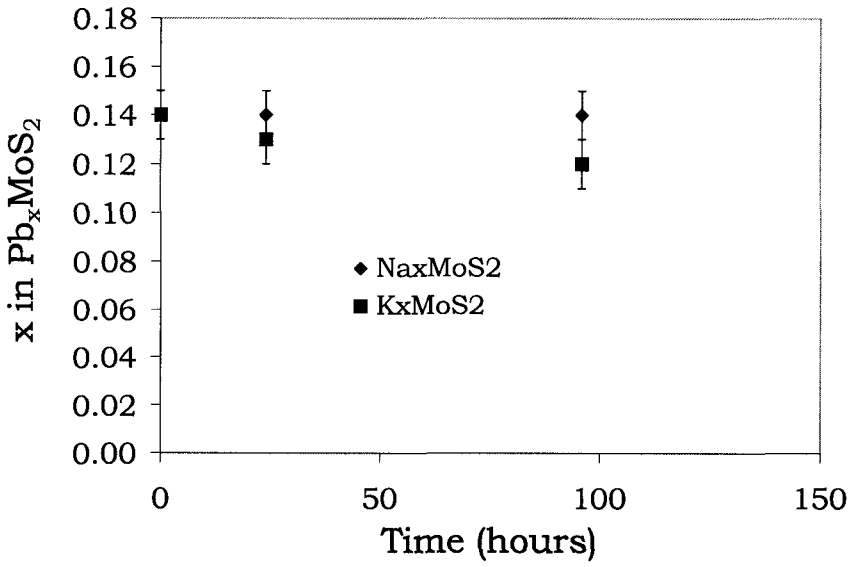

Figure 2.14 Pb^{2+} extraction (aerobic) as a function of time.

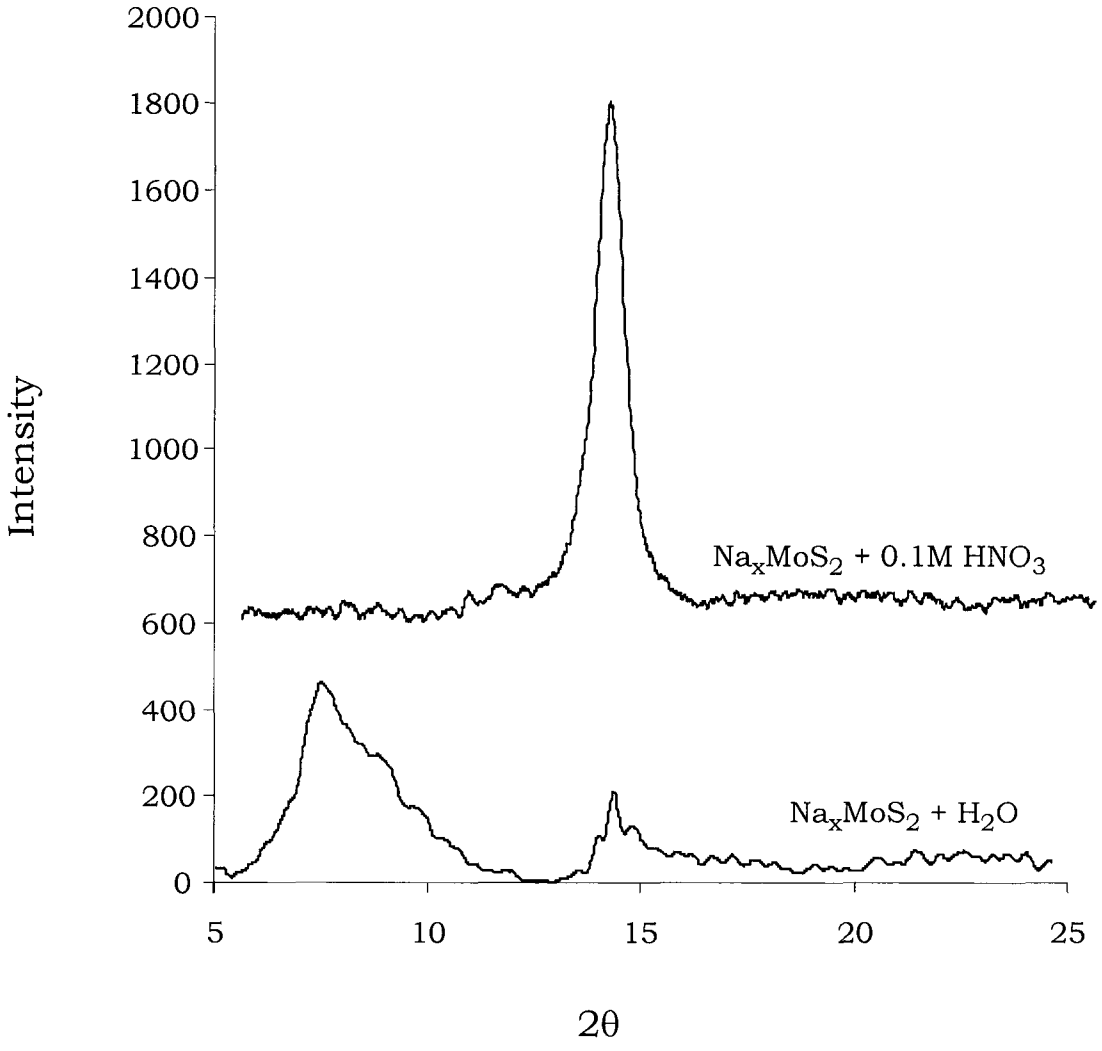

Figure 2.15 X-ray diffraction pattern monitoring the degradation of Na_xMoS_2 in 0.1M HNO_3 and H_2O.

that showed the preference of MoS_2^{n-} for protons, is the reaction between Na_xMoS_2 and an acidic solution (0.1M HNO_3). According to the powder X-ray diffraction analysis shown in Figure 2.15, sodium was completely replaced by H^+ after a four hour contact even though it was shown to be relatively stable in distilled, deionized water.

This preference, and the ion exchange equilibrium was also apparent when the extraction capacity of Na_xMoS_2 for $Pb^{2+}(aq)$ was considered as a function of the initial pH of the solution (adjusted by the addition of an appropriate volume 0.1M HNO_3), seen in Figure 2.16. This decrease in capacity in increasingly acidic waste streams indicated that Na_xMoS_2 will become a less effective extractant than $Li_{1.3}MoS_2$ when the pH of the waste stream is low. This is contrary to what was discovered with $Li_{1.3}MoS_2$, which works more effectively at lower pH's because the high concentration of protons help to neutralize the $OH^-(aq)$ formed as a byproduct of the reduction of water. In neutral pH, this $OH^-(aq)$ production decreases the flocculation of the layers due to increased electrostatic repulsion of negative species in solution and renders $Li_{1.3}MoS_2$ a relatively ineffective extractant.[19]

Interestingly, this behavior is not seen when a sample of Pb_xMoS_2 is placed in a solution of 0.1M KNO_3, as shown in Figure 2.17. Unlike in the case with a high concentration of protons, potassium cations did not significantly replace the lead cations in the solid. This indicated that at neutral pH's the metal ion loaded extractant is stable to the intercalation of hard metal cations.

Conclusions

The research presented in this chapter has demonstrated that ion exchange materials with the general formula A_xMoS_2 are effective extractants

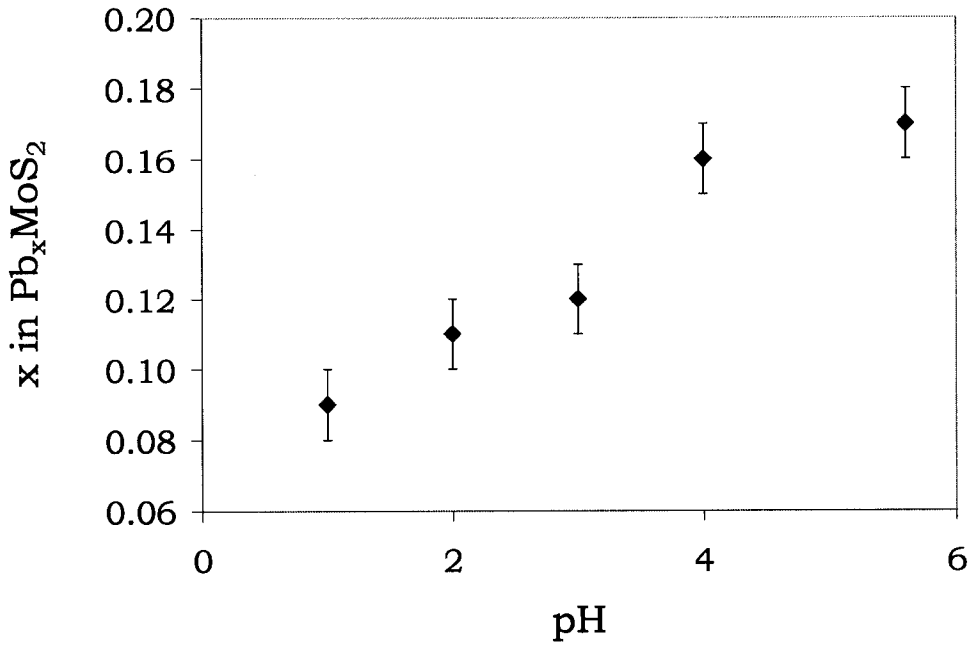

Figure 2.16 Extraction of Pb^{2+} by Na_xMoS_2 as a function of pH.

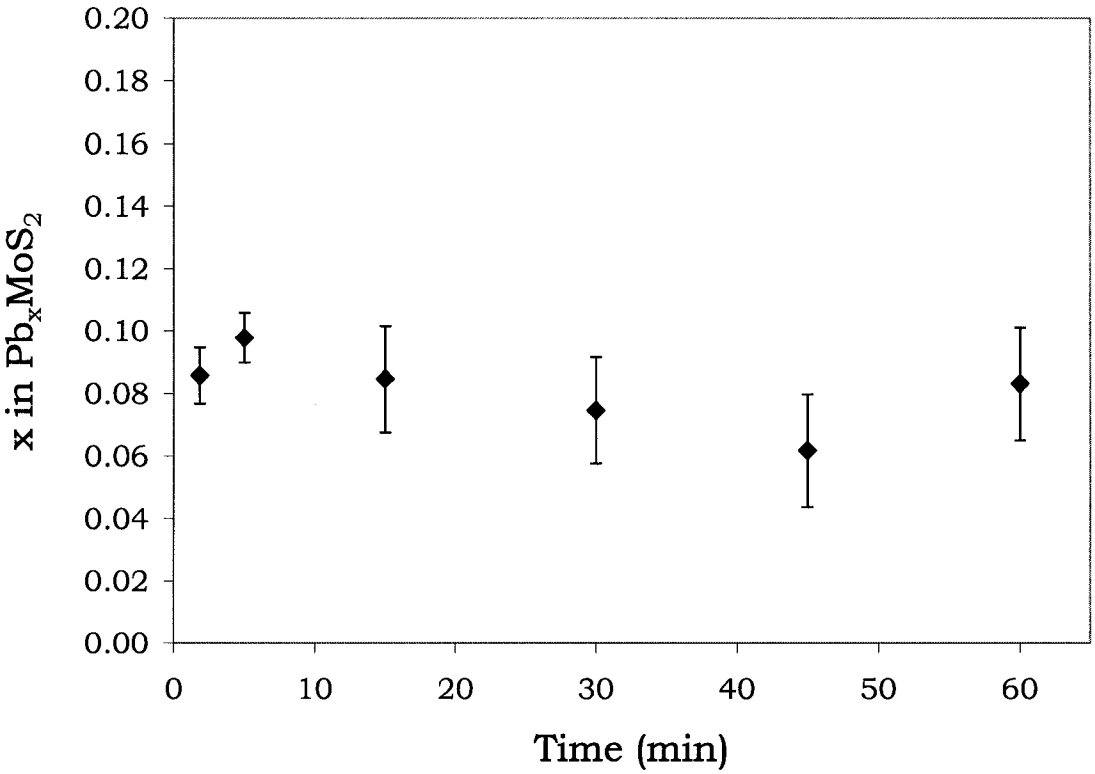

Figure 2.17 Decomposition of Pb_xMoS_2 in 0.1M KNO_3 over time.

for the removal of soft heavy metal cations from aqueous solution. It has been suggested that metal ion removal with $Li_{1.3}MoS_2$ is an effective, selective and recyclable system. However, the mechanism of cation extraction with this material is intimately tied to an exfoliation/flocculation mechanism involving the generation of hydrogen gas during the metal ion extraction step of the cycle.

One of the goals of this research was to remove the production of hydrogen gas from the extraction step, where it is most likely to pose safety concerns and increased cost in an actual remediation situation. In fact, no hydrogen gas was detected when the above-mentioned ion exchange materials were contacted with aqueous solutions containing contaminant metal cations. Therefore, ion exchange was limited to the diffusion of cations into and out of the solid. This mechanism was shown to be a disadvantage for the extractant H_xMoS_2, where the lack of surface area contact with the solution and a kinetic barrier to ion exchange became significant.

In the case of the extractants Na_xMoS_2 and K_xMoS_2, however, with the added advantage of an interlayer space that is initially 2-3 Å larger than that of H_xMoS_2, the kinetic barrier was eliminated. The extraction process was complete on a time frame similar to that of $Li_{1.3}MoS_2$. For this reason, Na_xMoS_2 and K_xMoS_2 have proven to be more effective extractants for the removal of heavy metal ions from aqueous solution. Neither of these extractants produce hydrogen gas as a byproduct of the extraction process, however both remove soft metal cations with final metal loadings similar to those seen with $Li_{1.3}MoS_2$. Other factors that were considered in each of these systems included their eventual degradation over time due to the eventual oxidation of the MoS_2^{n-} layers to neutral MoS_2 by atmospheric water. In addition, because of the affinity of the MoS_2^{n-} layers for protons, the capacity of these materials for metal cations decreased with increasing acidity, which may

be a concern in an actual remediation situation. Ultimately, the real advantage of these modified, less reduced systems lies in the relative ease of manipulation of the solids in a laboratory atmosphere as compared with $Li_{1.3}MoS_2$.

References and Notes

1. Cotton, F.A., et al. *Advanced Inorganic Chemistry,* Sixth Edition; John Wiley and Sons, Inc.: New York, 1999.
2. This distance refers to the distance in the 001 direction perpendicular to planes formed by molybdenum atoms in adjacent layers of MoS_2. In Figure 2.1A, this refers to the distance between the planes labeled *b* and *a*. In Figure 2.1B, this refers to the distance between the two planes labeled *b*. This value can also correspond to the distance between planes of complimentary sulfur atoms of adjacent layers. For example, the distance between plane *A* of the top layer and plane *A* of the bottom layer in Figure 2.1B.
3. Dines, M.B. *Mat. Res. Bull.* **1975**, *10*, 287-292.
4. Py, M.A.; Haering, R.R. *Can. J. Phys.* **1983,** *61,* 76.
5. Joensen, P. et. al. *Mat. Res. Bull.* **1986**, *21*, 457-461.
6. Gee, M.A., et al. *Mat. Res. Bull* **1986**, *21*, 543-549.
7. Originally, it was believed that metallic lithium between the MoS_2 layers of $LiMoS_2$ was responsible for the reduction of water. From this it is implied that even the layers in $LiMoS_2$ are neutral.
8. Divigalpitiya, W.M.R., et al. *Science* **1989,** *246,* 369-371.
9. Danot, M., et al. *Mat. Res. Bull.* **1994,** *29,* 833.
10. Golub, A.S., et al. *Mendeleev Commun.* **1993,** 199-200.
11. Golub, A.S., et al. *Russ. Chem. Bull.* **2001,** *50,* 2293-2303.
12. Heising, J.; Kanatzidis, M.G. *J. Am. Chem. Soc.* **1999,** *121,* 11720-11732.
13. Miremadi, B.K.; Cowan, T.; Morrison, S.R. *J. Appl. Phys.* **1991,** *69,* 6373-6378.
14. Joensen, P., et al. *J. Phys. C* **1987,** *20,* 4043-4053.

15. Yang, D.; Frindt, R.F. *Mol. Cryst. Liq. Cryst.* **1994,** *244,* 355-360.

16. Tsai, H.-L., et al. *Chem. Mater.* **1997,** *9,* 879-882.

17. Heising, J.; Kanatzidis, M.G. *J. Am. Chem. Soc.* **1999,** *121,* 638-643.

18. Gash, A.E., et al. *Environmental Science and Technology* **1998**, *32,* 1007-1012.

19. Gash, A.E., *Lithium Intercalated Transition-Metal Chalcogenides as Redox-Recyclable Extractants and Synthesis and Characterization of Group IVB Metal Bis(hydrogen monothiophosphate) Compounds*, Colorado State University, Fort Collins, CO., Ph.D. Dissertation, Fall 1999.

20. The existence of proton intercalated molybdenum disulfide was initially postulated by Schollhorn, however no direct evidence or stoichiometry for this compound was ever published.

21. Shriver, D.F.; Drezdzon M.A. *The Manipulation of Air Sensitive Compounds*; 2nd Edition; Wiley-Interscience: New York, 1986.

22. Murphy, D.W., et al. *Inorganic Chemistry* **1976**, *15,* 17-21.

23. Shriver, D.F.; Atkins, P.; Langford, C.H. *Inorganic Chemistry.* 2nd Edition; W.H. Freeman and Co.: New York, 1994,

24. Shannon, R.D. *Acta Crystallogr.* **1976**, *A32,* 751.

25. Schollhorn, R.; Weiss, J. *J. Less Common Metals* **1974**, *36,* 229-236.

26. Schollhorn, R. et. al. *J. Less Common Metals* **1978**, *58,* 55-60.

27. Roder, U. et. al. *J. Chem. Phys.* **1981**, *75,* 412-417.

28. Roder, U., et al., *J. Chem. Phys.* **1982**, *77,* 4627-4631.

29. Alexiev, V., et al., *Chem. Mater.* **1999**, *11,* 1742-1746.

30. Wypych, F.; Schollhorn, R. *J. Chem. Soc., Chem. Commun.* **1992**, 1386-1388.

31. Calculation of metal loading was based on a material with the molecular weight of 177.89 $gmol^{-1}$. If a molecular weight of 285.18 $gmol^{-1}$ is used

(assuming $Na_{0.75}(H_2O)_6MoS_2$), then the loaded extractant has the stoichiometry $Ag_{0.78}MoS_2$. This infers a 1:1 exchange between $Na^+(aq)$ and $Ag^+(aq)$ in the interlayer space.

Chapter III

Synthesis and Characterization of Thiospinels with the Formula $Cu_2MSn_3S_8$ (M = Mn, Fe) and Derivatives

Introduction to the Spinel Structure Type

Compounds adopting the spinel structure-type are considered interesting solid state electrode materials due to their open, flexible structure and ability to accept and exchange small ionic species.[1-4] The unit cell content of a compound adopting the spinel structure is $A_8B_{16}X_{32}$.[5] The structure is derived from the NaCl parent structure in which vacancies are created in octahedral sites of the parent cell ($Na_{32}Cl_{32}$) to generate the formula $Na_{16}Cl_{32}$. New cations, designated A, fill one quarter of the tetrahedral vacancies to generate the formula $A_8Na_{16}Cl_{32}$, which is not charge balanced unless A is divalent. This formula can also be written more generally as, $A_8B_{16}X_{32}$., where cations A and B are charged to balance the 32 X anions. Specifically, in a thiospinel, the X anions are sulfides (rather than oxides or halides). Therefore, the final unit cell contains 32 cubic-close-packed S^{2-} anions (in the designated 32e site), eight A cations located in tetrahedral holes (designated 8a sites) and sixteen B

cations located in octahedral holes (designated 16d sites). A ball and stick and a polyhedral depiction of the thiospinel structure are shown in Figures 3.1 and 3.2, respectively. The polyhedral view best illustrates the tetrahedral A cations (blue spheres) located in channels lined with sulfide anions (yellow surfaces). An important characteristic of the spinel structure are the unoccupied 16c (octahedral), 8b and 48f (tetrahedral) sites that are available to facilitate ion movement through the solid. In Figure 3.3, one example of a vacant site, the 48f site, can be visualized using green spheres. These vacant sites are integral to a spacious yet three-dimensionally stabilized solid that lends itself well to repeated ion exchange applications.

Ion Mobility in Various Thiospinel Compounds

A large body of literature is devoted to an investigation of the structure and ionic conductivity of thiospinels and their potential use as lithium ion batteries. In 1985, Schöllhorn and Payer reported a cubic form of titanium disulfide formed by the extraction of copper from $CuTi_2S_4$. The compound TiS_2 was then electrochemically intercalated with lithium cations to form $LiTi_2S_4$.[6] Following this, attempts to understand the structure of the solid after copper extraction and lithium insertion were also made.[3, 4, 6-8]

Copper extraction from and lithium insertion into thiospinels with the formula $Cu_2MSn_3S_8$ (M = Mn, Fe, Co, Ni) was first reported in 1996 by Jumas and co-workers.[9] These compounds adopted the spinel structure with Cu^+ in tetrahedral 8a sites and a combination of M^{2+} and Sn^{4+} cations randomly distributed in the 16d sites, 25 and 75% of the time, respectively. The parent solids were synthesized through a solid state reaction using a stoichiometric combination of the elements at 700°C for eight days.

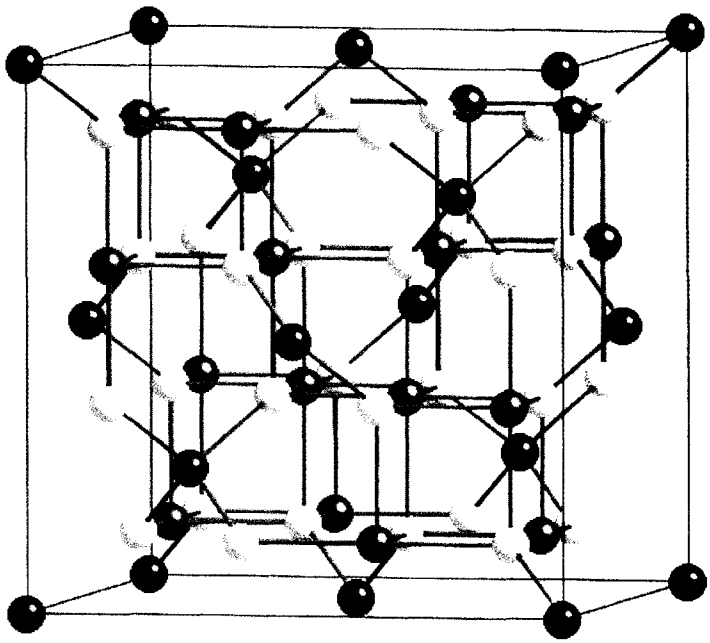

Figure 3.1 Ball and stick model of the thiospinel unit cell, AB_2S_4. Yellow spheres represent sulfide ions, blue spheres represent tetrahedrally coordinated A ions and gray spheres represent octahedrally coordinated B ions. The black outline defines the unit cell.

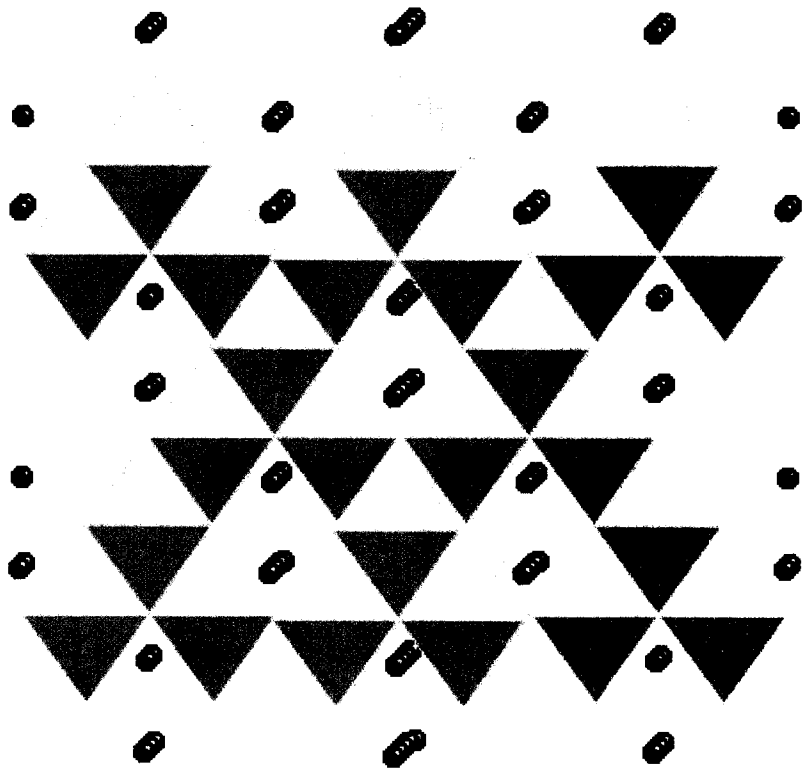

Figure 3.2 Polyhedral representation of the thiospinel AB_2S_4 structure showing BS_6 octahedra (yellow) and A cations (blue) in tetrahedral sites filling the channels.

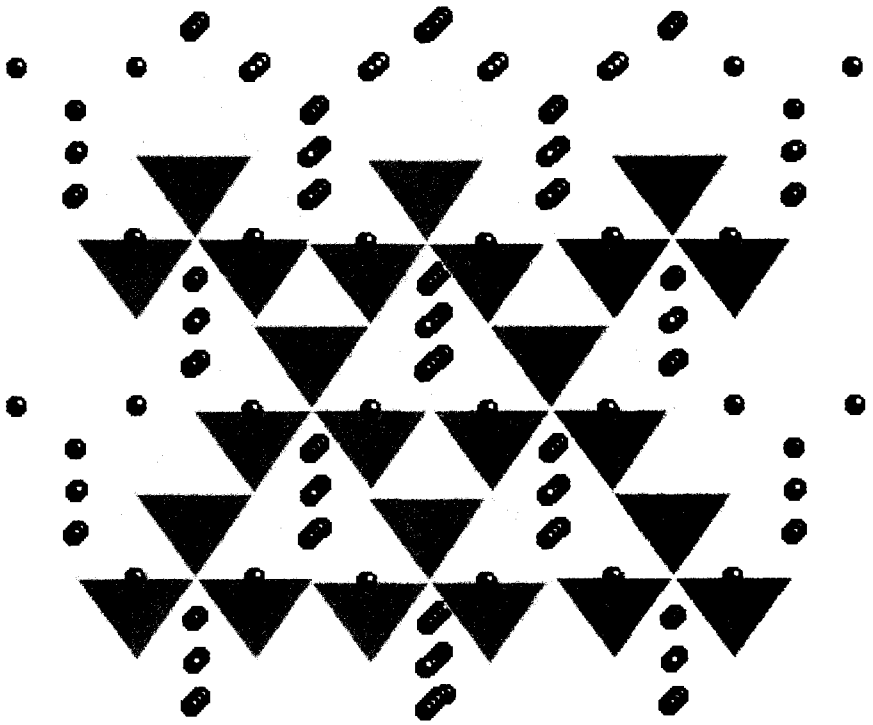

Figure 3.3 Polyhedral view of the spinel structure as seen in Figure 3.2, showing the tetrahedral, 48f, vacancies (green spheres).

To test the lithium ion conductivity of these compounds, lithium was first introduced into the solid using electrochemical methods. This produced powders with very low crystallinity due to loss of long range order resulting from diffusion of cations through the solid. In addition, X-ray diffraction revealed the presence of metallic copper, resulting from the reduction of Cu^{+} to Cu^{0} and migration of the copper out of solid.

Structural degradation was partially avoided using a chemical pretreatment step in which the solid was first oxidized, to remove a portion of the copper cations from the solid, thereby introducing vacancies in the previously occupied 8a sites. A saturated solution of I_2 in CH_3CN oxidized the transition metal from M^{2+} to M^{3+} that caused simultaneous expulsion of Cu^{+} into solution in order to maintain charge neutrality in the solid. The maximum copper extraction for $Cu_2FeSn_3S_8$ was reported to be approximately eight percent after a two-week treatment with I_2, resulting in a compound with the stoichiometry $Cu_{1.84}FeSn_3S_8$. Copper extraction increased the number of vacant sites in the channels and lithium insertion did not cause reduction to metallic copper. However, the oxidized compounds similarly lost long range order with large lithium discharge and eventually became amorphous. The oxidation and reduction reactions described above are summarized in Equations 3.1 and 3.2.

$$Cu_2MSn_3S_8(s) + (x/2)\, I_2(org) \longrightarrow Cu_{2-x}MSn_3S_8(s) + x\, CuI(org) \qquad (3.1)$$

$$Cu_{2-x}MSn_3S_8(s) + y\, Li \longrightarrow Li_yCu_{2-x}MSn_3S_8(s) \qquad (3.2)$$

There have been numerous other attempts at the insertion of lithium into similar structures, including a class of thiospinels based on a Cu_2S-In_2S_3-SnS_2 system.[10-13] These approaches also used chemical reduction with *n*-

butyllithium and also reported reduction of copper to Cu^0 along with a phase transformation to the rock salt structure. Ultimately, retention of structure only occurred when less than one equivalent of lithium was inserted.

Direct Synthesis of Cation Deficient Thiospinels

Other attempts have been made to increase the number of vacancies in the thiospinel structure using direct solid state synthesis. Garg and co-workers were the first to publish the synthesis of a cation deficient thiospinel in the $Cu_2MSn_3S_8$ family with the formula $Cu_{5.47}Fe_{2.9}Sn_{13.1}S_{32}$.[14] Single crystals were grown from a solid state reaction containing a 1:1:3:8 molar ratio of Cu:Fe:Sn:S. The goal of this reaction was to produce a material with the stoichiometry $CuFeSn_3S_8$, containing half as much copper as seen in $Cu_2FeSn_3S_8$. However, this idealized stoichiometry was not obtained. Instead, a product with a higher molar ratio of Sn^{4+} was produced, allowing for lower ratios of both Cu^{1+} and Fe^{2+}. This was the first example of a thiospinel of this type exhibiting a Sn/Fe ratio higher than three, resulting in a compound deficient in both copper and iron.

A second method for producing cation deficient spinels was also reported by Garg using the substitution of a higher valent atom, namely Si^{4+}, for Fe^{2+} in the solid.[15] This approach reduced the number of copper equivalents needed to charge balance the eight sulfide equivalents. The ratio of reactants loaded into this reaction were 3.31:1:4:12:32 of Cu, Si, Fe, Sn, and S respectively. The single crystals were found to have the formula $Cu_{5.5}Si\square_{1.5}Fe_4Sn_{12}S_{32}$.(where $\square$ is representative of a vacancy in the solid). Silicon was present in 13% of the 8a sites and either copper (69%) or a vacancy (18%) occupied the remaining 8a sites. Therefore, substitution of tetravalent silicon in this system reduced the

relative amount of copper present by reducing the number of cations needed for charge balance, however the presence of the silicon atoms in the tetrahedral sites did not substantially increase the overall number of vacancies found in these channels. No lithiations or electrochemical studies have yet been reported with these cation deficient thiospinels.

It is our hypothesis that thiospinels are ideal candidates for the ion exchange of heavy metals from aqueous solution for a number of reasons. Foremost, the soft Lewis-basic channels found in these structures provide a thermodynamic driving force for the preferential inclusion of soft heavy metal cations over hard ones, similar to the behavior of MoS_2 and $H_2Zr(PSO_3)_2$. In addition, the proposed flexible spinel structure will allow ion mobility and therefore ion exchange. Ion exchange extraction is a softer method of inserting different cations into the spinel structure as compared to reduction with chemical reducing reagents such as *n*-butyllithium. Therefore, retention of structure is expected.

Finally, the potential redox activity of the transition metal in $Cu_2MSn_3S_8$ provides the opportunity for redox-recyclability. This redox activity also allows for activation of the extractant using electrochemical rather than chemical methods, as well as the processing of these materials into electrochemical sensors for metal cations in solution. Unfortunately, no other reports have focused on the ion exchange ability of these solids, nor has any research been reported to date regarding the synthesis of compounds using lithium cations directly substituted for copper.

This chapter will discuss the design of a variety of new compounds based on the $Cu_2MSn_3S_8$ family with the goals of producing ion exchange extractants for soft metal cations. This research stemmed from a need to introduce a chemically hard and environmentally benign cation into the solid to ion

exchange for soft metal cations in solution. Copper is considered a chalcophillic cation and the driving force for ion exchange, forcing copper into aqueous solution is expected to be limited. Furthermore, copper is not an ideal cation to release into the decontaminated waste produced after ion exchange occurs.

Different techniques were employed to synthesize new spinel compounds. Initially, chemical oxidation and reduction was investigated, similar to the approaches used by Jumas. These reactions did not effectively change the bulk composition of the powders that were used. Therefore, direct synthesis of cation deficient thiospinels by reducing the amount of metal loaded into the solid state reaction, similar to the approach used by Garg, was investigated as a method of removing the chemical oxidation step from the extractant synthesis. This technique was beneficial because as a bulk technique, under ideal conditions, it produced an extractant with a homogeneous composition, whereas chemical oxidation and reduction was limited to the surface of the solid.

Novel compounds crystallizing with the spinel structure were also directly synthesized with lithium or sodium cations replacing copper in the structure. Example stoichiometries for these solids are $Li_2FeSn_3S_8$ or $Na_2FeSn_3S_8$. This is the first time that direct synthesis using high temperature techniques has been used to introduce lithium into these structures.

Finally, ion exchange reactions to introduce protons into the solid, similar to the approach used to synthesize H_xMoS_2, were employed and the reaction products are discussed. These compounds were designed to be ion exchange extractants with the following characteristics: (1) selectivity for soft metal cations over hard ones (2) fast ion exchange (3) synthesis without the use or production of toxic or dangerous chemical agents and (4) oxidative stability.

Experimental

Distilled water was purified and deionized (to 18 MΩ) with a Barnstead NANOPure purification system. Nitric acid (Mallinckrodt), hydrochloric acid (Mallinckrodt), acetonitrile (Fisher Scientific) and metal nitrate salts were reagent grade or better and were used as received. Reagents for syntheses were used as follows: *n*-Butyllithium (2.5M in hexane, Aldrich), iron powder (grade 1, Johnson Matthey), manganese powder (-50 mesh, 99.9%, Aldrich), tin powder (-325 mesh, 99.8%, Alfa Aesar), sulfur (Johnson Matthey), lithium sulfide (98%, Aldrich), iodine (sublimed, Baker), sodium hydrosulfite (85%, Aldrich), sodium carbonate (anhydrous, Fisher). Na_2S_2 was synthesized by a combination of the elements in liquid ammonia, as described elsewhere.[16] Purified, anhydrous hexane was prepared by stirring over H_2SO_4 (Mallinckrodt), flowing through activated basic alumina (Aldrich, 150 mesh) and distillation from sodium metal. Schlenk, glovebox and high vacuum techniques were employed for some experiments.[17]

Powder X-ray diffraction (PXRD) measurements were recorded with a Philips diffractometer using Cu-Kα radiation. XRD patterns were taken of samples on frosted glass sample holders. XRD patterns of air-sensitive samples were taken by preparing the sample and holder in a nitrogen atmosphere glove box and then placing a piece of transparent tape over the sample. Diffraction data was analyzed using JADE (MDI) software. Powder patterns were compared to those in the PDF database. X-ray photoelectron spectra (XPS) were taken using a Physical Electron 5800 XPS-Auger Spectrometer.

Compounds with the chemical formula $Cu_2MSn_3S_8$ (M = Mn, Fe) were synthesized according to a modified procedure initially described by Lavela and

co-workers.[9] For a typical 5.00 g synthesis, the appropriate stoichiometric amounts of the elements (as described in Table 3.1) were loaded into a quartz ampoule in a nitrogen atmosphere glovebox. The ampoule was sealed under dynamic vacuum on a high vacuum manifold. The sealed ampoule was placed in a tube furnace and heated to 300 °C at a rate of 25 °C/hour, held at 300 °C for 24 hours and then heated to 700 °C at a rate of 25 °C/hour and held for 192 hours (8 days). The reaction was cooled to room temperature at a rate of 25 °C/hour. This synthesis typically gave a mixture of products. In order to obtain a single-phase product, the entire reaction mixture was reground with a mortar and pestle in the nitrogen atmosphere glovebox and loaded into a second ampoule and sealed as described above. This second ampoule was again placed in a tube furnace and heated at 25 °C/hour to 700 °C for 50 hours. The product of this second reaction was a highly crystalline black powder with a spinel structure. The procedure described by Lavela only included the initial heating of the solid to 700 °C without further heating.[9]

Results and Discussion

A representative X-ray powder diffraction analysis of a spinel with the general formula $Cu_2FeSn_3S_8$ synthesized in our laboratory can be seen in Figure 3.4. These powders were highly crystalline and could be indexed to the naturally occurring mineral rhodostannite. Each reflection in the pattern is representative of a plane of atoms in the solid, pictorially represented in Appendix A. The relative intensities of these reflections are representative of the concentrations of cations found in the planes causing diffraction. Copper atoms are present in the 020 plane ($2\theta = 24.2°$, d = 3.68 Å) and the 242 plane ($2\theta = 42.5°$, d = 2.13 Å). When copper atoms are extracted from the solid,

Table 3.1 Typical stoichiometric ratios used in the synthesis of $Cu_2MSn_3S_8$.

	$Cu_2MnSn_3S_8$	$Cu_2FeSn_3S_8$
Cu (s) (g, mmoles)	0.7998, 12.58	0.7989, 12.57
M (s) (Mn, Fe) (g, mmoles)	0.3457, 6.293	0.3510, 6.285
Sn (s) (g, mmoles)	2.2408, 18.88	2.2382, 18.86
S (s) (g, mmoles)	1.6139, 50.34	1.6121, 50.28

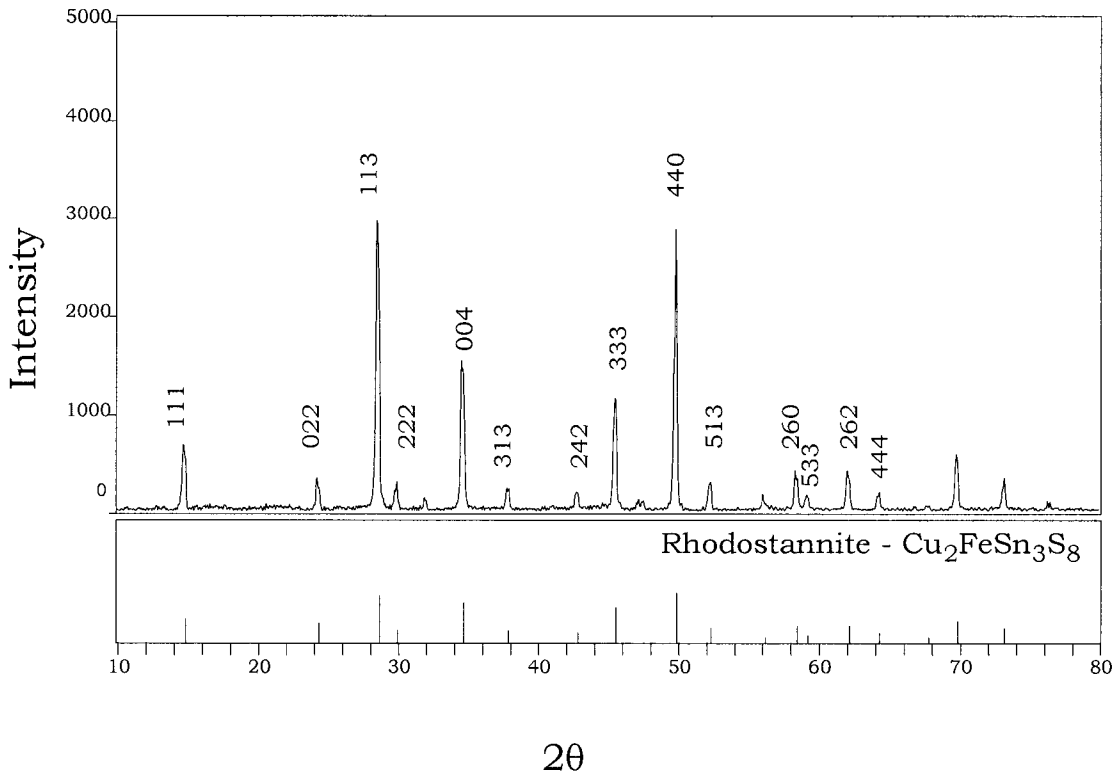

Figure 3.4 PXRD analysis of as prepared $Cu_2FeSn_3S_8$ together with the Inorganic Crystal Diffraction Database (ICDD) standard, file # 29-0558.

the relative intensities of these two reflections are expected to decrease. This qualitative method of determining the removal of copper from this structure has also been used by Jumas.[9]

Chemical Synthesis of Oxidized Spinels

The first approach to synthesizing new spinel compounds focused on the chemical oxidation of the parent compounds $Cu_2FeSn_3S_8$ and $Cu_2MnSn_3S_8$. Both parent solids were contacted with a saturated solution of iodine in acetonitrile at room temperature for four days, after which time the solutions were filtered and washed with acetonitrile to remove any excess copper iodide. The powder X-ray diffraction analyses of the resulting 'oxidized' spinels can be seen in Figures 3.5 and 3.6. This comparison shows very little change in either the 020 or the 242 reflections, indicating that little or no copper was extracted from the bulk material. In addition, when the solids were digested in *aqua regia* and the metal ion stoichiometries were determined by ICP-AES, there was no detectable change in the copper or transition metal stoichiometry. For example, a digestion of the parent spinel resulted in materials with the formulae $Cu_{1.9}Mn_{1.1}Sn_3S_8$ and $Cu_{1.7}Fe_{1.1}Sn_3S_8$. The chemically treated materials were found to have the formulae $Cu_{1.9}Mn_{0.8}Sn_3S_8$ and $Cu_{1.8}Fe_{1.0}Sn_3S_8$.

A comparison of the X-ray photoelectron spectra of $Cu_2MnSn_3S_8$ to that of the product of its oxidation is shown in Figures 3.7 and 3.8. In $Cu_2MnSn_3S_8$, all atoms were found to be in single oxidation states. In the oxidation product, only one oxidation state is seen for copper, with a decrease in the signal to noise ratio of the copper 2p peaks. This decrease in intensity

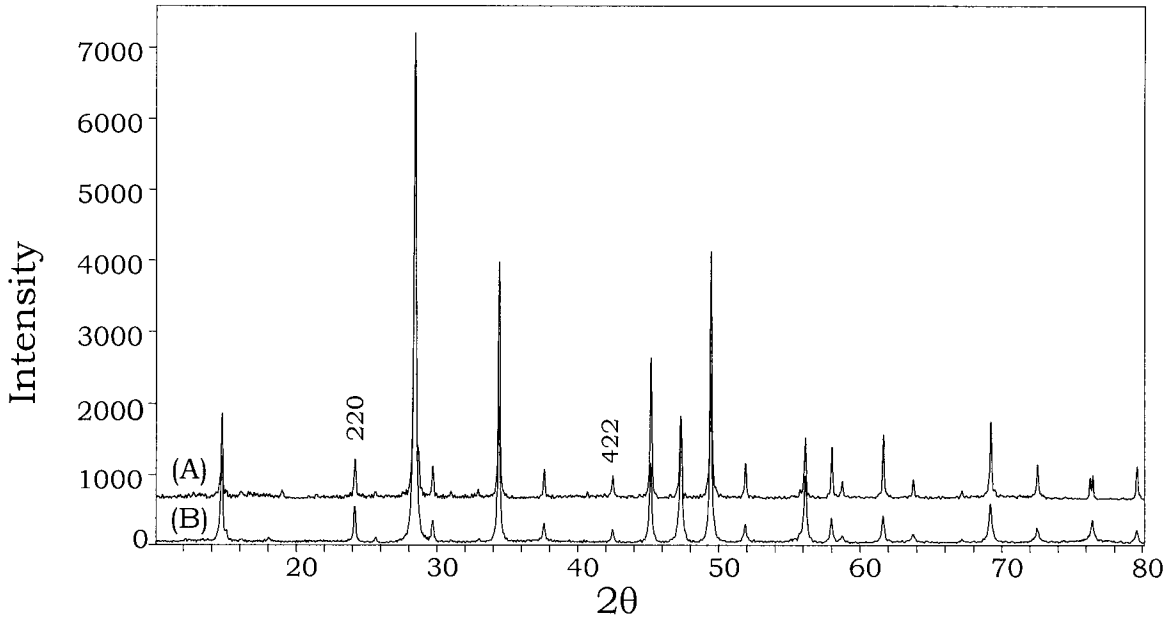

Figure 3.5 Powder X-ray diffraction analysis of (A) $Cu_2MnSn_3S_8$ and (B) $Cu_2MnSn_3S_8$ after oxidation with I_2/CH_3CN.

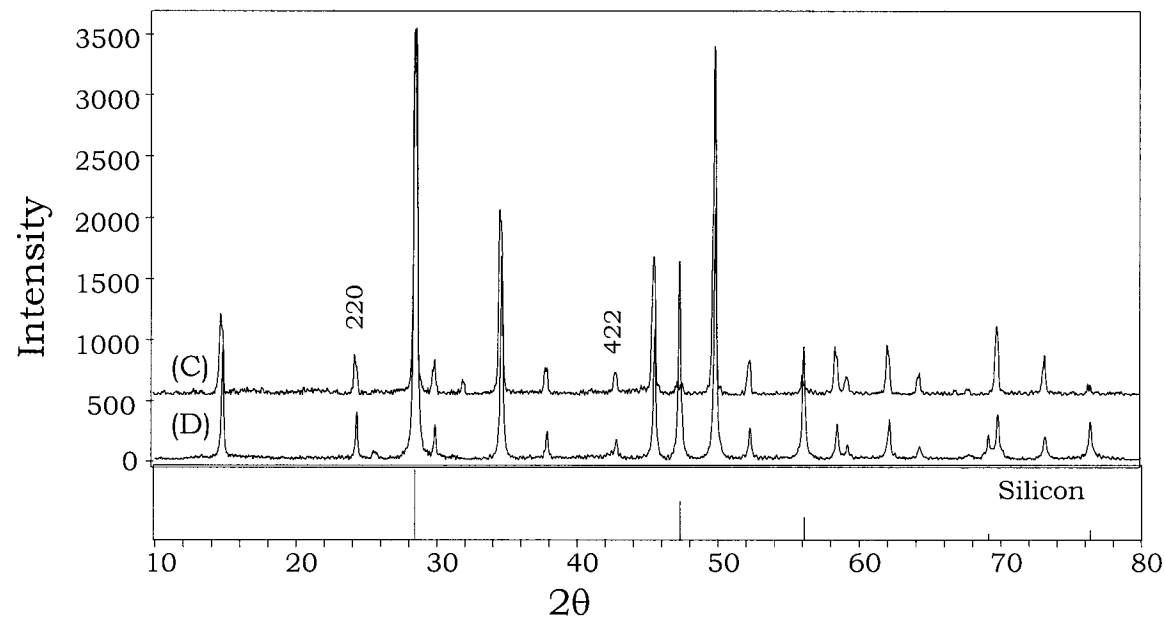

Figure 3.6 Powder X-ray diffraction analysis of (C) $Cu_2FeSn_3S_8$ and (D) $Cu_2FeSn_3S_8$ after oxidation with I_2/CH_3CN.

qualitatively indicated that the concentration of copper atoms on the surface of the solid had decreased. The Mn $2p_{1/2}$ and $2p_{3/2}$ peaks in $Cu_2MnSn_3S_8$ were single peaks, separated by approximately 9 eV. In the oxidized compound, Figure 3.8b, a new set of peaks appeared at higher binding energies relative to the initial peaks. The emergence of a new set of manganese peaks indicated partial oxidation of the manganese.

In the oxidation product of $Cu_2FeSn_3S_8$, only one oxidation state was found for copper with a similar decrease in the signal to noise ratio. In the case of iron analysis, Figure 3.8d, determination of oxidation state of iron was not possible due to interference from an intense Sn $3p_3$ that falls in the same binding energy range as the most intense iron peak ($2p_{3/2}$). From the manganese data, however it appeared that the transition metal was oxidized with simultaneous expulsion of copper from the solid.

It is important to note here, that XPS is a surface analysis technique. Therefore, partial oxidation of surface atoms does not necessarily indicate oxidation of the bulk material. In fact, oxidation of the manganese was shown to be incomplete, indicating that the bulk of the material was not oxidized, due to poor diffusion of the oxidant into the solid particles. Because of incomplete oxidation and relatively long reaction times, oxidation using iodine was determined to be an impractical route to producing cation deficient thiospinels with significant copper extraction.

Solid State Synthesis of Cation Deficient Thiospinels

A different approach to the synthesis of cation deficient compounds was the direct, solid state synthesis of materials with the defect stoichiometries: $CuMnSn_3S_8$, $Cu_2Sn_3S_8$ and $CuFeSn_3S_8$. Because of the possibility of multiple

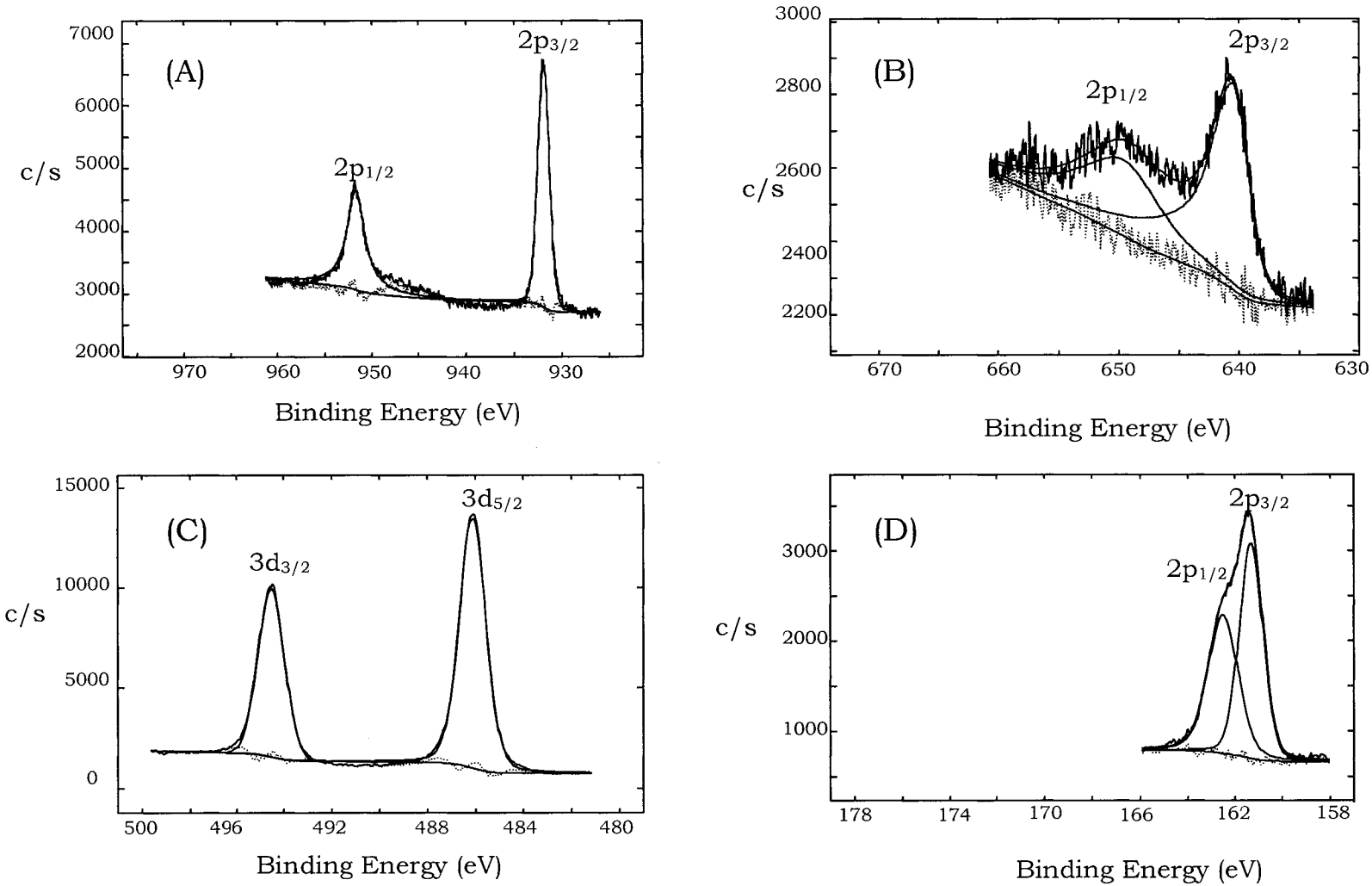

Figure 3.7 High Resolution (HRES) XPS analysis of $Cu_2MnSn_2S_8$ (parent) powder. (A) Cu 2p (B) Mn 2p (c) Sn 3d (D) S 2p.

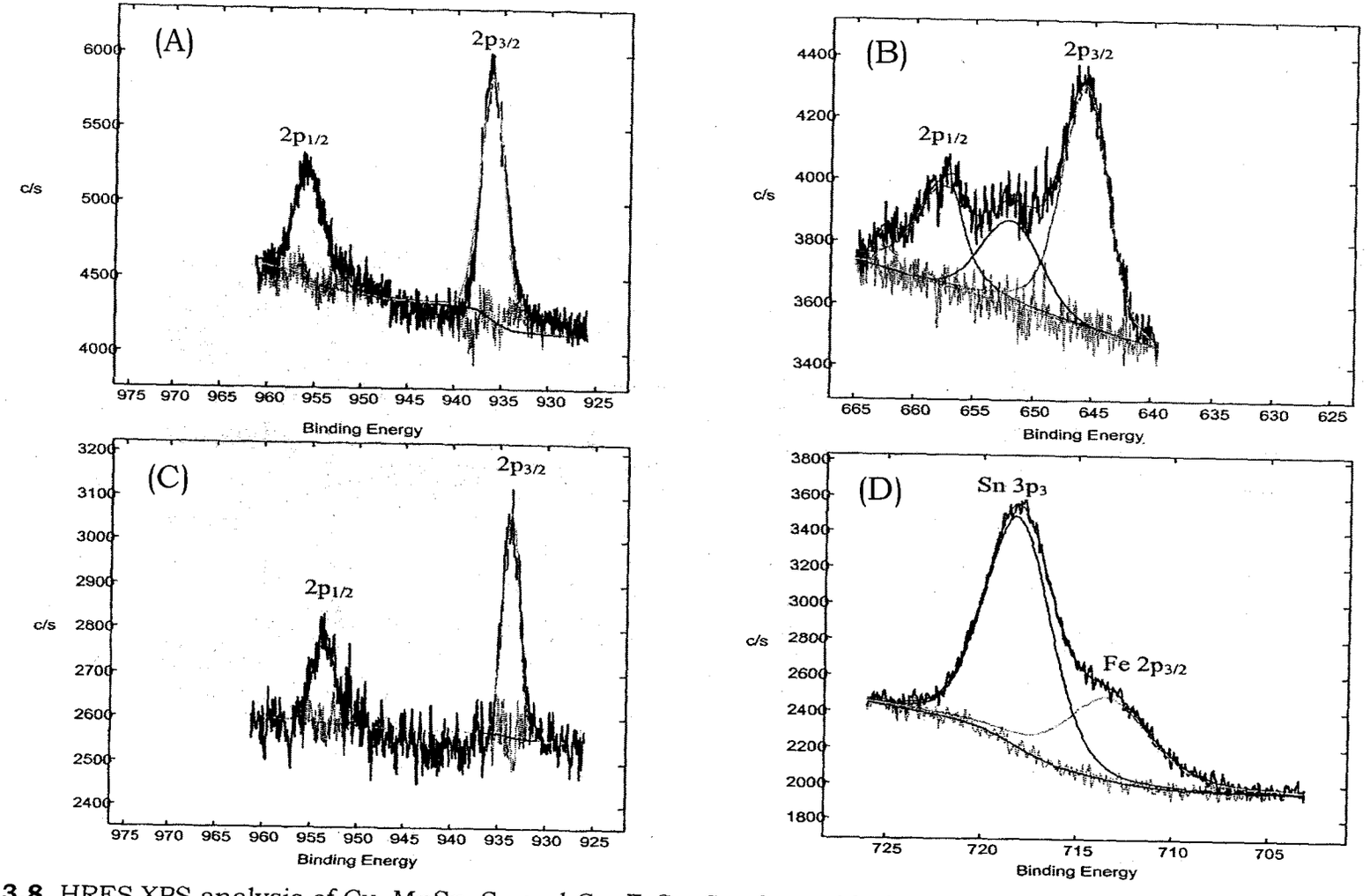

Figure 3.8 HRES XPS analysis of $Cu_2MnSn_3S_8$ and $Cu_2FeSn_3S_8$ after oxidation with I_2/CH_3CN (a) Cu 2p (b) Mn 2p (c) Cu 2p (d) Fe 2p.

oxidation states of both copper and the transition metal, reduction in the molar equivalents of either copper or transition metal can be compensated for by an increase in the oxidation state of another atom in the structure. For example, in the case of $CuMnSn_3S_8$, either copper can be oxidized Cu^{2+} (as compared with the parent compound) or manganese can be oxidized to Mn^{3+}.

For these reactions, the correct stoichiometric ratio of the elements was loaded into a fused silica ampoule and heated as described in the experimental section. The product of each reaction, similar to the parent compound, was a fine, black powder. X-ray powder diffraction analysis, seen in Figure 3.9, revealed that all three of the solids crystallized with the spinel structure.[18] A closer comparison of the diffraction pattern of $CuMnSn_3S_8$ with that of $Cu_2MnSn_3S_8$, seen in Figure 3.10, shows a significant decrease in the 022 and 242 reflections, indicating defects or vacancies in copper positions. This is the first example of a spinel of this type with as many as half of the cations removed from the tetrahedral sites with retention of the structural integrity of the solid.

X-ray photoelectron spectroscopy was used to examine the oxidation states of the atoms in $Cu_2Sn_3S_8$. It was expected that copper would be present as Cu^{2+} in order to charge balance S^{2-} and Sn^{4+}. It was found, however, that a fraction of both the copper and sulfur were present as oxidized species, as can be seen in Figure 3.11. The exact ratios of Cu^{+}/Cu^{2+} and S^{2-}/S_n^{2-} cannot be determined from these data due to the complex and overlapping sulfur signals.

Once it had been determined that direct synthesis produced oxidized materials with a significant number of cation deficiencies, the next step was chemical reduction of the solids. Based on literature precedent, reduction of $CuMnSn_3S_8$, $Cu_2Sn_3S_8$ and $CuFeSn_3S_8$, was attempted using *n*-butyllithium. This method resulted in powders that, according to powder X-ray diffraction,

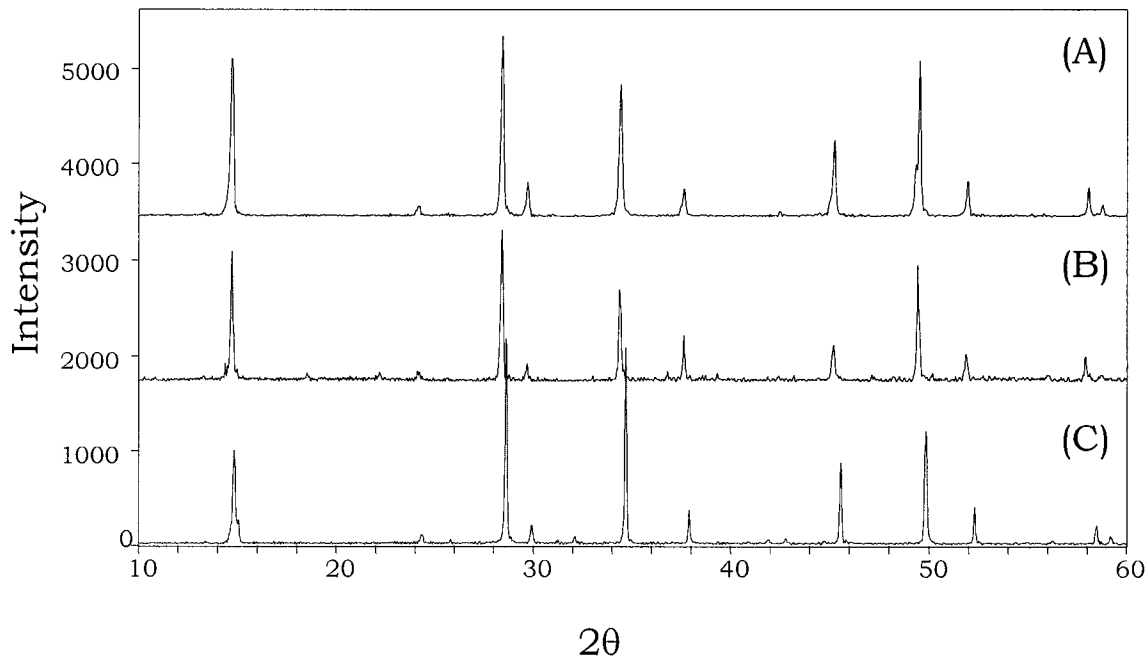

Figure 3.9 Powder X-ray diffraction analysis of (A) $CuMnSn_3S_8$ (B) $Cu_2Sn_3S_8$ (C) $CuFeSn_3S_8$.

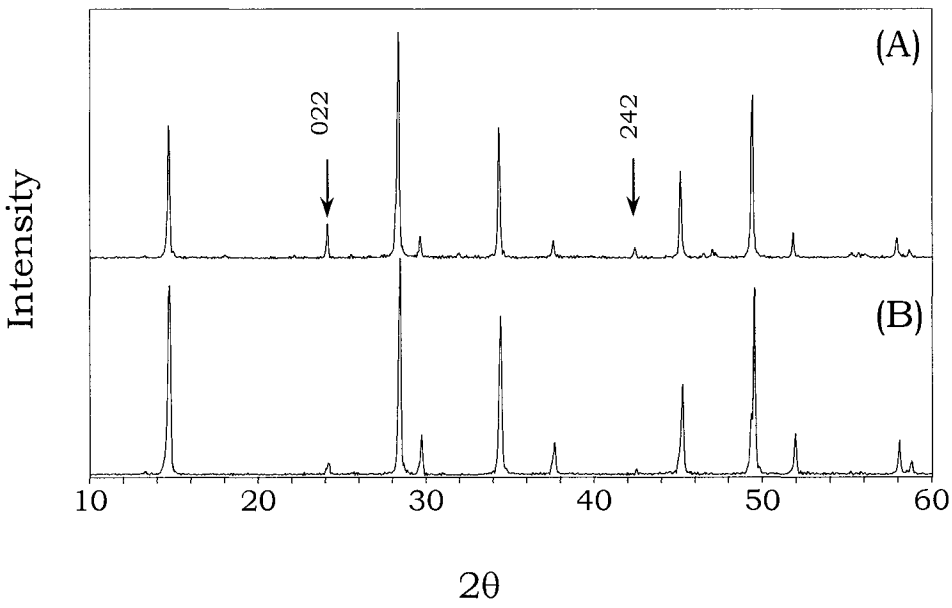

Figure 3.10 X-ray powder diffraction comparison of (A) $Cu_2MnSn_3S_8$ and (B) $CuMnSn_3S_8$ showing a reduction in intensity of 022 and 242 reflections.

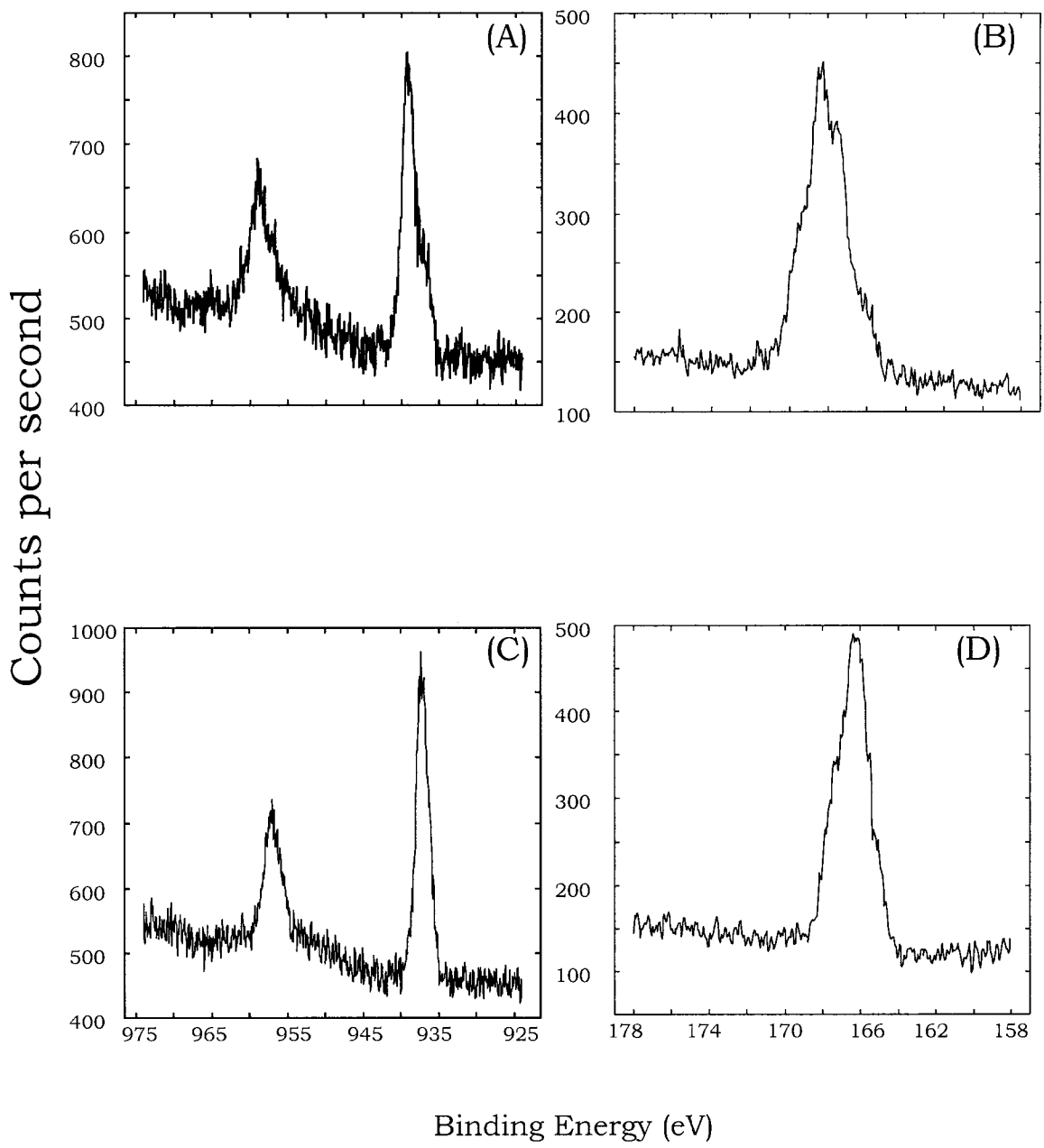

Figure 3.11 HRES XPS analysis of (A) Cu 2p peaks of $Cu_2Sn_3S_8$ (B) S 2p peaks of $Cu_2Sn_3S_8$ (C) Cu 2p peaks of $Cu_2Sn_3S_8$ after reduction with $Na_2S_2O_4$ and (D) S 2p peaks of $Cu_2Sn_3S_8$ after reduction with $Na_2S_2O_4$.

had lost the spinel structure and could not be otherwise structurally characterized.

To replace butyllithium as a reducing agent, $CuMnSn_3S_8$ and $Cu_2Sn_3S_8$ were reduced using a basic solution of $Na_2S_2O_4$. This reductant was chosen because of its mild nature compared with that of *n*-butyllithium. A comparison of the powder diffraction data of $CuMnSn_3S_8$ and the product of the reaction with $Na_2S_2O_4$ can be seen in Figure 3.12. There was a very small increase in the a parameter of the unit cell (from 10.399(1) Å in $Cu_2MnSn_3S_8$ to 10.417(2) in the reduced compound), however there were no detectable changes in the relative intensities of the reflections. There also appeared to be a small increase and sharpening of the 002 reflection. Both of these changes were too small to make any clear conclusions about structural changes in the solid. Therefore, it was concluded from X-ray data that less than 5% of the solid was reduced, if any reduction had occurred at all.

The same is true with respect to the reduction of $Cu_2Sn_3S_8$. In Figures 3.11C and 3.11D, the XPS analysis of the reduction products show reduction of copper to Cu^+, however the sulfur peaks appear unaffected. These results are similar to the oxidation reactions described in the previous section. If any of the reduction reactions were successful, they were confined to the surface of the solid and did not represent reduction of the bulk powder. Overall, chemical reduction was relatively slow and incomplete and a new approach was needed to introduce hard metal cations, such as H^+, Li^+ or Na^+, into the solid.

Solid State Synthesis of $ACuFeSn_3S_8$ and $A_2FeSn_3S_8$ (A = Li, Na)

Compounds with lithium or sodium atoms substituting for either half or all of the copper atoms were successfully synthesized through solid state

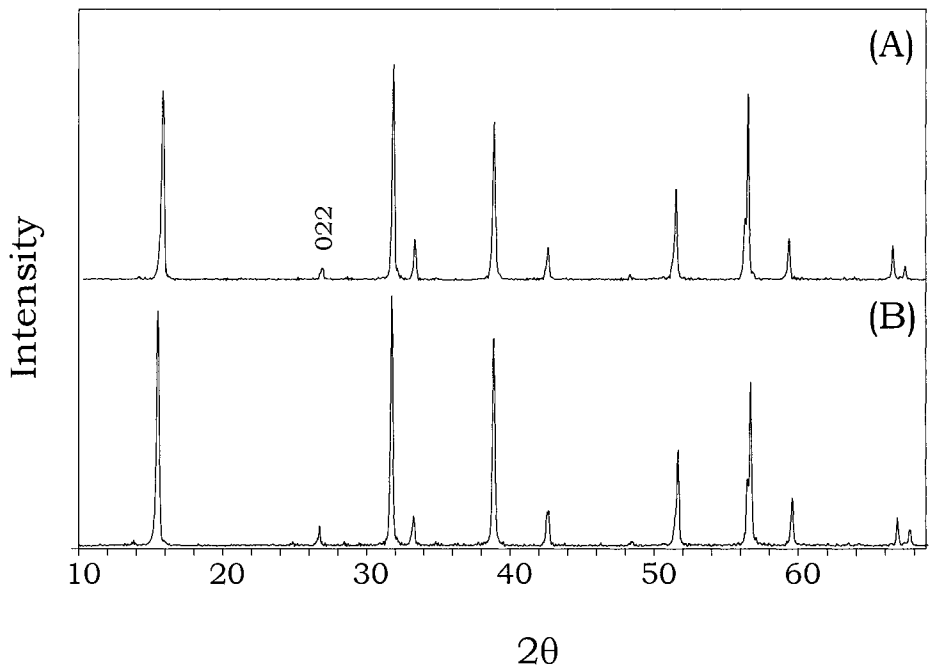

Figure 3.12 Powder X-ray diffraction comparison of (A) $CuMnSn_3S_8$ and (B) $CuMnSn_3S_8$ after reduction with $Na_2S_2O_4$.

reactions using Li_2S and Na_2S_2. The goal of this research was the production of extractants with the formula $LiCuFeSn_3S_8$, $Li_2FeSn_3S_8$, $NaCuFeSn_3S_8$, and $Na_2FeSn_3S_8$. Initially, it was hypothesized that complete substitution of an alkali metal for copper to form either $Li_2FeSn_3S_8$ or $Na_2FeSn_3S_8$ might create too much structural instability to maintain the spinel phase. For this reason, $LiCuFeSn_3S_8$ and $NaCuFeSn_3S_8$ were also synthesized with the intent of providing structural stability for the spinel phase with copper atoms, but allowing a significant number of hard metal cations available for ion exchange. The reactions used to produce these solids are described in Equations 3.3 through 3.6.

$$0.5\ Li_2S(s) + Cu(s) + Fe(s) + 3\ Sn(s) + 7.5\ S(s) \longrightarrow LiCuFeSn_3S_8(s) \quad (3.3)$$

$$Li_2S(s) + Fe(s) + 3\ Sn(s) + 7\ S(s) \longrightarrow Li_2FeSn_3S_8(s) \quad (3.4)$$

$$0.5\ Na_2S_2(s) + Cu(s) + Fe(s) + 3\ Sn(s) + 7\ S(s) \longrightarrow NaCuFeSn_3S_8(s) \quad (3.5)$$

$$Na_2S_2(s) + Fe(s) + 3\ Sn(s) + 6\ S(s) \longrightarrow Na_2FeSn_3S_8(s) \quad (3.6)$$

Each reaction yielded a black powder, uniform in appearance. The powder X-ray diffraction patterns of the products from Equations 3.3 and 3.4 are shown in Figure 3.13. Both of these materials are highly crystalline with a diffraction pattern indicative of a spinel structure. One clear difference between the diffraction pattern of $Li_2FeSn_3S_8$ and the standard $Cu_2FeSn_3S_8$ is the absence of the 022 and 242 reflection. This was expected if all of the copper atoms were replaced by lithium because of the lower atomic scattering factor of lithium compared to copper. In the case of $LiCuFeSn_3S_8$, the 022 reflection is still present, although less intense, due to the substitution of only 50% of the copper atoms for lithium.

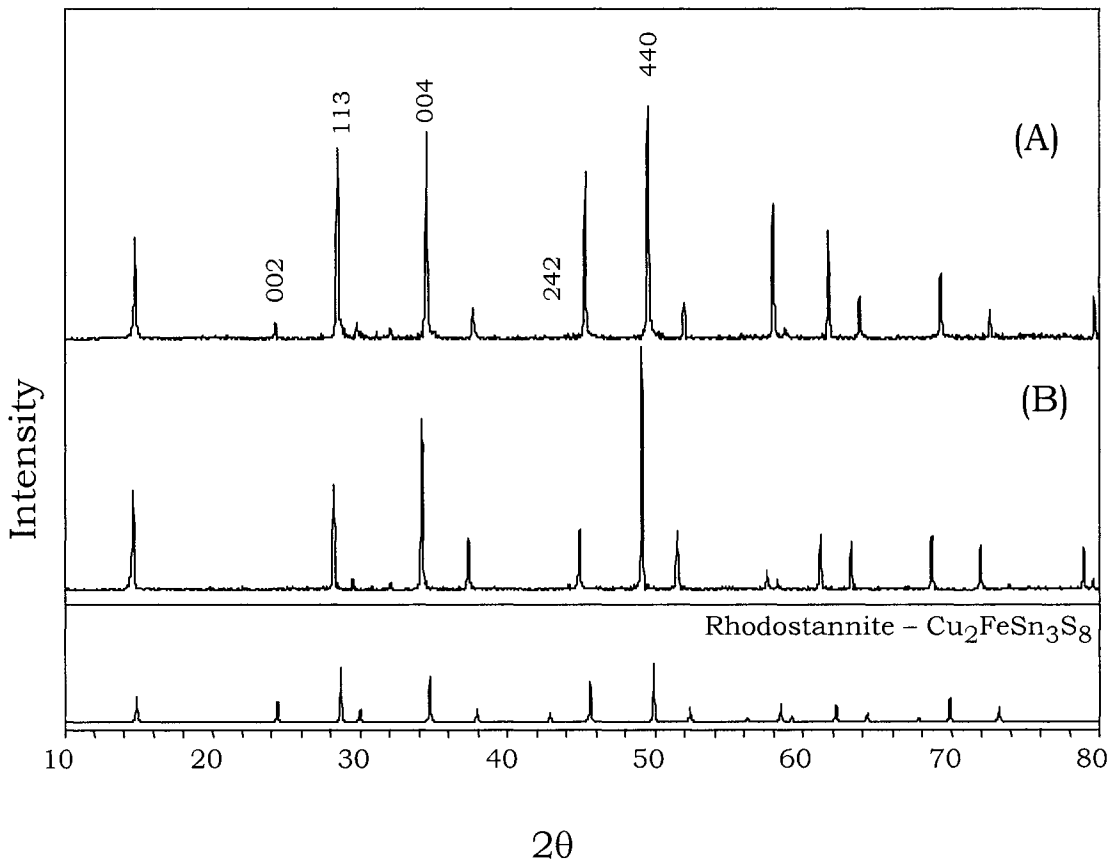

Figure 3.13 Powder X-ray diffraction comparison of (A) $LiCuFeSn_3S_8$ and (B) $Li_2FeSn_3S_8$. Included is the ICCD standard file for rhodostannite.

In addition, the relative intensities of the 113 and 004 reflections are reversed from those of the parent spinel, $Cu_2FeSn_3S_8$. This inversion of relative intensity had been previously used as an explanation for the migration of indium cations (strong scattering atoms) out of tetrahedral sites and into octahedral sites during the electrochemical lithiation of α-$Li_{16.26}Sn_{3.90}S_{32}$.[12] In both $LiCuFeSn_3S_8$ and $Li_2FeSn_3S_8$, the presence of more strongly scattering cations (Fe, Sn) in octahedral holes and relatively weak scattering cations (Li) in tetrahedral holes is expected to produce a similar effect. In addition, the ratio of the 113/004 reflection is smaller in the diffraction pattern of $LiCuFeSn_3S_8$, compared with the ratio of the 113/004 reflection of $Li_2FeSn_3S_8$ because of the addition of one equivalent of copper atoms in the 8a site. The increase in the 440 reflection is also indicative of a structure based on octahedral cation occupancy. Along with the 004, this reflection can be used as a reference to the 220 and 002 reflections of the NaCl rock salt structure. The NaCl structure could be used as a reference in the lower limit of this series with no atoms present in tetrahedral sites and therefore no diffraction.[11]

The powder diffraction analysis of the products of Equations 3.5 and 3.6 can be seen in Figure 3.14. From this, it is apparent that $NaCuFeSn_3S_8$ is a mixture of two different phases, one having the spinel structure (denoted with asterisks), the other with an as yet undetermined structure. In a comparison with the structure of $Na_2FeSn_3S_8$, it is apparent that the $Na_2FeSn_3S_8$ phase is common to both products. This indicated that the product of the reaction proposed in Equation 3.5 was actually a one to one mixture of $Cu_2FeSn_3S_8$ and $Na_2FeSn_3S_8$ as shown in Equation 3.7.

$$0.5\ Na_2S_2(s) + Cu(s) + Fe(s) + 3\ Sn(s) + 7\ S(s) \longrightarrow 0.5\ Cu_2FeSn_3S_8(s) + 0.5\ Na_2FeSn_3S_8(s) \qquad (3.7)$$

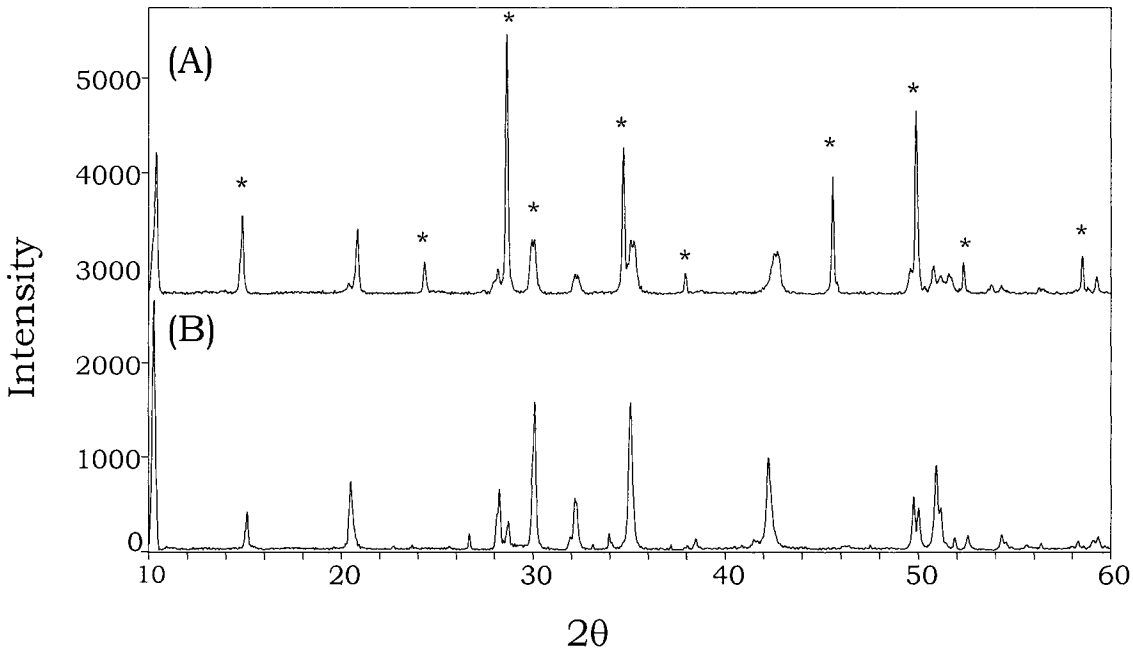

Figure 3.14 PXRD analysis of (A) $NaCuFeSn_3S_8$ and (B) $Na_2FeSn_3S_8$. Asterisks on pattern (A) denote the reflections due to a spinel phase.

This result was not surprising because isostructural substitution of a sodium cation for copper is not as likely as a substitution of lithium for copper. Foremost, there is larger difference in the atomic radius of sodium and copper (1.1 Å for Na^+ compared to 0.74 Å for Cu^+, Δ = 0.36 Å) as compared with the difference between lithium and copper (0.73 Å for Li^+).[19] In addition, sodium is most commonly found with octahedral coordination in the solid state compared to copper which, in this structure, is present in a tetrahedral site. Isostructural substitution is therefore not as likely with sodium as with lithium. Instead of isostructural substitution, sodium could have filled the vacant 16c octahedral sites. Had this happened, the powder pattern would resemble the simulated pattern in Figure 3.15. Again, this simulated pattern shows an increase in the relative intensity of the 004 and 440 reflections as a result of a structure based on octahedral coordination of the atoms (as seen in the NaCl structure).

One interesting feature seen in the diffraction pattern of $Na_2FeSn_3S_8$ (Figure 3.14B) is the intense reflection at $2\theta = 10°$ corresponding to an interplanar distance of 8.8 Å. This large cell parameter is not typical for thiospinels and could be indicative of a layered structure. Unfortunately, this sample is not crystalline enough for it to be a candidate for Rietfield refinement or more rigorous structural analysis and the exact structure remains undetermined.

Proton Activated Spinels

An interesting thiospinel analogue that was discovered during the course of various extraction experiments (to be discussed in Chapter IV) was a proton intercalated or activated spinel. This material was synthesized by contacting the parent spinel, either $Cu_2MnSn_3S_8$ or $Cu_2FeSn_3S_8$ with an acidic, aqueous

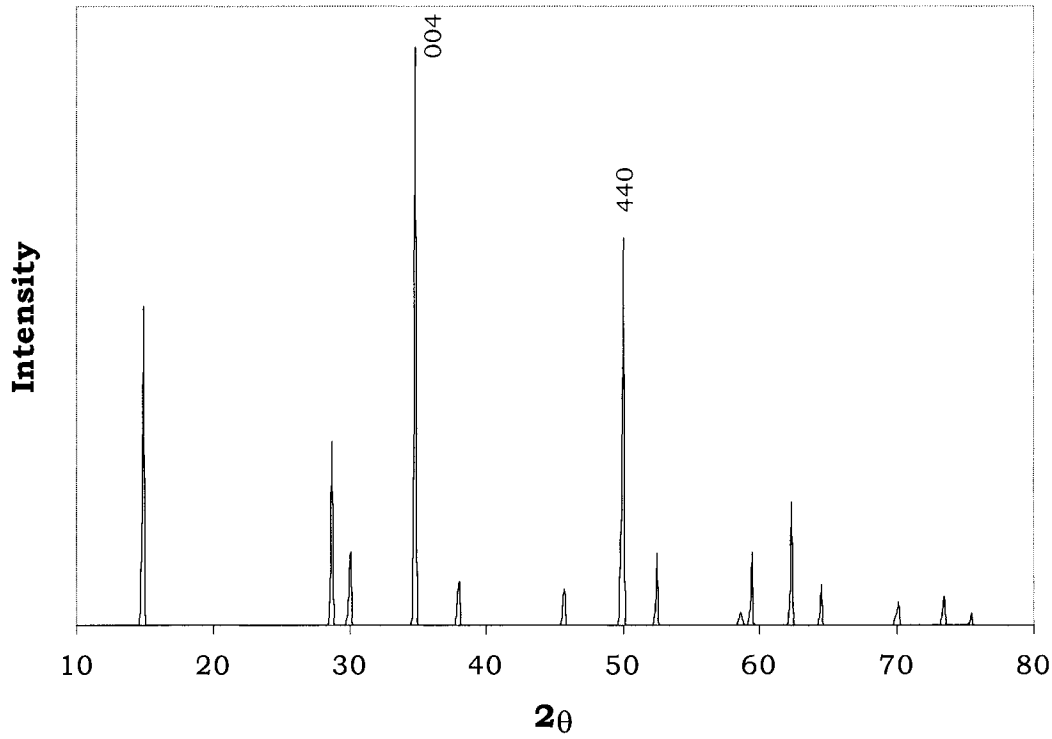

Figure 3.15 Simulated X-ray diffraction pattern of $Na_2FeSn_3S_8$ assuming sodium occupation of one half of the available 16c octahedral sites.[Palmer, 2001 #25][Palmer, 2000 #26]

solution. This product is similar to H_xMoS_2 produced in the reaction between $Li_{1.3}MoS_2$ and 0.1M HNO_3. As was the goal in the synthesis of alkali metal containing thiospinels such as $Na_2FeSn_3S_8$ discussed in the previous section, this 'activation' inserts an environmentally inert cation, H^+, into the parent material that will produce a less toxic decontaminated waste stream after ion exchange.

Proton-activated spinels were initially synthesized through a reaction of $Cu_2FeSn_3S_8$ with a solution of 0.1M HNO_3, aerobically. The stoichiometry of the resultant compound was calculated by analyzing the concentrations of copper, iron and tin in the filtrate after the reaction, in addition to testing the pH of the solution before and after extraction. The variation of copper and iron stoichiometry as a function of contact time is shown in Figures 3.16 and 3.17. From these two plots, it can be seen that both copper and iron were extracted from the solid, rather than selective extraction of one cation over the other. No tin was detected in the filtrate of either sample. The stoichiometries ranged from $H_{0.10}Cu_{1.96}Fe_{0.97}Sn_3S_8$ after a 24 hour contact of 0.1M HNO_3 to $H_{0.18}Cu_{1.90}Fe_{0.96}Sn_3S_8$ after 72 hours, showing that the amount of ion exchange is small (less than 5% of the total ions possible), and very slow (in that there is not a great increase in extraction after six days of contact). Using a different acid, 0.1M HCl for example, did not significantly change these results, as can be seen in the triangle plots of Figures 3.16 and 3.17.

Because of the inability to detect protons with powder X-ray diffraction, and because there appears to be loss of both copper and iron from the structure, this ion extraction does not produce significant changes in the intensities of reflections in the diffraction pattern, shown in Figure 3.18. The spinel phase is still present, however, and no deviation from the initial phase, or the formation of binary or ternary sulfides can be detected that would

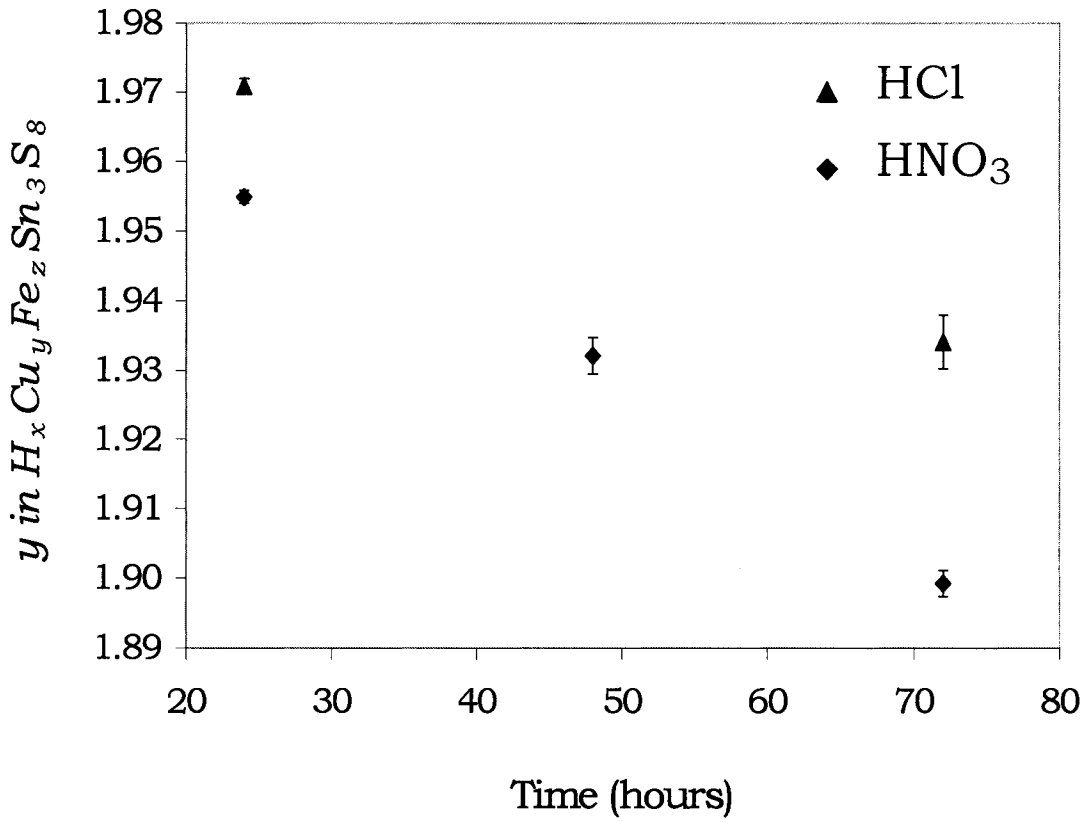

Figure 3.16 Variation of copper stoichiometry, y in $H_xCu_yFe_zSn_3S_8$, as a function of time using 0.1M HCl (triangles) and 0.1M HNO_3 (diamonds).

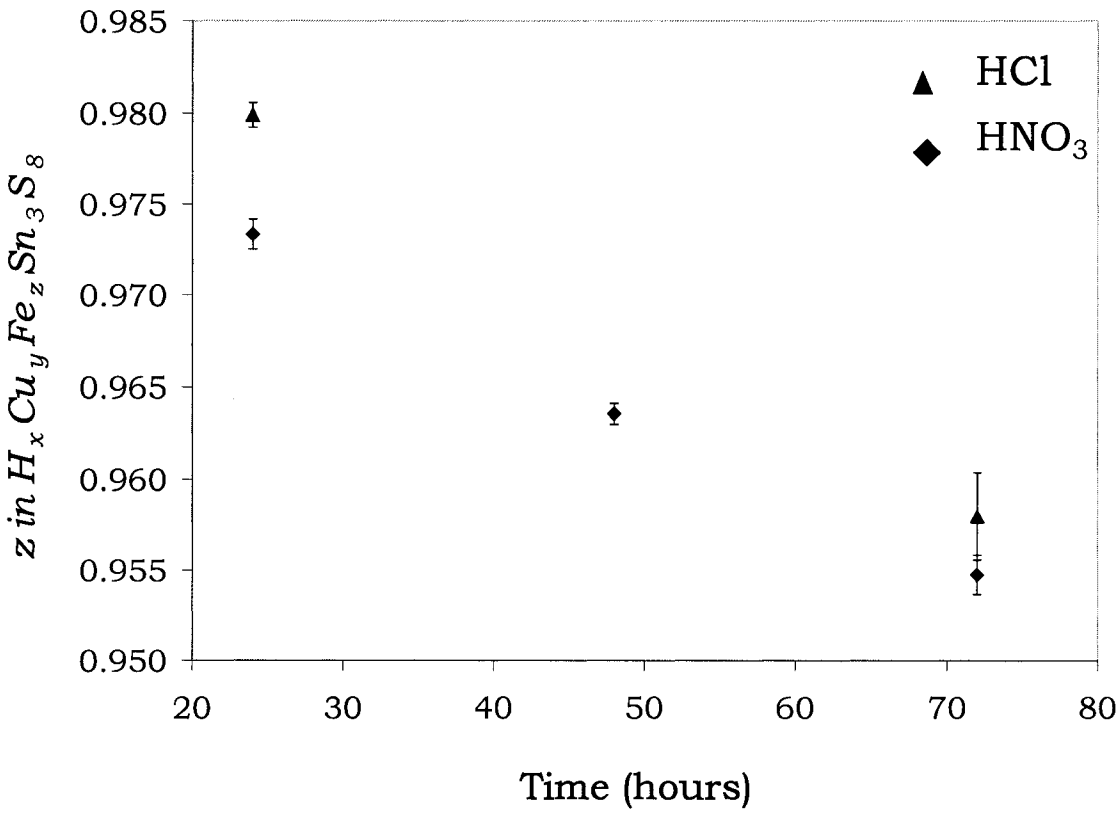

Figure 3.17 Variation of iron stoichiometry, z in $H_xCu_yFe_zSn_3S_8$ as a function of time using 0.1M HCl (triangles) and 0.1M HNO_3 (diamonds).

indicate decomposition.

This same behavior was seen with the manganese analog of the parent, $Cu_2MnSn_3S_8$. ICP analysis and pH measurements on the filtrate of a reaction between $Cu_2MnSn_3S_8$ and 0.1M HNO_3 after 48 hours, indicated that the product had a resultant stoichiometry of $H_{0.37}Cu_{1.98}Mn_{0.82}Sn_3S_8$. This stoichiometry was consistent with the results seen with $Cu_2FeSn_3S_8$ in that only a small amount of copper was extracted from the parent spinel, with the transition metal, in this case manganese, being the more commonly exchanged atom. The manganese extraction in this case is greater than the extraction of iron under the same conditions. This leads to a significant amount of proton intercalation into the resultant product.

Proton-activated thiospinels are important candidates to consider as heavy metal ion extractants. These new materials provide an avenue by which exchange of intercalated protons can be compared to copper or transition metal in the parent spinel, or lithium in the lithiated spinels $Li_2FeSn_3S_8$ and $LiCuFeSn_3S_8$.

Conclusions

This chapter introduced the synthesis and characterization of new thiospinels based on the parent compounds $Cu_2FeSn_3S_8$ and $Cu_2MnSn_3S_8$. The first approach, as discussed previously in the literature, used chemical oxidation with iodine to extract copper from the structure as the result of oxidation of the transition metal from M^{2+} to M^{3+}. This produced compounds with very little structural change, as evidenced by powder X-ray diffraction and very little copper extraction, as evidenced by partial surface oxidation of manganese using X-ray photoelectron spectroscopy. In addition to small

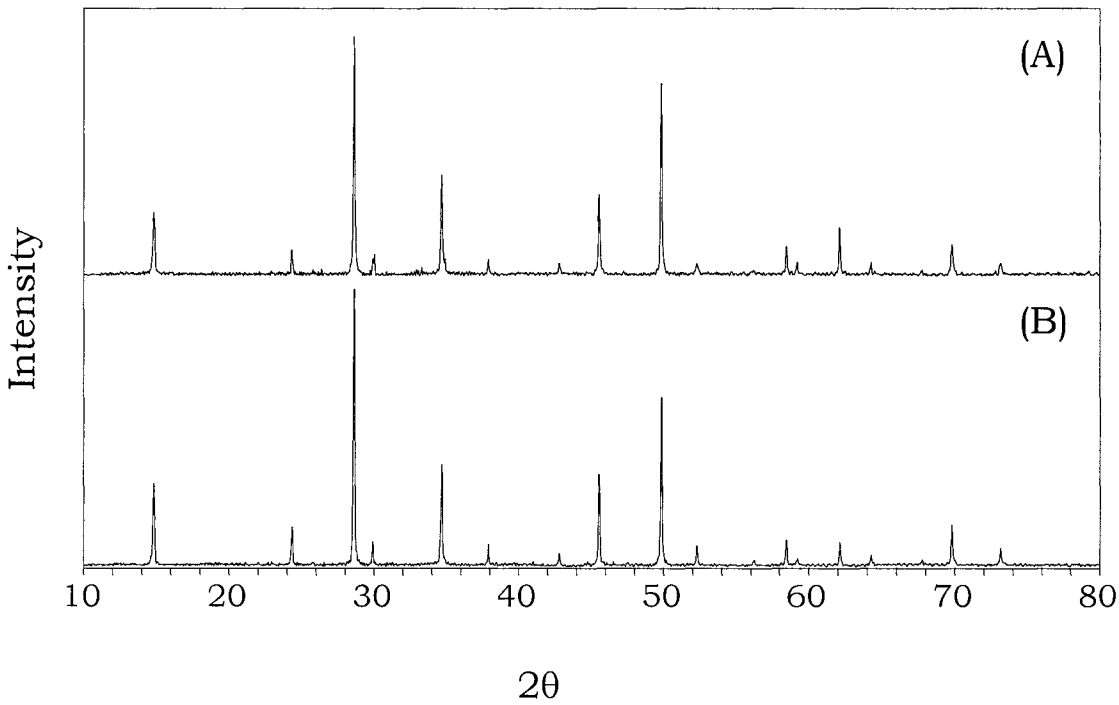

Figure 3.18 X-ray diffraction comparison of (A) $Cu_2FeSn_3S_8$ (parent) and (B) $H_xCu_yFe_zSn_3S_8$.

amounts of oxidation, these reactions were relatively slow (on the order of days) and were therefore concluded to be inefficient methods of creating new thiospinel materials.

Direct, solid state synthesis of cation deficient thiospinels yielded three novel compounds that crystallized with the spinel structure, $CuMnSn_3S_8$, $Cu_2Sn_3S_8$ and $Cu_2FeSn_3S_8$. Chemical reduction using $Na_2S_2O_4$ and *n*-butyllithium was also unsuccessful in producing spinels containing significant amounts of either sodium or lithium and, in the case of *n*-butyllithium, decomposition of the starting material resulted. Chemical techniques for introducing alkali metal cations into the spinel structure were also considered to be ineffective.

In order to introduce alkali metal cations into the solids, four new compounds were prepared using direct synthetic methods. These syntheses yielded the spinels $Li_2FeSn_3S_8$ and $LiCuFeSn_3S_8$, where lithium is believed to substitute into the tetrahedral vacancies previously occupied by copper, and a new compound with an as yet undetermined structure, $Na_2FeSn_3S_8$.

Finally, in a method similar to the protonation of $Li_{1.3}MoS_2$ to produce H_xMoS_2, the parent spinels $Cu_2MnSn_3S_8$ and $Cu_2FeSn_3S_8$ were contacted with acidic solutions of either 0.1M HNO_3 or 0.1M HCl. This caused extraction of small amounts of both copper and transition metal after periods as short as twenty four hours. No significant structural degradation was observed over this time period, indicating that an ion exchange reaction with protons produced a proton containing thiospinel, novel to this class of compounds. In Chapter IV, the relative extraction capabilities of the above mentioned compounds will be evaluated and compared.

References

1. Eisenberg, M., *Proc.-Power Sources Symp.* **1978**, *28th*, 155-157.
2. Eisenberg, M., *Journal of the Electrochemical Society* **1980**, *127*, 2382-2383.
3. Sinha, S.; Murphy, D.W. *Solid State Ionics* **1986**, *20*, 81-84.
4. James, A.C.P.W.; Goodenough, J.B.; Clayden, N.J. *Journal of Solid State Chemistry* **1988**, *77*, 356-365.
5. Spinels are also commonly referred to with the empirical formula AB_2X_4.
6. Schollhorn, R.; Payer, A. *Angewandte Chemie* **1985**, *24*, 67-68.
7. James, A.C.P.W.; Goodenough, J.B. *J. Power Sources* **1989**, *26*, 277-283.
8. Imanishi, N., et al., *J. Power Sources* **1993**, *43-44*, 619-625.
9. Lavela, P., et al., *J. Mat. Chem.* **1996**, *6*, 41-47.
10. Dedryvere, R., et al., *Electrochim. Acta* **2000**, *46*, 127-135.
11. Dedryvere, R., et al., *Chem. Mat.* **2000**, *12*, 1439-1445.
12. Elidrissi Moubtassim, M.L., et al., *Chem. Mat.* **1998**, *10*, 968-973.
13. Branci, C., et al., *Chem. Mat.* **1999**, *11*, 2846-2850.
14. Garg, G., et al., *Mat. Res. Bull.* **2001**, *36*, 2429-2435.
15. Garg, G., et al., *J. Solid State Chem.* **2001**, *161*, 327-331.
16. Liao, J.-H. and M.G. Kanatzidis, *Inorg. Chem* **1992**, *31*, 431-439.
17. Shriver, D.F.; Drezdzon, M.A. *The Manipulation of Air Sensitive Compounds*. 2nd. Ed.; Wiley-Interscience: New York, 1986.
18. The synthesis of $MnSn_3S_8$ was also attempted, in which manganese would be present as Mn^{4+}, however this product did not yield a crystalline product of a single phase.
19. Shannon, R.D., *Acta Crystallogr.* **1976**, *A32*, 751.

Chapter IV

Evaluation of Thiospinel Compounds as Heavy Metal Cation Extractants in Aqueous Solution

Introduction

In Chapter III, the thiospinels $Cu_2FeSn_3S_8$, $Cu_2MnSn_3S_8$ and novel analogs were introduced. Prior to this work, no ion exchange studies had been done on these types of compounds, nor had any cation other than lithium been inserted, post synthesis, into the thiospinel structure. This chapter describes an investigation of the aqueous ion exchange capabilities of the parent thiospinels $Cu_2FeSn_3S_8$ and $Cu_2MnSn_3S_8$ for different metal cations including $Hg^{2+}(aq)$, $Pb^{2+}(aq)$, and $Ag^{+}(aq)$ at different pH's and for varying lengths of time. The analysis will consider percent metal ion removal as a function of contact time, structural changes that occur as the result of ion exchange, the mechanism of ion exchange through mass balance experiments and finally, metal ion recovery. The relative capabilities and extraction systems of the derivatives described in Chapter III to those of the parent extractants will also be compared.

Experimental

Distilled water was purified and deionized (to 18 MΩ) with a Barnstead NANOPure purification system. Nitric acid (Mallinckrodt), hydrochloric acid (Mallinckrodt), and metal nitrate salts were reagent grade or better and were used as received. Extractants were prepared according to procedures described in Chapter III.

In a typical ion exchange experiment, a given solid was contacted with 20.0 mL of a $M(NO_3)_n$ solution in either 0.1M HNO_3 or deionized water in a capped, glass scintillation vial. Mixtures were prepared so that the initial extractant to metal ion ratio was either 1/1 or 5/1. The vials were constantly agitated at room temperature using a Labline shaker bath set at a shaking rate of 300. At the appropriate time, typically 24 hours, the extractions were filtered through 20 mL plastic syringes fitted with 0.2 μm, non-sterile surfactant-free cellulose acetate (SFCA) filters (Nalge Nunc International). The solid was rinsed with 20 mL of deionized water and dried under dynamic vacuum, without heating, overnight. Three replicate extractions were performed for each set of extraction conditions and a blank sample (metal ion solution with no ion exchange solid added) was run with each set.

The concentrations of metal ions were determined by inductively-coupled plasma atomic emission spectrometry (ICP-AES) using a Perkin-Elmer P400 ICP atomic-emission spectrometer equipped with a high salt nebulizer (the emission lines monitored were 670.781 nm for lithium, 589.592 nm for sodium, 324.754 nm for copper, 238.204 nm for iron, 257.610 nm for manganese, 189.989 nm for tin, 194.227 nm for mercury, 220.353 nm for lead, and 328.068 nm for silver. Calibration curves, which were linear in concentration over the range 1.00 to 0.0500 mM, were constructed using known concentrations of metal

salts in each particular aqueous solution studied. Matrix matching was used for all experiments. For each sample, five readings of the ICP-AES intensity were recorded and averaged.

Percent metal ion removed was calculated by subtracting the metal ion concentration of the sample, $[M^{n+}]_s$, from metal ion concentration of the blank (metal ion solution without extractant added), $[M^{n+}]_b$, divided by the blank metal ion concentration, multiplied by 100 % as described in Equation 4.1:

$$\text{Percent removed} = \left(\frac{([M^{n+}]_b - [M^{n+}]_s)}{[M^{n+}]_b} \right) \times 100\% \qquad (4.1)$$

The distribution coefficient, K_d (mL/g), is a figure of merit used to compare different extraction systems. The calculation of K_d , shown in Equation 4.2, takes into account the initial and final metal ion concentration; volume of waste solution, V; and mass of the extractant, m. An extractant with a high K_d (> 10,000) has a high selectivity for that metal ion. This occurs under a combination of conditions, including a very low final sample concentration, an extraction solution with a large volume, or when the mass of the extractant used is small. For the purposes of this dissertation, K_d values were single point determinations for a given set of conditions.

$$K_d = \left(\frac{([M^{n+}]_b - [M^{n+}]_s)}{[M^{n+}]_s} \right) \left(\frac{V}{m} \right) \qquad (4.2)$$

Mass balance experiments were performed in order to verify the ion exchange reaction by considering the initial and final concentrations of all metal ions in solution before and after the extraction. The metal ion concentrations were determined by ICP-AES analysis of the filtrate and included analysis of heavy metal ion, copper and transition metal. No tin was

detected in the filtrate of any extraction performed. The pH's of selected solutions were monitored using an Orion 720A pH meter.

Differential scanning calorimetry (DSC) data were collected on a TA Instruments 2920 Differential Scanning Calorimeter. Powdered samples were sealed in aluminum pans and heated at 10 °C/min under a flow of nitrogen. Thermogravimetric/mass spectroscopic analyses were performed on a TA Instruments 2950 Thermogravimetric Analyzer interfaced with a Balzers Thermostar Mass Spectrometer. The thermal unit was ramped at 10 °C/minute under a constant flow of He carrier gas. Evolved gasses were analyzed using multiple ion detection mode.

Results and Discussion

Ion Exchange at Neutral pH

$Cu_2FeSn_3S_8$ and $Cu_2MnSn_3S_8$ were found to remove Hg^{2+} and Ag^+ from solution. A representative plot of the percent Hg removed by $Cu_2FeSn_3S_8$ and $Cu_2MnSn_3S_8$ from solution versus time can be seen in Figure 4.1. The initial extractant to metal ion ratio used for both of these experiments was one to one. These ion exchange materials do not remove a considerable amount of mercury from solution, a maximum of 30% in the case of $Cu_2FeSn_3S_8$ and 60% in the case of $Cu_2MnSn_3S_8$, and at a significantly slower rate than the MoS_2 system, which is 100% complete within ten minutes.

As a comparison, $Cu_2FeSn_3S_8$ was also used to extract Pb^{2+}(aq), Ba^{2+}(aq), Mg^{2+}(aq) and Na^+(aq) from solution. After a 48 hour extraction with a five to one extractant to metal ion ratio, less than two percent of each metal ion was removed from solution. Since Ba^{2+}, Mg^{2+} and Na^+ are considered hard Lewis

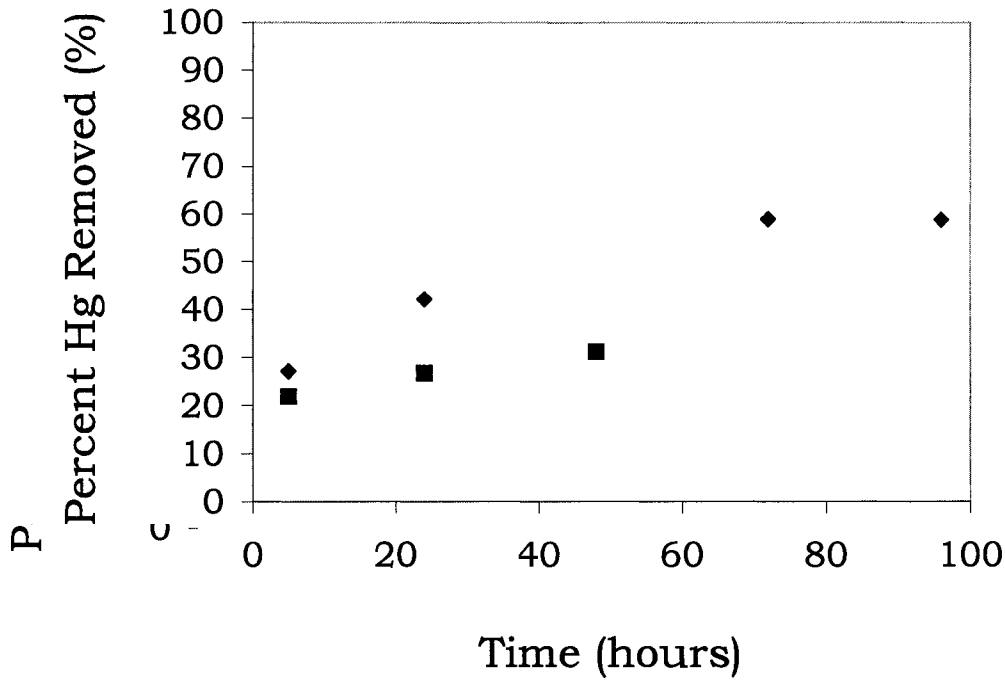

Figure 4.1 Hg^{2+}(aq) extraction as a function of time with $Cu_2FeSn_3S_8$ (squares) and $Cu_2MnSn_3S_8$ (diamonds).

acids, this result is not surprising. In the case of Pb^{2+}, however, which is considered a borderline soft Lewis base, the explanation for the low affinity is not clear. The ionic radius of Pb^{2+} (1.33Å, 6-coordinate) is significantly larger than that of Hg^{2+} or Ag^{+} (~ 1.1 Å for 6-coordinate mercury and 4-coordinate silver)[1] which could result in a diffusion barrier into the solid. It is possible that size is the limiting factor in the exchange of a cation as large as Pb^{2+}.

These initial experiments concluded that metal ion extraction with $Cu_2MSn_3S_8$ was not efficient. In order to explore the extraction process further and to understand the mechanism by which metal ion extraction was occurring, with the hope that an improved understanding of the mechanism of ion exchange would allow a rational approach to the improvement of the extractants, mass balance experiments were developed to investigate these systems. Figure 4.2 shows a bar graph comparing the number of μmoles of copper in the filtrate after extraction with the number of μmoles of mercury extracted from solution. It is clear from this figure that the charge equivalents of mercury removed from solution was not equal to the charge equivalents replaced into solution by Cu^{+} cations (assuming the exchange of one mercuric cation into the solid for two cuprous cations out of the solid). For this reason, new hypotheses had to be developed to explain these data.

Instead of an ion exchange reaction involving one mercuric cation and two cuprous cations, extraction of a $Hg(NO_3)^{+}$ ion pair could have occurred that would only require the exchange of one cuprous cation per $Hg(NO_3)^{+}$ exchanged into the solid. Similarly, a $Hg(NO_3)_2$ complex could have adsorbed to the sulfide rich surface of the material without ion exchange. This ion pair extraction behavior had been postulated in the Strauss and Dorhout laboratories using a MoS_2/sol-gel composite material for mercury extractions.[2] This would

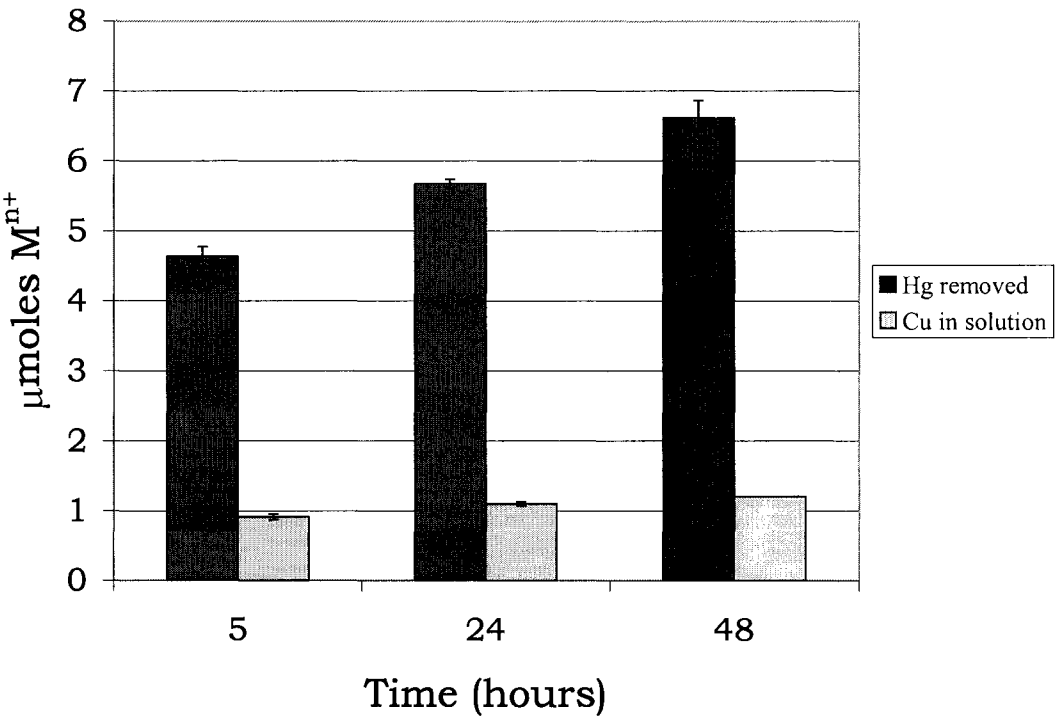

Figure 4.2 Comparison of $Cu^{+}(aq)$ in solution vs. $Hg^{2+}(aq)$ removed.

result in fewer copper equivalents present in the extraction filtrate than expected based on the equivalents of mercury extracted from solution, assuming a one to two mercury to copper ion exchange ratio.

A second possibility was that both copper and transition metal cation, Fe^{2+} in this case, were exchanging out of the solid. The mass balance equations would then involve the incorporation of some fraction of each type of exchange: two cuprous cations exchanging for one mercuric cation and one ferrous cation exchanging for one mercuric cation. The ion exchange equation and mass balance relationship are shown in Equations 4.3 and 4.4 assuming a one to one initial extractant to metal ion ratio and a 100% extraction of mercury from solution. This mechanism becomes more complicated when one considers the extraction of tin cations from the solid as a result of ion exchange. As noted in the Experimental section of this chapter, however, no tin was detected in any of the extraction mixtures analyzed over the course of this research. For this reason, tin will no longer be considered a potential exchangeable cation.

$$Cu_2FeSn_3S_8(s) + Hg^{2+}(aq) \longrightarrow HgCu_{2-x}Fe_{1-y}Sn_3S_8(s) + xCu^{+}(aq) + yFe^{2+}(aq) \qquad (4.3)$$

where $x + y = 1$

and $[Hg^{2+}] = \frac{1}{2}[Cu^{+}] + [Fe^{2+}]$ (4.4)

A third possible mechanism involved reduction of Hg^{2+} to Hg_2^{2+} or Hg^0 with concurrent oxidation of the spinel and expulsion of a copper cation in order to maintain charge neutrality. This reduction/oxidation scheme is explained with Equations 4.5 through 4.7.

Oxidation	$2Cu_2FeSn_3S_8 \longrightarrow 2CuFeSn_3S_8 + 2Cu^+ + 2e^-$	(4.5)
Reduction	$Hg^{2+} + 2e^- \longrightarrow Hg^0$	(4.6)
Overall	$2Cu_2FeSn_3S_8 + Hg^{2+} \longrightarrow 2CuFeSn_3S_8 + Hg^0 + 2Cu^+$	(4.7)

Reduction of Hg^{2+} to form Hg^0 was also seen in the MoS_2 system and can occur whenever a strong enough reducing agent is present along with Hg^{2+}.[3] With this mechanism, the equivalents of copper expelled from the solid was twice the number of equivalents of mercury extracted from solution and the mass balance experiments would not be able to distinguish this redox mechanism from ion exchange. Evidence for or against this mechanism could only be obtained using elemental analysis of the final solid using a technique such as XPS or a structural change upon substitution monitored by powder X-ray diffraction. If the mechanism for removal of mercury involved reduction of Hg^{2+} to Hg^0, there would be no evidence of this in the elemental analysis, nor should there be any structural change.

Another possibility, seen in the $H_2Zr(PSO_3)_2$ system, was the degradation of the parent structure to release sulfide with concomitant formation and precipitation of mercuric sulfide as described in Equation 4.8. This reaction would necessitate the expulsion of cations, copper for example, to maintain charge neutrality. Again, mass balance experiments would not be able to distinguish between this mechanism and an ion exchange mechanism without decomposition since the equivalents of copper in solution would be two times as large as the number of equivalents of mercury extracted.

$$Cu_2FeSn_3S_8(s) + Hg^{2+}(aq) \longrightarrow FeSn_3S_7(s) + HgS(s) + 2Cu^+(aq) \qquad (4.8)$$

It is important to note that Equations 4.5 through 4.8 are idealized situations in which only copper cations are released into solution, with the formation of single compounds such as $CuFeSn_3S_8$ or $FeSn_3S_7$. These reactions would most likely also involve the expulsion of both iron and tin cations and the formation of other binary and ternary sulfides involving different ratios of copper, iron, tin and sulfur. Evidence of these types of reactions would be seen in powder X-ray diffraction by the appearance of either mercuric sulfide or other metal sulfides.

An attempt was made to differentiate between these mechanisms with $Cu_2FeSn_3S_8$ by monitoring the concentrations of both copper and iron in the extraction filtrate as well as monitoring the diffraction pattern of the resultant solid for structural changes and XPS analysis for qualitative elemental analysis. Unfortunately, because of the low solubility of iron hydroxide in water at pH 5 under aerobic conditions, the concentrations of iron in the filtrates were difficult to monitor and were not representative of the amount of iron extracted from the solid. For this reason, the mass balance experiments from this point forward will discuss ion exchange reactions using $Cu_2MnSn_3S_8$.

In order reduce the possibility of a redox reaction from occurring, the contaminant metal ion of interest was changed to silver. Silver has a less favorable reduction potential than mercury (Ag^+/Ag^0 = 0.799 V; Hg^{2+}/Hg^0 = 0.852 V)[4] indicating that formation of silver is not as likely, based on the requirement of a stronger reducing agent. In addition, if silver metal were to form, evidence for this would be seen in the diffraction pattern of the final solid.

The results of mass balance experiments between $Cu_2MnSn_3S_8$ and $Ag^+(aq)$ are presented in Table 4.1. These data represent the molar equivalents of silver removed from solution and the combined equivalents of both copper and manganese replaced into solution after 5 and 24 hour extractions.

Table 4.1 Mass balance experiment monitoring $Ag^+(aq)$, $Cu^+(aq)$ and $Mn^{2+}(aq)$ cation movement into and out of the solid during $Ag^+(aq)$ extraction with $Cu_2MnSn_3S_8$.

	Contact Time (hours)	
M^{n+} (mmoles)	5	24
Ag^+ Into Solid	12.0(8)	19(1)
Cu^+ Out of Solid	2.5(4)	3.00(7)
Mn^{2+} Out of Solid	3.82(9)	7.2(2)

A bar graph comparing the molar equivalents of charge resulting from the exchanging cations (i.e. charge into the solid = $1x[Ag^{+}]$; charge out of the solid = $1x[Cu^{+}] + 2x[Mn^{2+}]$) can be seen in Figure 4.3. It is clear from the graph that the balance of charge equivalents into and out of the solid indicate an ion exchange reaction rather than ion pair extraction.

Powder X-ray diffraction was used to monitor the structural changes of the solid after extraction. If a redox mechanism were functioning, this technique would show the formation of Ag^{0} in the powder pattern. In addition to the presence of new Ag^{0} reflections, the relative reflection intensities would be unchanged after the extraction from the spinel phase.

A comparison of the powder X-ray diffraction patterns of $Cu_2MnSn_3S_8$ and $Ag_{1.9}Cu_{1.97}Mn_{0.93}Sn_3S_8$ (i.e. the product of a 24 hour extraction) can be seen in Figure 4.4. The first feature of the diffraction pattern in Figure 4.4A to be noted is the absence of any diffraction lines from elemental silver, the reference pattern for which is shown as stick pattern below the figure. In addition, the relative intensity of the 440 refection increased as compared to the relative intensity seen in the parent pattern. The 440 reflection is representative of a plane in the lattice containing the previously vacant 48*f* tetrahedral holes. This indicates that the silver atoms could fill tetrahedral holes in the structure. Finally, there appears to be a very small decrease in the relative intensities of the 111 and 151 reflections. These reflections are indicators of planes containing manganese atoms that are being removed from the structure as a result of ion exchange.

In addition to physical characterization by PXRD, XPS was used to qualitatively determine the presence of silver in the loaded extractant. Figure 4.5 shows the survey scan of a powder sample of $Cu_2MnSn_3S_8$ after a silver extraction. In addition to clear peaks arising from the presence of silver, there

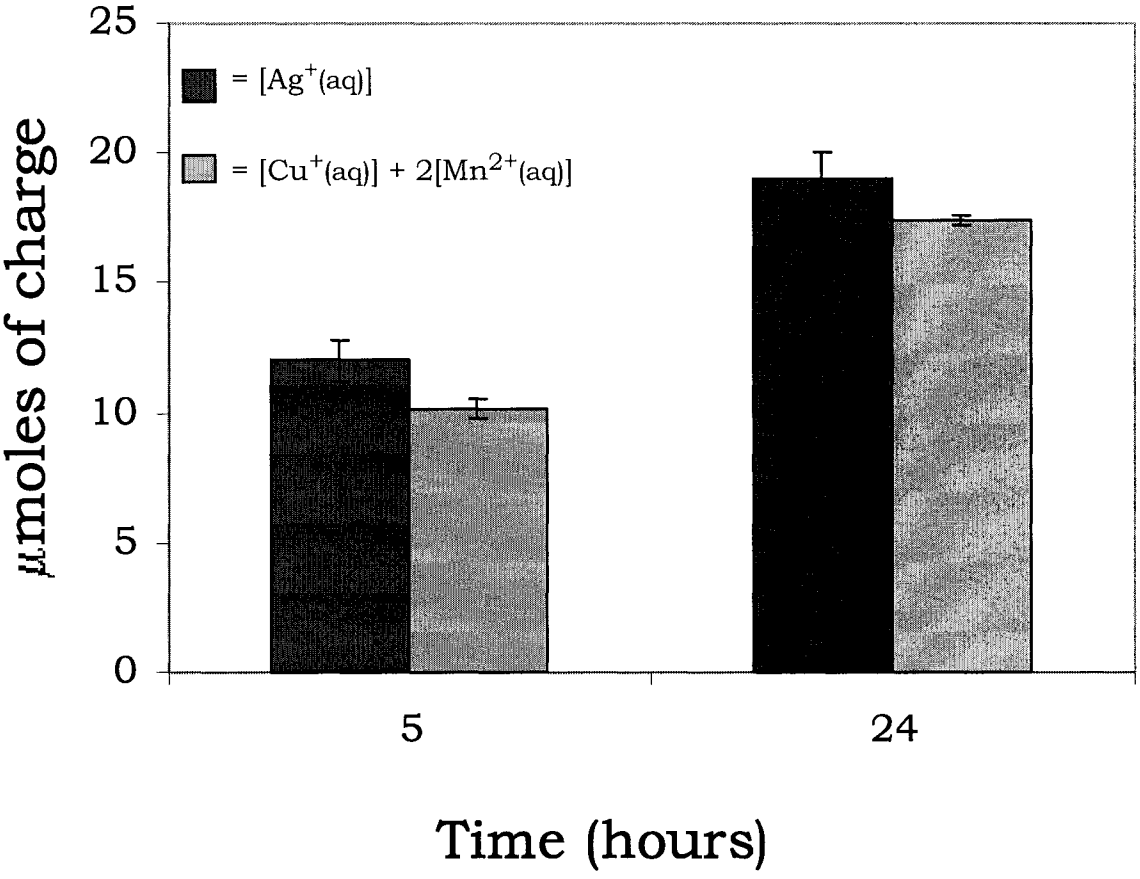

Figure 4.3 Mass balance analysis of $Cu_2MnSn_3S_8$ and $Ag^+(aq)$.

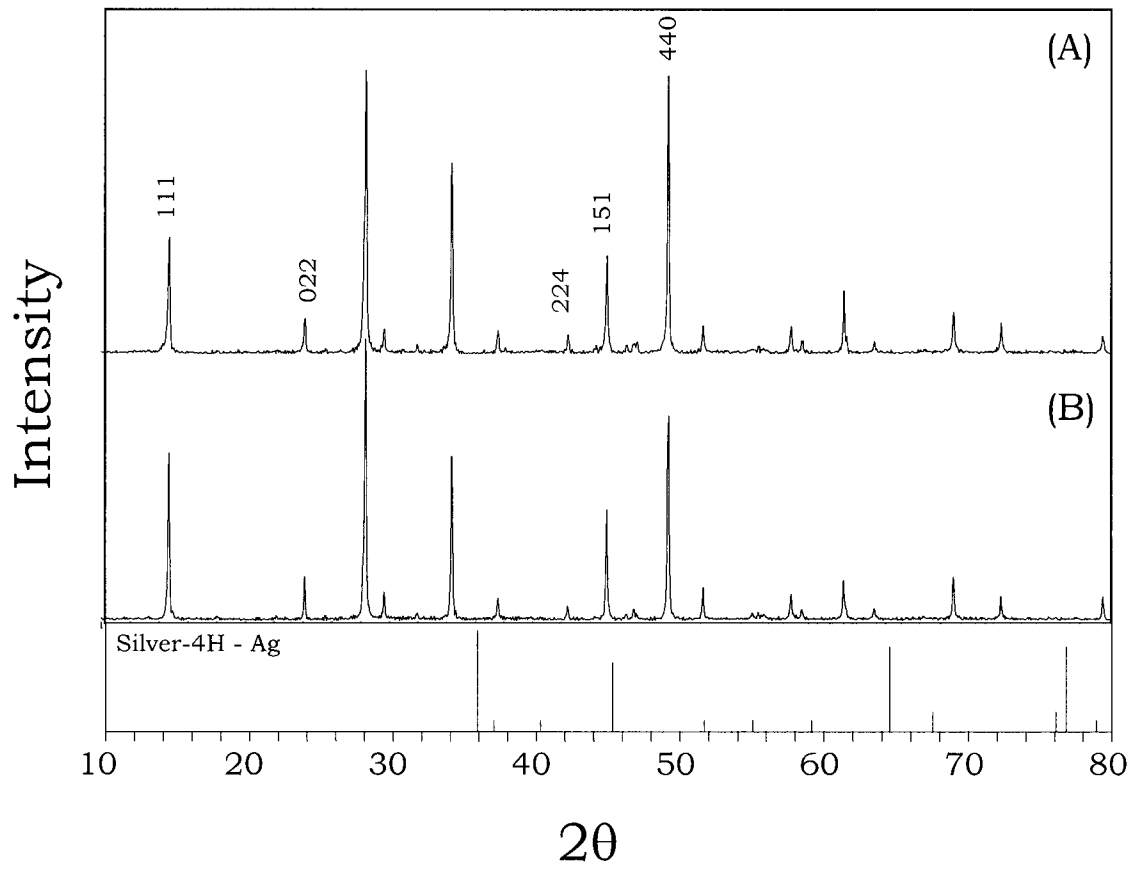

Figure 4.4 Powder X-ray diffraction analysis of (A) $Ag_{0.19}Cu_{1.97}Mn_{0.93}Sn_3S_8$ and (B) $Cu_2MnSn_3S_8$. Included is the Inorganic Crystal Diffraction Database (ICDD) standard file for the 4H phase of silver, # 41-1402.

did not appear to be any evidence for nitrogen, that would be present in the case of ion pair extraction of $AgNO_3$ (N1s ~ 407–408 eV).[5]

The ICP and XRD data combined can be used to construct a mass balance equation for this ion exchange reaction shown in Equation 4.9. It is interesting to note that the exchange of manganese appears to be favored over exchange of copper. This is most likely due to the chalcophillic nature of copper over manganese according to Goldschmidt's classification.[6, 7]

$$Cu_2MnSn_3S_8(s) + 0.19Ag^+(aq) \longrightarrow Ag_{0.19}Cu_{1.97}Mn_{0.93}Sn_3S_8(s) + 0.03Cu^+(aq) + 0.07Mn^{2+}(aq) \quad (4.9)$$

Ion Exchange at Low pH

In order to examine ion exchange with the extractant solid and extraction of heavy metal cations from solution with a pH = 1, similar extraction experiments were performed with a 1:1 extractant:mercury ion ratio in 0.1 M HNO_3. As can be seen in Figure 4.6, the final percentage of mercury extracted by $Cu_2MnSn_3S_8$ after 4 hours is significantly smaller than what was extracted from non-acidic media (15% vs. 60%). One hypothesis to explain this difference in the amount of mercury extracted from solution is the presence of competing exchange reactions between mercuric cations and protons, similar to the behavior in $H_2Zr(PO_3S)_2$ and $H_{0.78}MoS_2$. The affinity of $Cu_2MnSn_3S_8$ for protons was clear when $Cu_2MnSn_3S_8$ was contacted with nitric acid solutions (of pH ranging from 0 to 3) in the absence of metal ions. Ion exchange occurred between manganese cations in the solid and protons in solution and as a result, manganese was detected in the filtrate. The results of three experiments to determine the behavior of $Cu_2MnSn_3S_8$ in nitric acid can be seen in Figure 4.7.

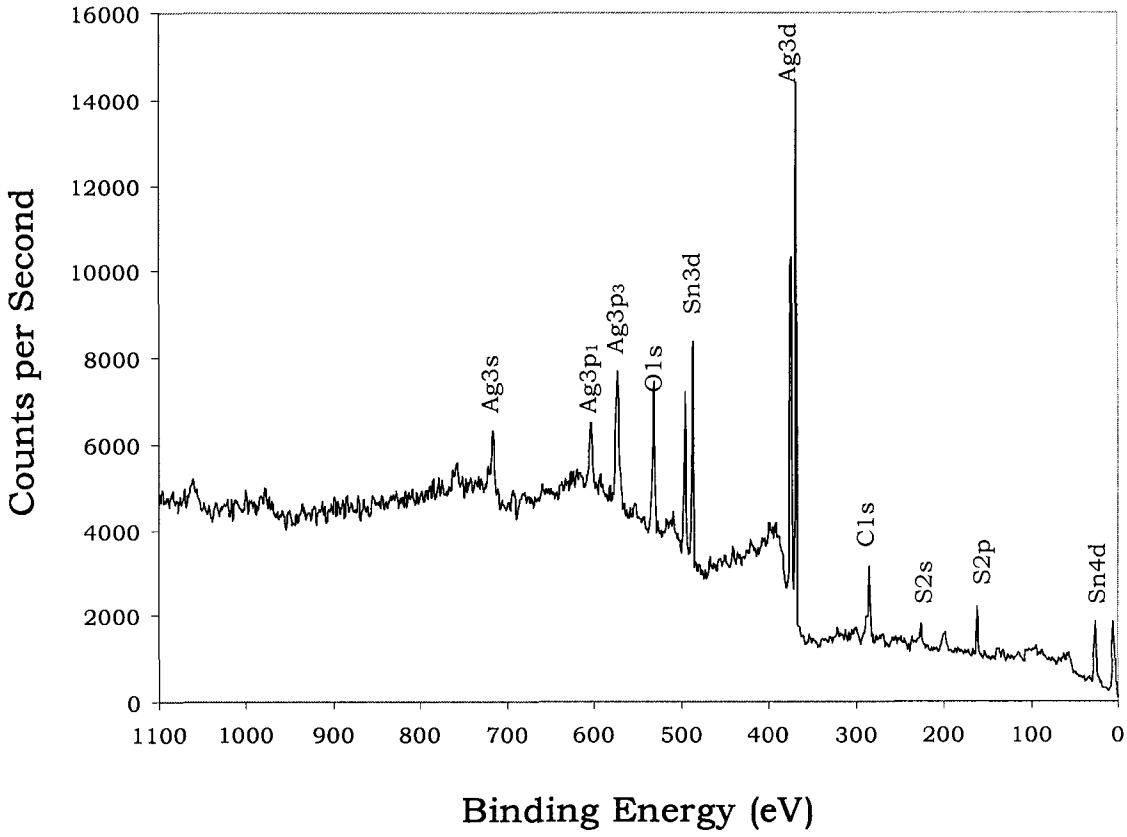

Figure 4.5 X-ray photoelectron spectra of $Ag_{0.19}Cu_{1.97}Mn_{0.93}Sn_3S_8$.

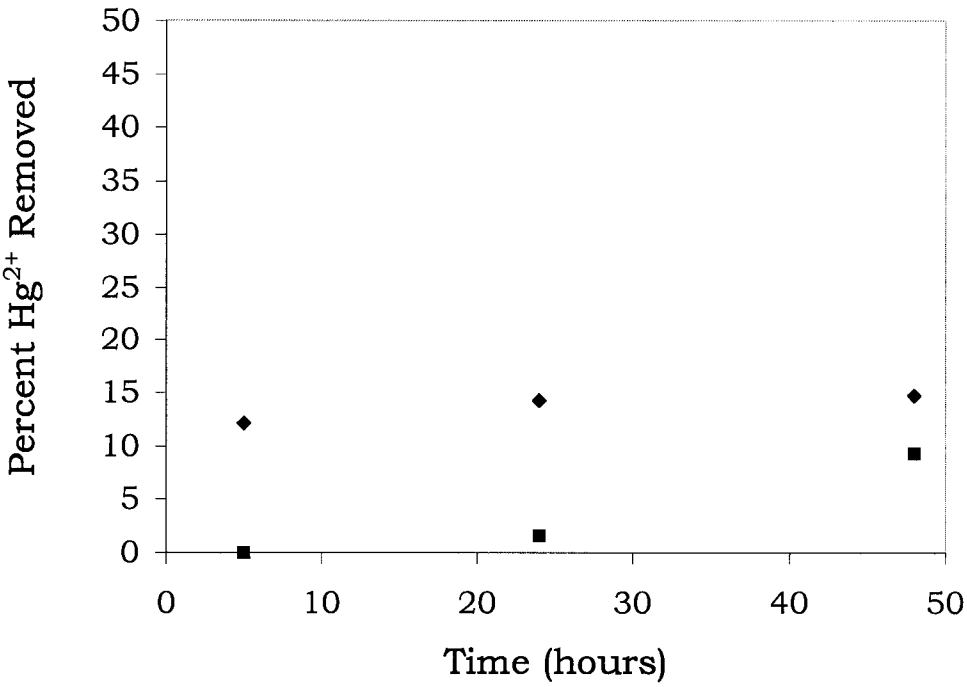

Figure 4.6 Hg^{2+}(aq) extraction as a function of time with $Cu_2MnSn_3S_8$ (diamonds) and $Cu_2FeSn_3S_8$ (squares) from 0.1M HNO_3

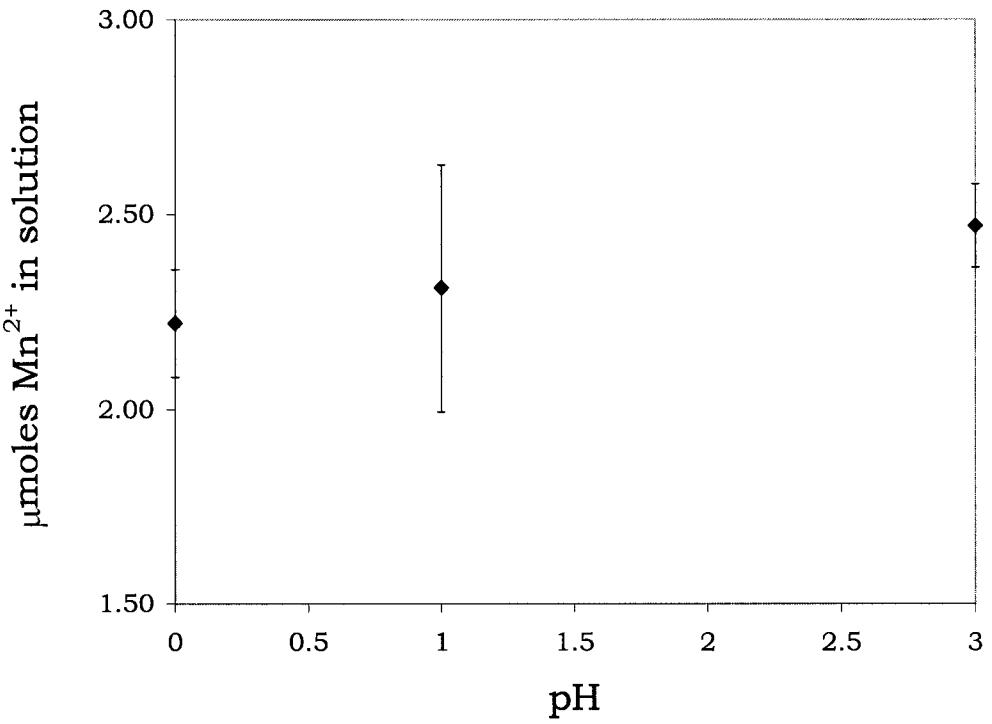

Figure 4.7 Removal of Mn from $Cu_2MnSn_3S_8$ in various concentrations of HNO_3

A reaction of this type, using 0.1M HNO_3 for 48 hours produced the material discussed in Chapter III, $H_{0.19}Cu_{1.97}Mn_{0.83}Sn_3S_8$.

The extraction capability decrease was also seen in mercury extractions using $Cu_2FeSn_3S_8$. In a five hour extraction, the level of mercury decreased from 22% in distilled, deionized water to 0% (within the error of the instrument) in 0.1M nitric acid. After 48 hours, only 9.6% of the mercury was extracted from solution as compared to 30% in d^2H_2O. These results were compared to those of $Cu_2MnSn_3S_8$ in Figure 4.6. Similarly, for silver extractions with $Cu_2FeSn_3S_8$, the percent metal ion removed ranged from 3% after a five hour extraction to only 12% after a 48 hour contact time.

The conclusion that can be drawn from the data collected from acidic metal ion extractions is that these materials do not make effective extractants for metal ions at low pH (i.e. relatively low ion extraction over long contact times). However, the formation of proton intercalated thiospinels was advantageous because it represented a new class of compounds to be tested as ion exchange extractants. An extractant that exchanges protons instead of transition metals generates a 'decontaminated' waste stream containing a more environmentally friendly cation than either manganese or copper. In addition, the available protons are smaller cations and less likely to experience diffusion barriers through the solid, potentially making metal ion extraction faster. Finally, the presence of a hard exchangeable cation such as a proton will provide a thermodynamic driving force according to hard/soft acid/base theory.

Metal Ion Removal Using Proton Activated Thiospinels

The ability of the proton-included (or activated) materials for removing metal ions from solution can be seen in Table 4.2. The most significant result

to note is the increased efficiency with which the proton activated compound, $H_{0.18}Cu_{1.90}Fe_{0.96}Sn_3S_8$ removed Hg^{2+}, Ag^{+}, Pb^{2+} and Ba^{2+} from solution as compared with the unactivated compound, $Cu_2FeSn_3S_8$. One of the challenges using $Cu_2FeSn_3S_8$ as an extractant, as noted in the previous section, is its relatively low extraction rates over long extraction times as compared with other extraction systems studied ($Li_{1.3}MoS_2$, for example). With only a five hour contact, $H_{0.18}Cu_{1.90}Fe_{0.96}Sn_3S_8$ removed five times as much mercury compared to $Cu_2FeSn_3S_8$. In addition, metal ions that had not been previously extracted by $Cu_2FeSn_3S_8$, such as Pb^{2+} and Ba^{2+} were removed by $H_{0.18}Cu_{1.90}Fe_{0.96}Sn_3S_8$. In the case of Pb^{2+}, the percent of metal ion extracted increased sixty-fold.

These data suggested that the exchange of protons out of the solid is thermodynamically favorable and the hypothesis that hard cations would exchange more effectively than softer ones was supported. In addition, the series of cations analyzed in Table 4.2 supported the hypothesis that this type of extractant, a soft Lewis base, would preferentially include soft Lewis acids over hard Lewis acids. Mercury and silver are considered soft Lewis acids and were extracted to the greatest degree. Lead and barium are best described as borderline and were extracted to a lesser degree than mercury or silver. Finally, magnesium, the hardest cation on the list, was not extracted to any considerable degree, even by $H_{0.18}Cu_{1.90}Fe_{0.96}Sn_3S_8$.

The increase in the amount of lead removed is most probably due a combination of thermodynamic and kinetic effects. The increased void space present in the lattice of $H_{0.18}Cu_{1.90}Fe_{0.96}Sn_3S_8$ due to removal of both copper and iron atoms from the structure, and replacement with small cations (protons), was large enough to allow incorporation of a larger cation. The lattice was also responsible for the faster extraction rate of other metal cations. By

Table 4.2 Percent removal and K_d comparison between $Cu_2FeSn_3S_8$ and the proton-activated analog, $H_{0.18}Cu_{1.90}Fe_{0.96}Sn_3S_8$. Values reflect percent metal ion removed after a five hour extraction with a 5:1 extractant to metal ion ratio.

	$Cu_2FeSn_3S_8$		$H_{0.18}Cu_{1.90}Fe_{0.96}Sn_3S_8$	
	Percent Removed(%)	K_d	Percent Removed (%)	K_d
Hg^{2+}	18	350	94	3800
Ag^{+}	5.4	14	> 99	$> 10^8$
Pb^{2+}	0.5	1	30	130
Ba^{2+}	1.5	4	34	140
Mg^{2+}	0.3	1	0.0	0

decreasing diffusion barriers through the solid, ion exchange was enhanced.

Mass balance studies were also used to monitor the ion exchange reaction of the proton activated thiospinels. Using a combination of ICP analysis and pH measurements of the aqueous solution before and after ion extraction, it was shown that the ion exchange equation describing the removal of silver ions using $H_{0.37}Cu_{1.98}Mn_{0.82}Sn_3S_8$ is:

$$H_{0.37}Cu_{1.98}Mn_{0.82}Sn_3S_8(s) + 0.20Ag^+(aq) \longrightarrow$$
$$Ag_{0.20}H_{0.25}Cu_{1.93}Mn_{0.82}Sn_3S_8(s) + 0.12H^+(aq) + 0.05Cu^+(aq) \qquad (4.10)$$

This experiment confirms that silver ion extraction using the proton activated manganese compound was as effective as was shown for the iron analog. This equation also verifies that the majority of silver extracted in this system was removed with the exchange of one equivalent of protons (accounting for approximately 60% of the ion exchange) as was also postulated in the case of $H_{0.18}Cu_{1.90}Fe_{0.96}Sn_3S_8$. A small amount of copper was also exchanged out of the solid but no manganese was detected in the filtrate. These data counter extraction experiments previously discussed with $Cu_2MnSn_3S_8$. In Equation 4.9, more manganese was exchanged than copper, indicating that the exchange for manganese was more favorable. In the proton activated thiospinel, however, copper was the favored cation. This is probably due to the decreased concentration of manganese on the surface of the extractant particles. The depletion of manganese occurred during the formation of $H_{0.37}Cu_{1.98}Mn_{0.82}Sn_3S_8$ when more manganese was initially exchanged out of the solid than copper.

Metal Ion Removal Using New Spinel Derivatives:

$A_2FeSn_3S_8$ and $ACuFeSn_3S_8$ (A = Li, Na)

As described in Chapter III, novel spinel derivatives were synthesized using high temperature solid state techniques, similar to those used in the synthesis of the parent spinels. This method was used to create analogs to the $Cu_2MSn_3S_8$ solids containing hard Lewis acids such as lithium and sodium. It was shown in the previous discussion that substitution of protons for both copper and transition metal atoms greatly decreased the time required for ion exchange and also improved the ability of the extractant to remove certain metals such as Pb^{2+}(aq) and Ba^{2+}(aq) from solution. This hypothesis was suggested to explain the behavior of the increased extraction abilities of $A_2FeSn_3S_8$ and $ACuFeSn_3S_8$.

These four compounds behave somewhat differently during mercury extractions than the spinel compounds described to this point. Upon contact with a 1mM Hg^{2+}(aq) aerobic solution, $Li_2FeSn_3S_8$ appeared as a fine brown powder that was significantly harder to filter from solution than other extractants. ICP analysis of the filtrate indicated that 65.6% of the mercury had been extracted. Interestingly, however, all of the lithium was found to be concentrated in the filtrate. This was more than five times the amount of lithium needed to account for the extraction of Hg^{2+}(aq). In addition, the pH of the solution after extraction was approximately ten (using ColorpHast Indicator strips).

Figure 4.8 shows the powder diffraction analysis comparison of $Li_2FeSn_3S_8$ before and after a mercury extraction. Figure 4.8B indicates a decrease in the lattice parameter, a, of the mercury loaded material from approximately 10.48 Å to 10.25 Å. An increase in the intensity of the 111

reflection indicates mercury incorporation into the solid. From this diffraction analysis there did not appear to be any structural degradation of the solid, contrary to what was suggested by the pH and lithium concentration data. One can propose a redox-reaction for this extraction process whereby $Li_2FeSn_3S_8$ was a strong enough reducing agent to reduce water as proposed in Equation 4.11.

$$Li_2FeSn_3S_8 + 2H_2O \longrightarrow H_2 + 2OH^- + 2Li^+ + \square_2FeSn_3S_8 \quad (4.11)$$

When a smaller extractant to metal ion ratio was used (3:1), this problem apparently disappeared, including the fact that the solution was no longer difficult to filter and mercury extraction was greater than 99%. However, the pH of the resultant solution was also high (~ 10), indicating that the redox mechanism was still likely.

In the case of $LiCuFe_3Sn_3S_8$, mercury extraction with a 5:1 extractant to metal ion ratio after five hours was also >99%. The X-ray diffraction analysis of this system before and after mercury extraction is shown in Figure 4.9. Again, a decrease in the lattice parameter from 10.39 Å to 10.20 Å is seen. This change of ~ 0.2 Å is similar to that seen with $Li_2FeSn_3S_8$. The solid did not exhibit line broadening, decreases in absolute intensities, or new phases that would indicate decomposition. The lithium ion concentration found in the filtrate was more than would be expected from a simple ion exchange reaction with Hg^{2+}. Therefore, although there was no visible structural degradation of this solid, it is likely that oxidation was still occurring.

Both $Na_2FeSn_3S_8$ and $NaCuFeSn_3S_8$ were analyzed for their ability to extract mercury from solution. The results of the extraction experiments of $Hg^{2+}(aq)$, $Pb^{2+}(aq)$ and $Ag^+(aq)$, after a five hour contact, with a 5/1 extractant to

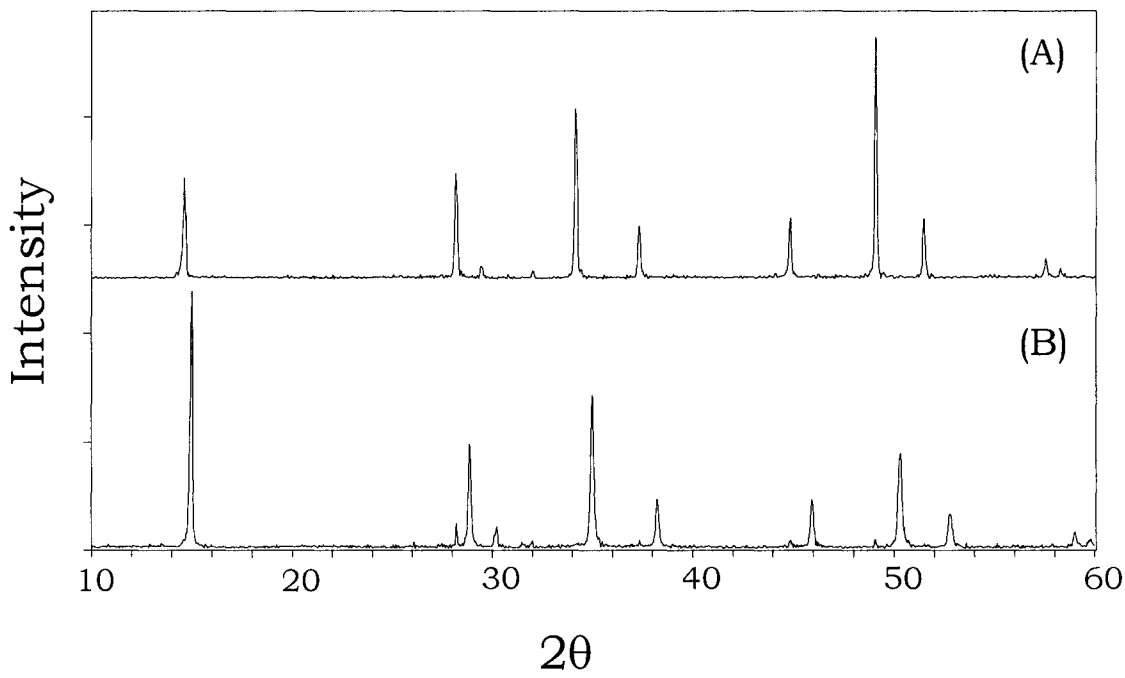

Figure 4.8 Powder X-ray diffraction comparison of (A) $Li_2FeSn_3S_8$ and (B) Hg-loaded $Li_2FeSn_3S_8$.

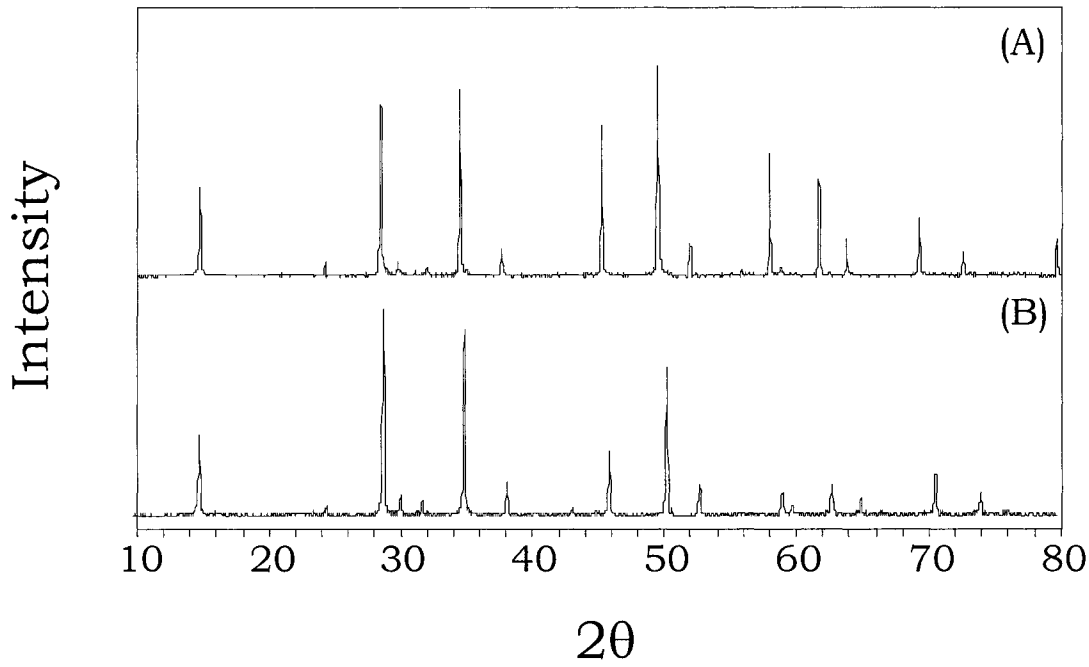

Figure 4.9 Powder X-ray diffraction comparison of (A) $LiCuFeSn_3S_8$ and (B) $Hg_{0.2}Cu_xFe_ySn_3S_8$.

metal ion ratio, including percent ion removal and K_d values are shown in Table 4.3. From these data it can be seen that both $Na_2FeSn_3S_8$ and $NaCuFeSn_3S_8$ were effective at removing these three soft metal ions from aqueous solution.

The extraction results between $Na_2FeSn_3S_8$ and $NaCuFeSn_3S_8$ are comparable, due to the fact that the sample of $NaCuFeSn_3S_8$ is actually a mixture of $Na_2FeSn_3S_8$ and $Cu_2FeSn_3S_8$ (see Chapter III). Because $Cu_2FeSn_3S_8$ had been shown to be relatively ineffective at removing $Hg^{2+}(aq)$, $Pb^{2+}(aq)$, and $Ag^{+}(aq)$ from solution in a five hour time period, it can be assumed that the active extractant in $NaCuFeSn_3S_8$ is actually $Na_2FeSn_3S_8$.

The powder X-ray diffraction analysis of the mercury, lead and silver extractions using $Na_2FeSn_3S_8$ are compared to the starting material in Figure 4.10. From this, it can be seen that most of the reflections present in the parent material above $2\theta = 20°$ weaken in intensity upon metal ion extraction; however, the three low angle reflections remain, with consistent relative intensities. In addition, the reflection at $2\theta = 10.3°$ (d = 8.59 Å) shifts to a smaller value by approximately 0.1 degrees. This corresponds to a d-spacing increase of 0.1 Å.

None of the patterns exhibit any evidence for the formation of metal sulfides (i.e. Ag_2S, HgS, or PbS) and the conclusion from this is that the compound is not significantly decomposing upon exposure to these cations. Unfortunately, as is the case with the parent compound, the diffraction patterns of the metal ion-included phases cannot be matched to any known compounds.

A similar behavior was observed in the structural changes of $NaCuFeSn_3S_8$, as would be expected. The powder diffraction patterns of mercury loaded $NaCuFeSn_3S_8$ and that of the parent structure are shown in Figure 4.11. This comparison shows that the reflections resulting from the

Table 4.3 Percent removal and K_d comparison of $Na_2FeSn_3S_8$ and $NaCuFeSn_3S_8$. Values reflect percent metal ion removed after a five hour extraction with a 5:1 extractant to metal ion ratio.

	Hg^{2+}		Pb^{2+}		Ag^{+}	
Extractant	Percent Removed (%)	K_d	Percent Removed (%)	K_d	Percent Removed (%)	K_d
$Na_2FeSn_3S_8$	97	8000	99	25000	98.3	16500
$NaCuFeSn_3S_8$	97	8700	99.9	25200	96.1	6530

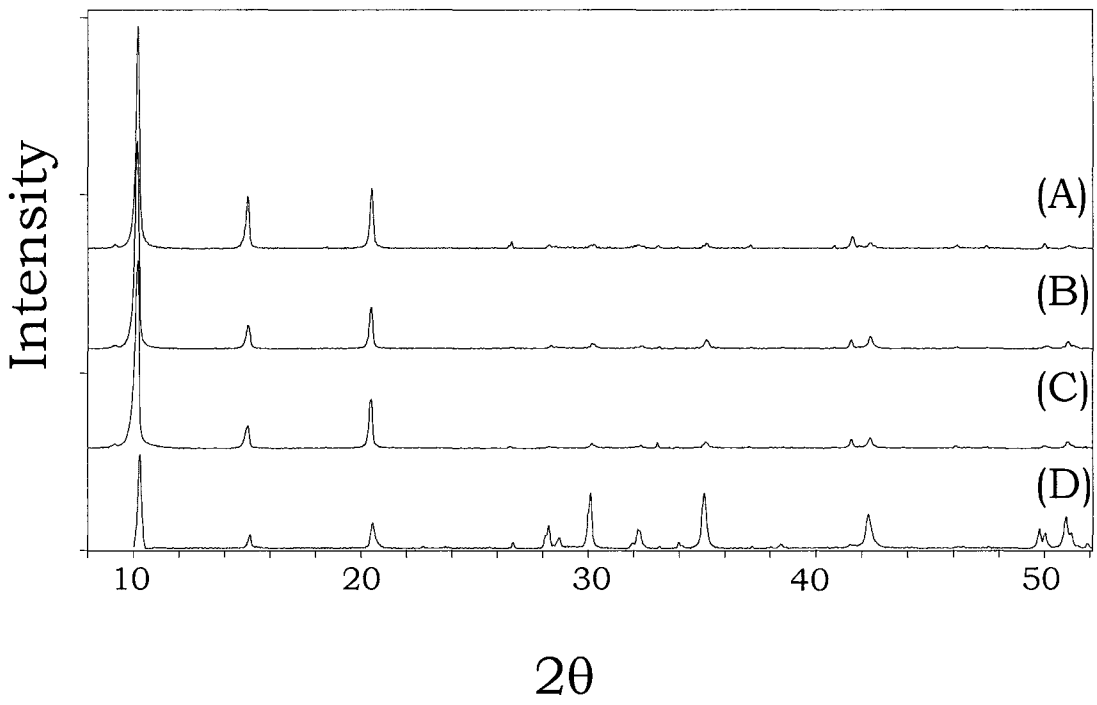

Figure 4.10 Powder X-ray diffraction comparison of (A) Ag-loaded $Na_2FeSn_3S_8$ (B) Hg-loaded $Na_2FeSn_3S_8$ (C) Pb-loaded $Na_2FeSn_3S_8$ and (D) $Na_2FeSn_3S_8$.

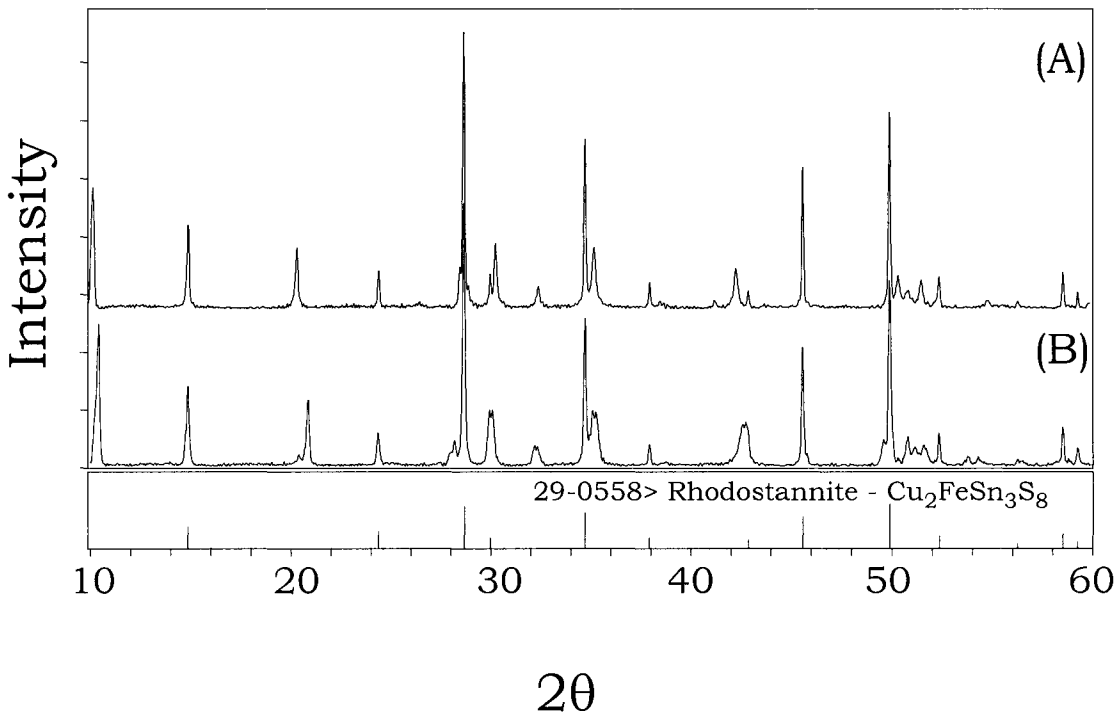

Figure 4.11 Powder X-ray diffraction comparison of (A) Hg-loaded $NaCuFeSn_3S_8$ and (B) $NaCuFeSn_3S_8$.

thiospinel $Cu_2FeSn_3S_8$ were not affected by contact with mercuric cations. Both the positions and relative intensities of these reflections remained constant. This is not unexpected, however since there was relatively little change in the structure of this pure phase upon contact with mercury, as previously described.

The reflections representing the $Na_2FeSn_3S_8$ phase have shifted to lower values of 2θ by approximately 0.1 degrees and indicate that the lattice parameter increased to a value near that of the 'pure' phase of $Na_2FeSn_3S_8$, previously described. In this case, the reflections at higher values of 2θ did not weaken significantly, but broadening occurred, indicating that the material was, in fact, becoming less crystalline.

Thermal Analysis/Recyclability Data

In Chapter II, the recovery of heavy metal from the loaded extractant described for the MoS_2 system included heating M_xMoS_2 to release elemental metal. The metal ion loaded materials described in this chapter were heated in a similar manner to determine their behavior under elevated temperatures and to see if metal ion recovery was possible through heating. The parent thiospinels prior to metal ion intercalation were found to be thermally stable. The thermal gravimetric analysis of a mercury loaded sample of $Cu_2MnSn_3S_8$, shown in Figure 4.12, however exhibits three main thermal events, the first at 178 °C due to water loss and the second and third at 287 °C and 348 °C due to loss of mercury. The two latter mass losses were confirmed to be loss of mercury by mass spectroscopy, monitored at 200.59 amu. XPS also confirmed loss of mercury from the surface of the solid, as seen in Figure 4.13. The Hg4f lines that were present in the sample after mercury extraction (Figure 4.13B)

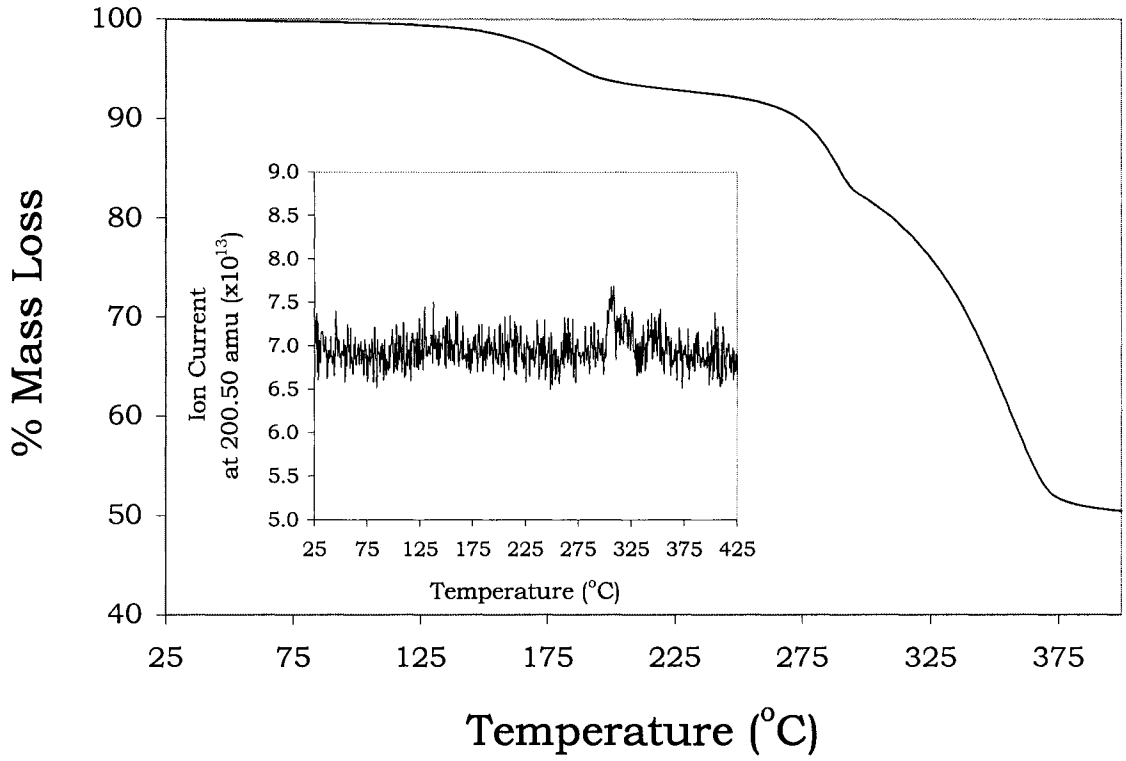

Figure 4.12 Thermal gravimetric analysis of Hg-loaded $Cu_2MnSn_3S_8$. Inset plot shows concurrent mass spectrum monitored at 200.59 amu during TGA scan.

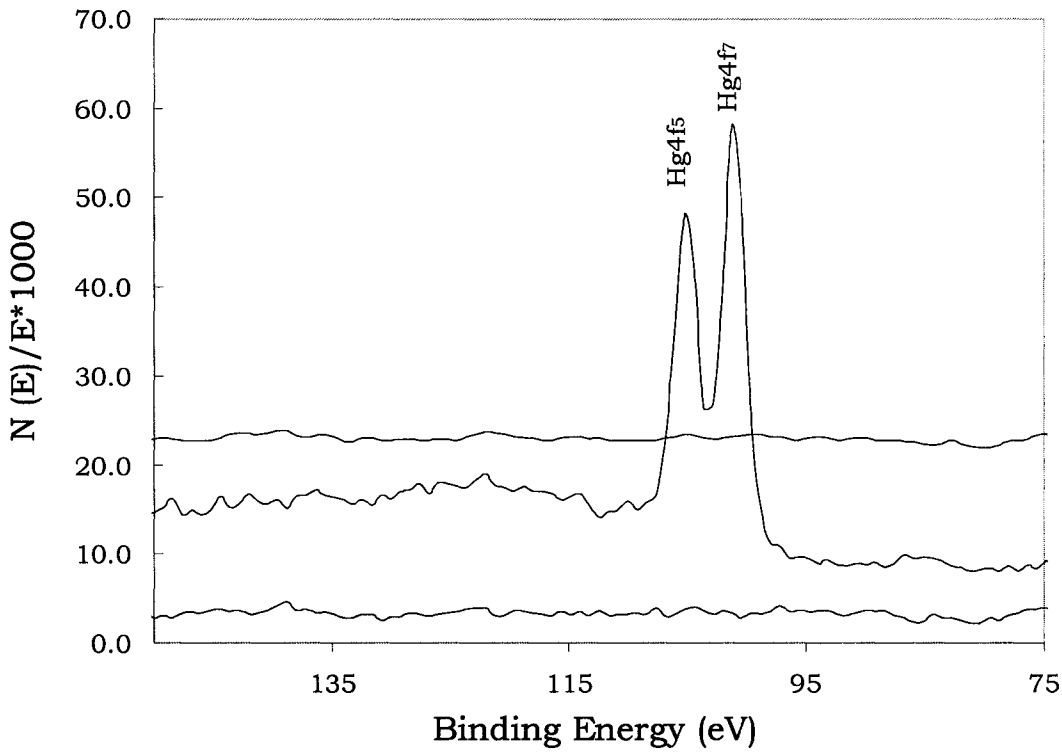

Figure 4.13 X-ray photoelectron spectra of Hg4f lines (A) $Cu_2MnSn_3S_8$ (B) $Cu_2MnSn_3S_8$ after Hg^{2+} exchange (C) $Hg_xCu_yMn_zSn_3S_8$ after heating to 500 °C.

were absent after heating to 500 °C (Figure 4.13C). This qualitatively shows the presence and absence of mercury through a heating cycle.

In the case of silver, the only thermal event apparent in the TGA (Figure 4.14), was the loss of water. This did not provide any information regarding the formation of Ag^0, however, because if silver metal had been formed, no mass loss was expected. The XPS analysis of the silver loaded solid after heating showed the disappearance of silver from the solid. The fact that silver was not found in the XPS is further evidence for its presence as reduced silver. If no redox reaction had occurred, the XPS spectrum would remain unchanged and would resemble that of Figure 4.5. The absence of the main silver peak at 370 eV indicated the formation of small particles of Ag^0 that, because of their physical location in the sample, were not detected by the XPS beam.

Further evidence for the deintercalation of silver from the structure came from the diffraction analysis of the heated material. Previously, silver metal ion intercalation had been evidenced by an increase in the relative intensities of the 440 and 004 reflections (see Figure 4.4). In Figure 4.16, the 440 reflection shows a decreased intensity compared to the 113 as does the 004 compared to the 151. This is evidence of reversion of the structure to $Cu_2MnSn_3S_8$.

This thermally-induced reduction of the target metal cation was also observed with the lithiated thiospinel, $LiCuFeSn_3S_8$. Figure 4.17 shows a comparison of three X-ray diffraction analyses of this extractant, $LiCuFeSn_3S_8$ before mercury extraction, after extraction and the changes in the structure that occur after heating the mercury loaded solid to 500 °C. The only small change that could be seen in the structure of this solid was an increase in the unit cell parameter of the material from the mercury loaded solid (10.200(2) Å) to 10.260(1) Å. This increase is a reversion back to the original cell parameter of 10.394(2) Å.

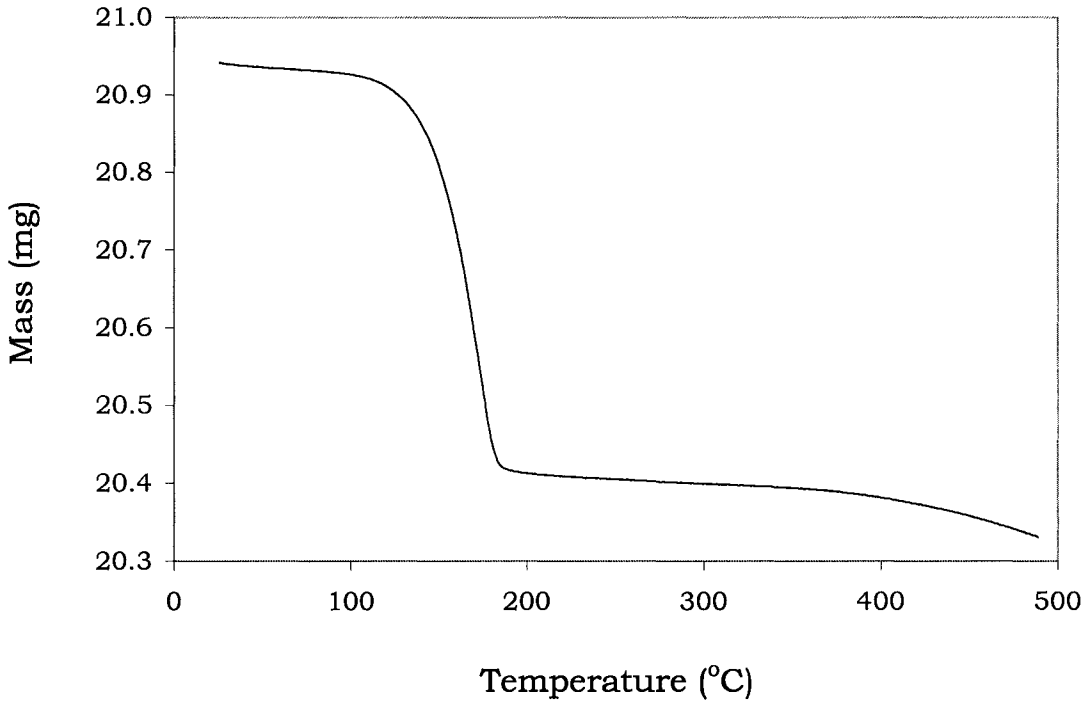

Figure 4.14 Thermal gravimetric analysis of Ag-loaded $Cu_2MnSn_3S_8$.

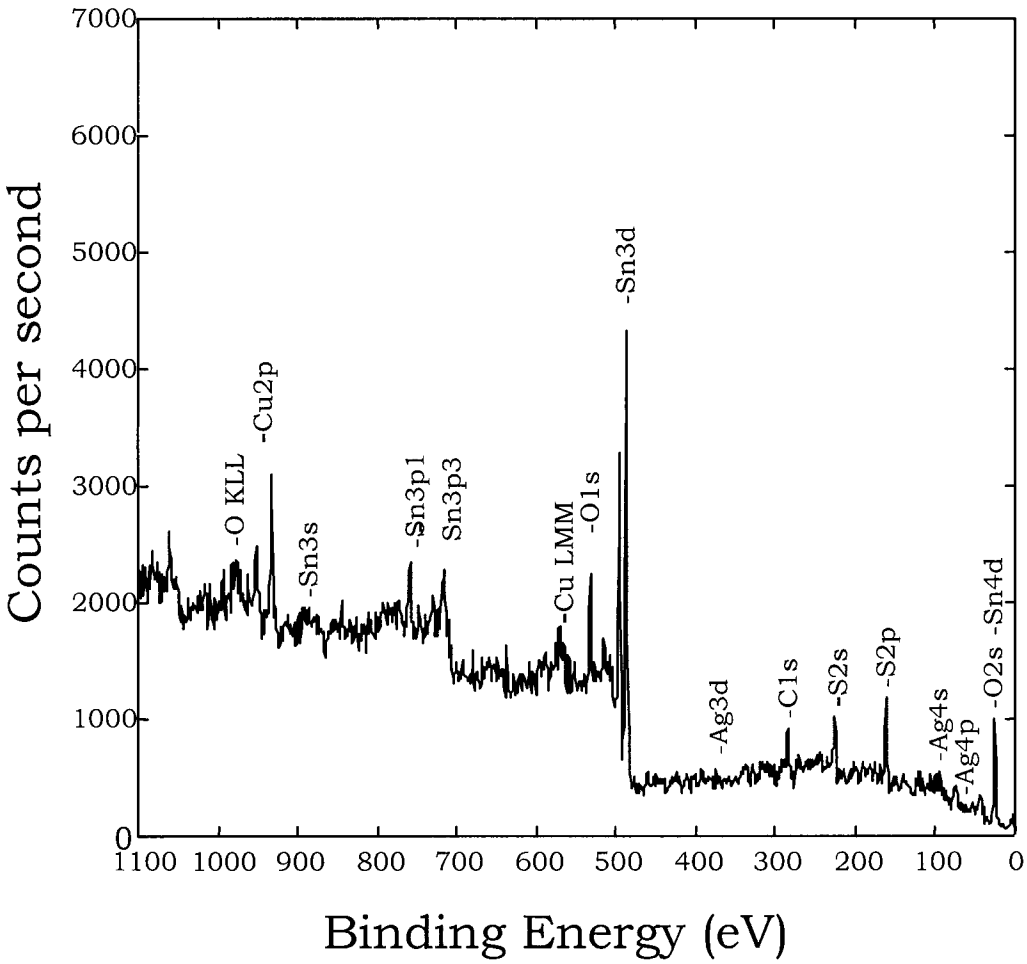

Figure 4.15 X-ray photoelectron spectrum of heat treated Ag-loaded $Cu_2MnSn_3S_8$.

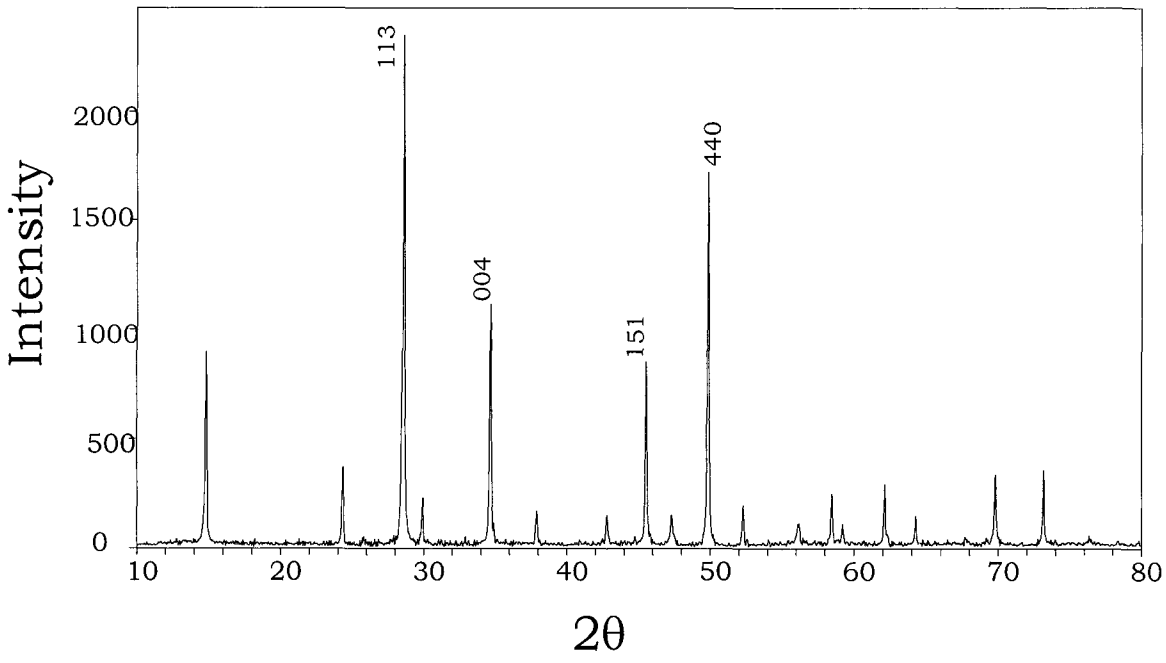

Figure 4.16 X-ray diffraction analysis of heat treated Ag-loaded $Cu_2MnSn_3S_8$.

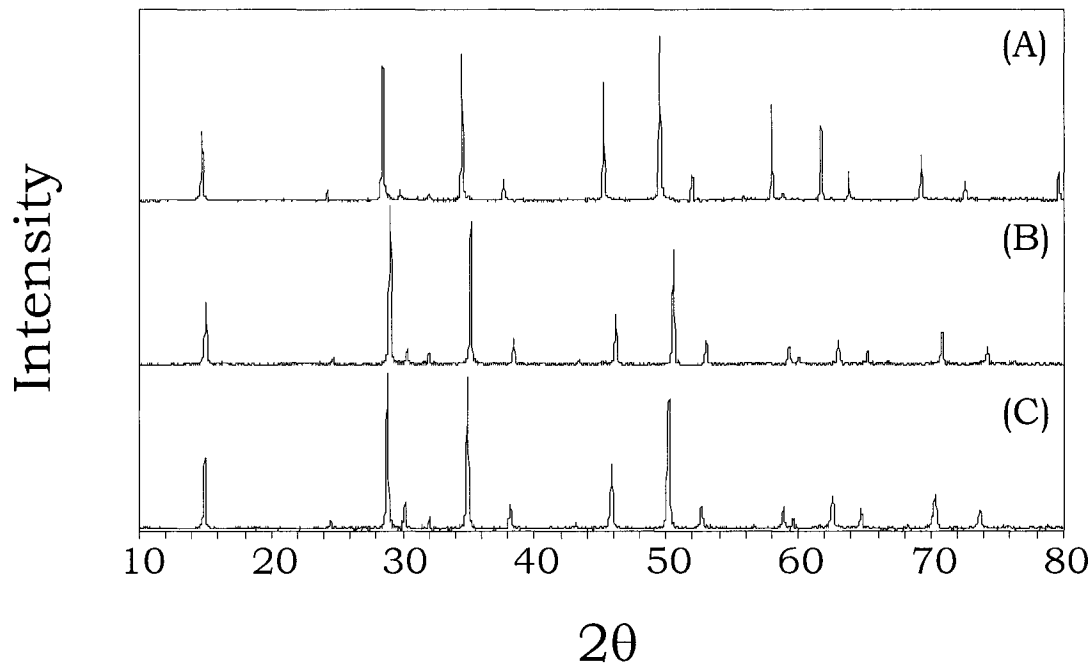

Figure 4.17 Powder X-ray diffraction comparison of (A) $LiCuFeSn_3S_8$ (B) $Hg_{0.2}Cu_xFe_ySn_3S_8$ and (C) $Hg_{0.2}Cu_xFe_ySn_3S_8$ after heating to 500 °C.

All of these data combines to indicate that thermal treatment to 500 °C is a viable method for deintercalating and recovering the target metal ion from the loaded solids. This method, as discussed in Chapter II is an inexpensive way reduce the secondary waste produced with this extractant to the smallest volume possible as well as to recycle the extractant through multiple extraction cycles.

Conclusions

This chapter discussed the viability of using various thiospinels as extractants for aqueous soft metal cations. It was found that the parent spinels were the least effective extractants synthesized, removing small percentages of the metal ion after relatively long extraction times. It was shown, however, using a combination of mass balance experiments and powder X-ray diffraction analysis that the mechanism of ion removal is ion exchange. Furthermore, this ion exchange involves both copper and transition metal. This exchange also produces a decontaminated waste stream that is newly contaminated with both copper and transition metal, which is considered to be another unattractive extraction cycle characteristic.

For these reasons, new thiospinels were derived and tested under similar conditions. The most promising extractants are the proton activated thiospinels, in that they have been shown to remove relatively more metal ion on a shorter time scale. In addition, these new thiospinels extract some metals, such as $Pb^{2+}(aq)$ that were not extracted by $Cu_2MnSn_3S_8$ or $Cu_2FeSn_3S_8$. The mechanism of metal ion extraction with the proton activated thiospinels was also shown to be ion exchange, with protons exchanging for the majority of metal ion cations. This is also an advantage because is inserts a relatively

innocuous cation into the decontaminated waste. Finally, the synthesis of the proton activated materials is easy and inexpensive.

The thiospinels $A_2FeSn_3S_8$ and $ACuFeSn_3S_8$ also removed significantly more metal cation than the parent thiospinels, however the mechanism of metal ion extraction was not clear. In the case of the lithiated compounds, structural degradation did not seem to occur, however mass balance experiments did not exhibit equivalent amounts of lithium exchanged out of the solid for the amount of mercury that was removed from solution (based on a 2:1 exchange). In addition, the increase in pH of the solution after ion exchange indicated reduction of water. The sodium compounds also removed significant quantities of metal ion from solution, however again, the mechanism by which this removal occurred was not clear. The further complication of inadequate structural characterization of the parent material made this system difficult to analyze.

Finally, it was shown that metal ion recovery was achieved by heating the sample to 500 °C. In the case of mercury, this resulted in the release of mercury vapors that could be collected. In the case of silver, structural analysis and X-ray photoelectron spectroscopy indicated the formation of silver metal. The resulting solids also maintained their structural integrity, indicating that reuse through multiple extraction cycles. This thermal behavior was observed with both the parent thiospinels as well as with one of the analogs, $LiCuFeSn_3S_8$.

References

1. Shannon, R.D., *Acta Crystallograpia* **1976**, *A32*, 751.
2. Hufford, F.D. Colorado State University, Fort Collins, CO, unpublished work.
3. Gash, A.E., Lithium Intercalated Transition Metal Chalcogenides as Redox-Recyclable Extractants and Synthesis and Characterization of Group IVB Metal Bis(Hydrogen Monothiophosphate) Compounds, Ph.D. Thesis, Colorado State University, Fort Collins, CO, 1999.
4. Harris, D.C., *Quantitative Chemical Analysis*. 3rd Edition. Ed.; W.H. Freeman and Company: New York, 1991.
5. Moulder, J.F., et al., *Handbook of X-ray Photoelectron Spectroscopy*. J. Chastain and R.C. King, Jr., Ed.; Physical Electronics, Inc.: Minnesota, 1995,
6. Shriver, D.F.; Atkins, P.; Langford, C.H. *Inorganic Chemistry*. 2nd Edition.; W.H. Freeman and Co.: New York, 1994.
7. Goldschmidt, V.M., *Geochemistry*. Muir, A. Ed.; Oxford University Press: London, 1958 (Reprinted from the corrected sheets of the first edition, 1954).

Chapter V

Extractant System Evaluations and Conclusions

The overall goal of this research was the investigation and development of extraction systems for the selective removal of soft heavy metal contaminant cations. The ideal system would satisfy a long list of requirements including: the elimination or reduction of hazardous reactants or byproducts from the synthetic or extraction step of the extraction cycle; completion of the extraction process on a short time scale (hours to a few days); stability under a variety of experimental conditions including structural, thermal, and oxidative stability as well as stability in a variety of different waste streams (i.e. acidic or basic, high concentrations of other metal cations or anions); recovery of the target element with production of a secondary waste stream of minimal volume; and the ability of the system to undergo multiple extraction cycles to ensure cost efficiency. In addition to recyclability, cost of materials and techniques required for synthesis as well as materials required for storage and transport of the extractant should be low. It would also be advantageous if the extractant had the ability to be used in a variety of different types of extraction scenarios such as: batch extractions, extractions using a column, or as part of an electrode or

electrochemical device. Finally, the use of environmentally benign cations as exchangeable cations out of the solid, so as to produce a decontaminated waste stream that is as environmentally sound as possible is important. No one extraction system is likely to meet all of the above-mentioned requirements, however optimization of extraction systems with all of these requirements in mind can lead to the improvement of currently flawed systems. The goal of this dissertation was to present an investigation of two different extraction systems: alkali intercalated molybdenum disulfides and transition metal tin thiospinels.

Alkali Intercalated Molybdenum Disulfide

Although $Li_{1.3}MoS_2$, had previously been shown to be a selective and effective extractant, the two main problems associated with this system were: the use and production of hazardous reagents during the extraction cycle (*n*-butyllithium in the activation of MoS_2 and production of hydrogen gas during exfoliation) and air (or oxidative) instability. H_xMoS_2, Na_xMoS_2 and K_xMoS_2 are improvements to this system in that they did not produce hydrogen gas during the metal ion extraction step of the extraction cycle. In the case of Na_xMoS_2 and K_xMoS_2, with the advantage of an interlayer space that is initially 2-3 Å larger than that of H_xMoS_2 (and native MoS_2), the kinetic barrier to ion exchange, introduced as a result of the elimination of exfoliation and flocculation mechanism, was eliminated. Similar metal ion loadings were realized on a time frame similar to that of $Li_{1.3}MoS_2$ and for this reason, Na_xMoS_2 and K_xMoS_2 are considered more ideal extractant systems.

In many respects, however, these newly developed extractants contain the same drawbacks as $Li_{1.3}MoS_2$. The synthesis of the less reduced extractants involved initial reduction with *n*-butyllithium. Reactivation of the

extractant after the first extraction cycle would also involve this method of reduction. Furthermore, hydrogen gas production was not eliminated from the overall extraction process, it was only moved to the extractant activation (or synthesis) step where it was more easily controlled. These materials were also shown to be oxidatively unstable, similar to $Li_{1.3}MoS_2$. Because of a powdery morphology, these extractants would not be particularly appropriate for use in a column or as an electrochemical device. Because of the oxidative instability, they would also not be appropriate in a permeable barrier extraction setup and would therefore only be useful in a batch process.

In some aspects, the MoS_2 analog systems are even less attractive than $Li_{1.3}MoS_2$. These extractants are not appropriate for use in waste streams with a low pH due to proton competition with metal cations and decreased metal ion loading. Because of the production of large amounts of OH^- as a result of the exfoliation/flocculation mechanism, $Li_{1.3}MoS_2$ is more appropriate for use at low pHs. In the case of H_xMoS_2, because of its small interlayer space and lack of exfoliation, exchange of some cations, such as lead, was not possible, and in all cases is slower than with $Li_{1.3}MoS_2$. Finally, there is an added cost associated with the incorporation of a second step during the synthesis of the extractant, as the MoS_2 analogs with fewer reducing equivalents could not be synthesized through any method other than exfoliation/flocculation in an alkali metal nitrate or nitric acid solution.

Transition Metal Tin Thiospinels

The thiospinels discussed in Chapters III and IV had not previously been examined as ion exchange extractants. The development of new compounds allows for the comparison of different extractants within this family.

To begin with, the synthesis of these extractants was relatively straightforward and did not involve the use of any hazardous chemicals. The only drawback was the relatively long reaction time required for synthesis (a minimum of two weeks). It is not yet known if these syntheses can be scaled up to produce crystalline powders with the spinel structure (the largest batch synthesized to this point was 5 g). The solid state synthetic method appears to be advantageous, in that a variety of new compounds, incorporating different metal cations in various oxidation states were prepared with relative ease. Furthermore, neither the synthesis of the extractant nor the extraction itself produced any hazardous byproducts. In the case of $Cu_2MSn_3S_8$, the decontaminated waste stream was contaminated with both copper and transition metal cations (not considered environmentally innocuous), however this problem was answered with the use of other extractants such as $Li_2FeSn_3S_8$ or the proton activated analogs.

In all cases, the alkali metal and proton intercalated spinels extracted soft heavy metal ions from solution more effectively than the parent compounds and on a faster time scale. The most promising extractants are the proton activated thiospinels, in that they removed relatively more metal ion on a shorter time scale than the parent spinels. In addition, these new thiospinels extracted some metals, such as $Pb^{2+}(aq)$, that were not extracted by $Cu_2MnSn_3S_8$ or $Cu_2FeSn_3S_8$. The mechanism of metal ion extraction with the proton activated thiospinels was shown to be ion exchange, with protons exchanging for the majority of metal ion cations. This is also an advantage because a relatively innocuous cation is introduced into the decontaminated waste. Finally, the synthesis of the proton activated materials was easy and inexpensive although, as was the case with H_xMoS_2, required an additional step.

Based on the extraction experiments performed to this point, the proton activated thiospinels can remove at least 50 mg Hg/g $H_{0.18}Cu_{1.90}Fe_{0.96}Sn_3S_8$. This number is significantly lower than the reported capacities of $Li_{1.3}MoS_2$ (580 mg Hg/g material) and the functionalized mesoporous silica discussed in Chapter I (505 mg Hg/g material) for two reasons. The first is that the maximum loading capacity of the proton activated thiospinel was never tested. This maximum would be reached with optimization of two experimental parameters. First, maximization of x and y in $H_{(x+2y)}Cu_{(2-x)}Fe_{(1-y)}Sn_3S_8$ would allow the maximum number of protons available for ion exchange. The maximum proton loading stoichiometry, with retention of a spinel structure is not known.

Maximum loading would also be obtained by decreasing the extractant to metal ion ratio from five. The maximum loading could be as high as 300 mg Hg/g material for a material with the idealized stoichiometry of $H_2FeSn_3S_8$, if one equivalent of mercury were exchanged for the two available equivalents of protons. This is still considerably lower than that reported for $Li_{1.3}MoS_2$, however significantly higher than that of activated carbon (1mg Hg/g material). The second reason that this figure of merit is lower for the thiospinel system is because of the use of a relatively heavy atom, tin. It is not known if tin can be effectively substituted with another metal atom, while retaining the spinel structure.

Another advantage associated with the thiospinel system is thermal and oxidative stability. No structural or chemical degradation was observed when these solids were exposed to or stored in air. Therefore, storage, transport and use in systems such as a permeable barrier extraction system would be more appropriate for the thiospinel compounds.

As was shown with the alkali metal intercalated molybdenum disulfides, mercury recovery was achieved by heating mercury loaded-$Cu_2MnSn_3S_8$ to 500 °C. This resulted in the release of mercury vapors that could be collected. The resultant, heated solid maintained its structural integrity, indicating that reuse through multiple extraction cycles was possible. This thermal behavior was observed with both the parent thiospinels as well as with one of the analogs, $LiCuFeSn_3S_8$.

Ultimately, the thiospinel system addresses the shortcomings of the A_xMoS_2 system, namely the use and production of hazardous chemicals during the extraction process. In addition, it was shown to outperform activated carbon based on mercury extractions. The oxidative, thermal stability and ease of synthesis indicate that this family of extractants would be ideal in a variety of different extraction scenarios.

Appendix A

Lattice Planes of the Spinel Structure

Parameters used to generate the following unit cell figures:

Crystal System: Cubic

Space Group #227: Fd–3m, origin at 0,0,0

a (Å) = 10.3

atomic coordinates:

Atom	x	y	z
Cu	0.125	0.125	0.125
Fe/Sn	0.500	0.500	0.500
S	0.250	0.250	0.250

Key to atoms (for clarity, atoms are not drawn to scale)

- ● Cu
- ● Fe/Sn
- ○ S

International Tables for Crystallography, Volume A: Space Group Symmetry, 2nd ed.; Theo Hahn, Ed.; Kluwer Academic Publishers: Boston, 1989.

Palmer, D. *Crystal Maker, version 5.0.3*; Crystal Maker Software: Oxfordshire, UK, 2001.

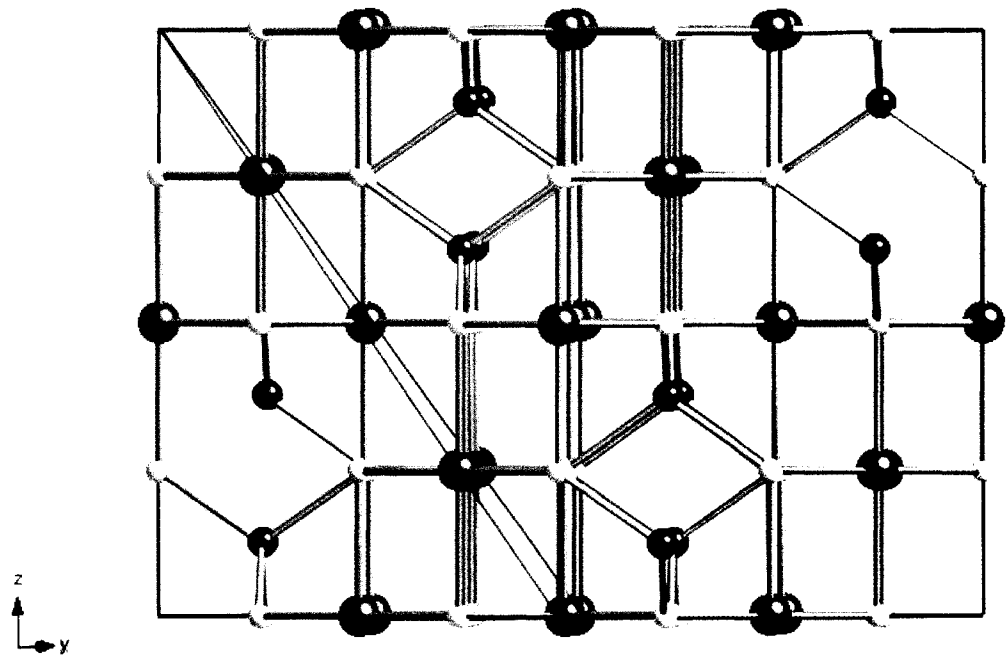

111

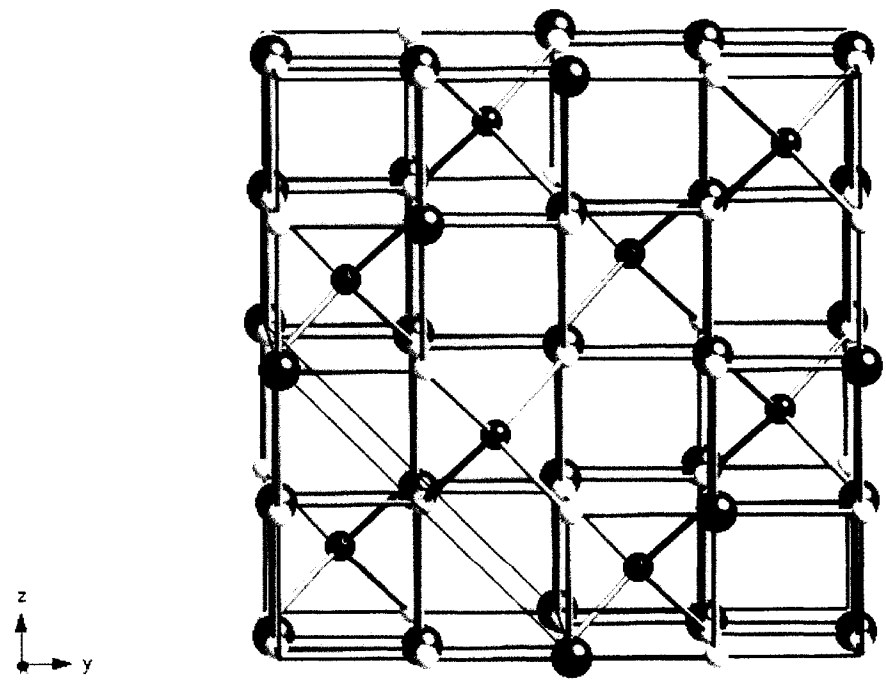

022

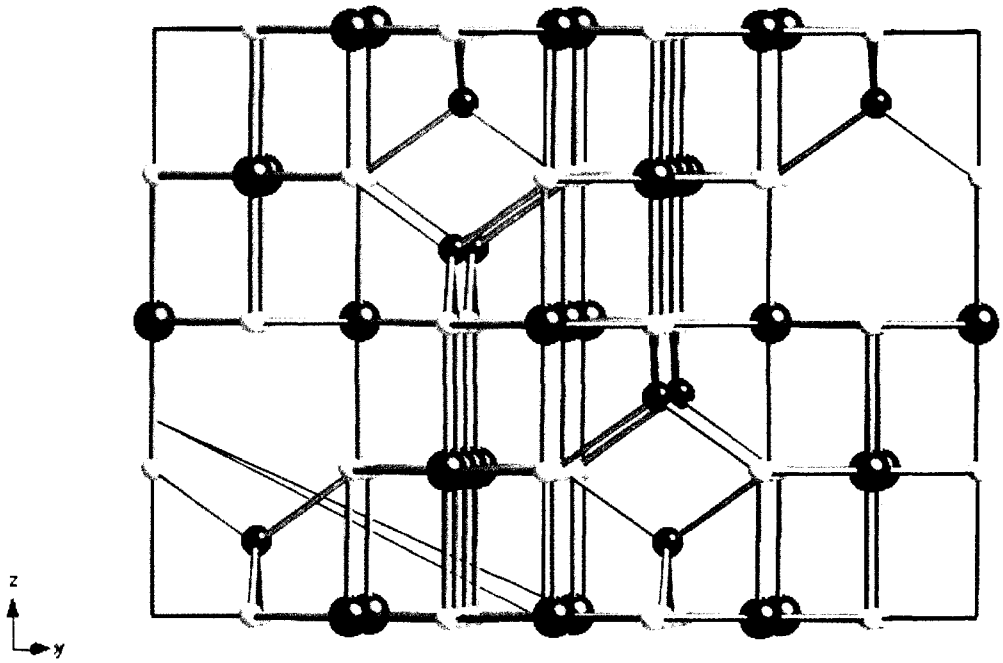

113

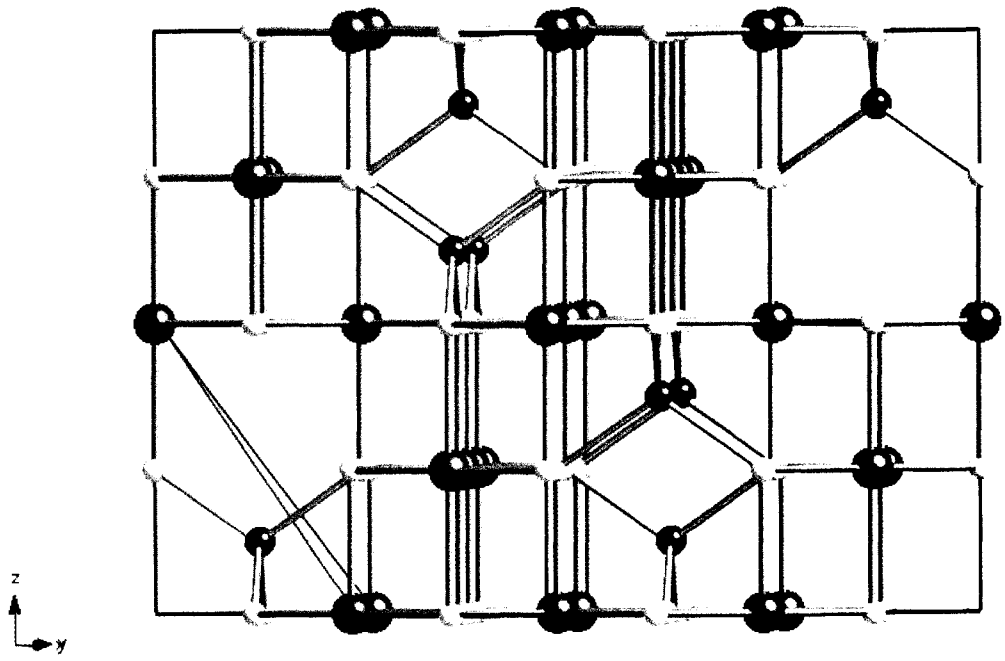

222

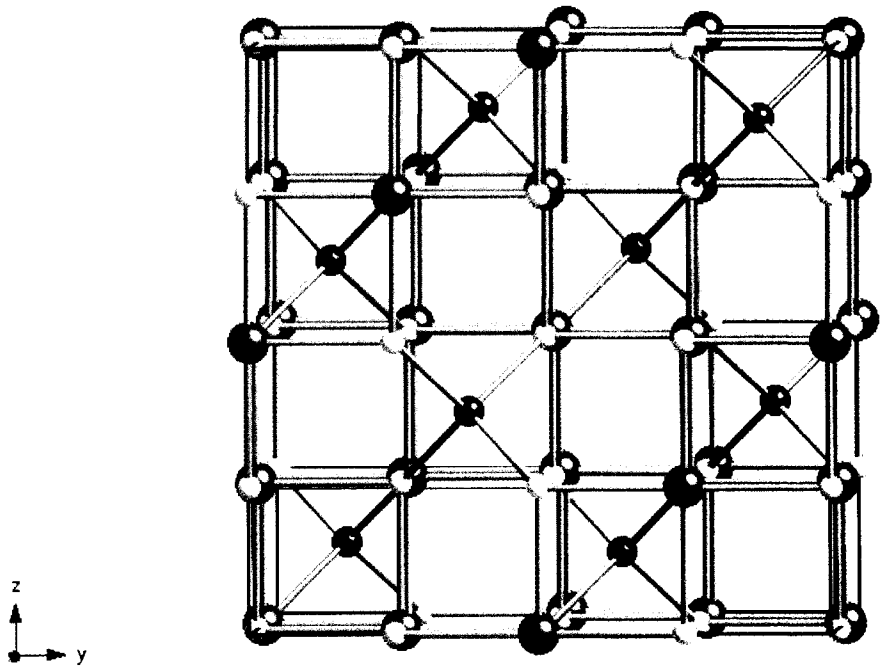

004

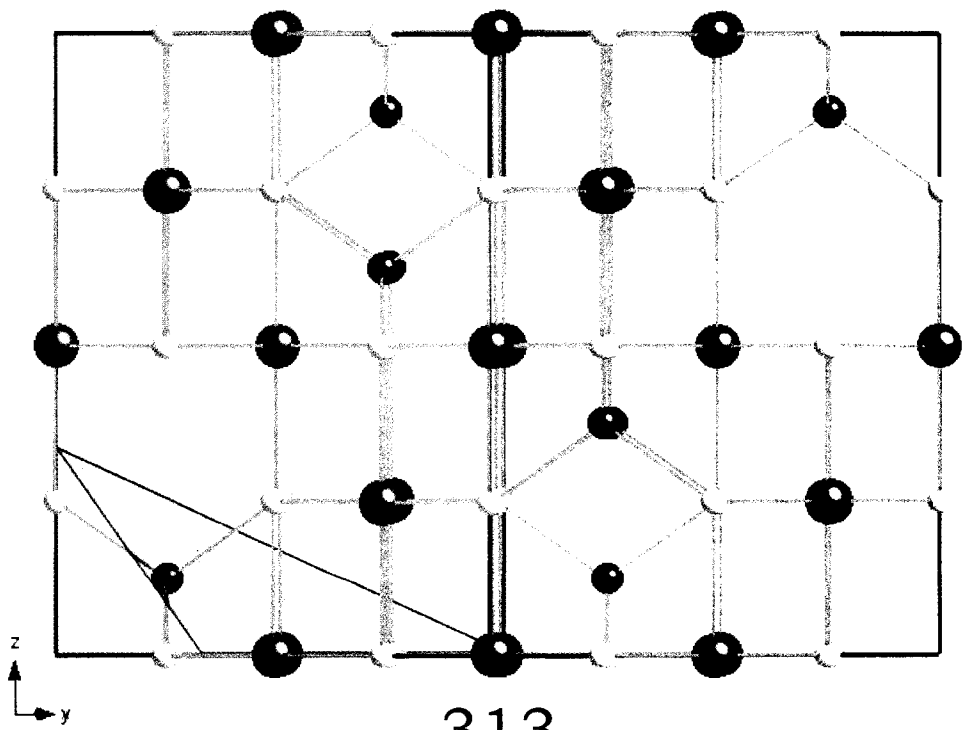

313

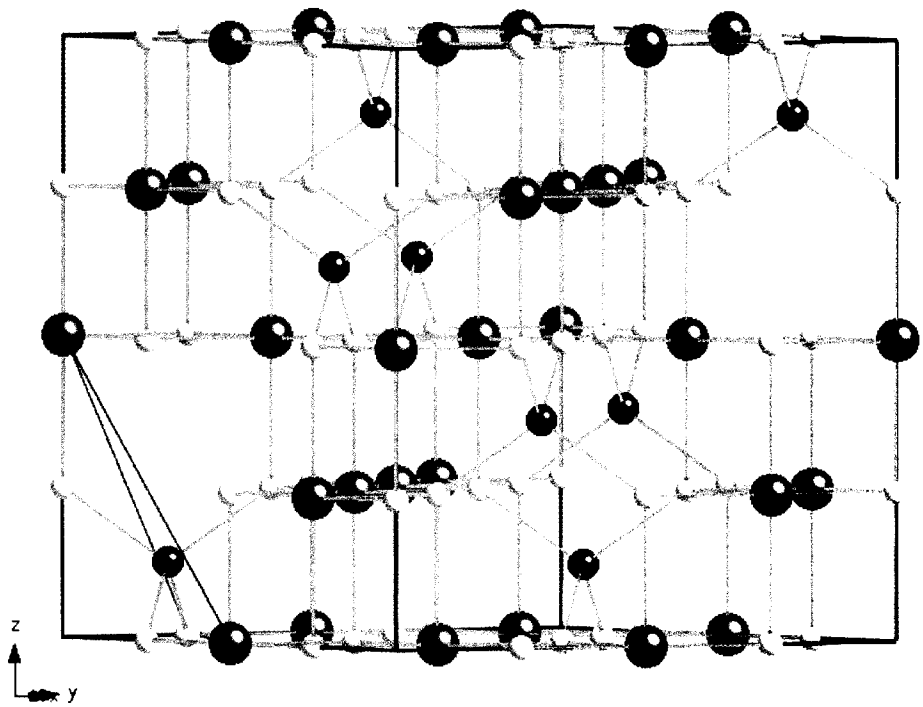

242

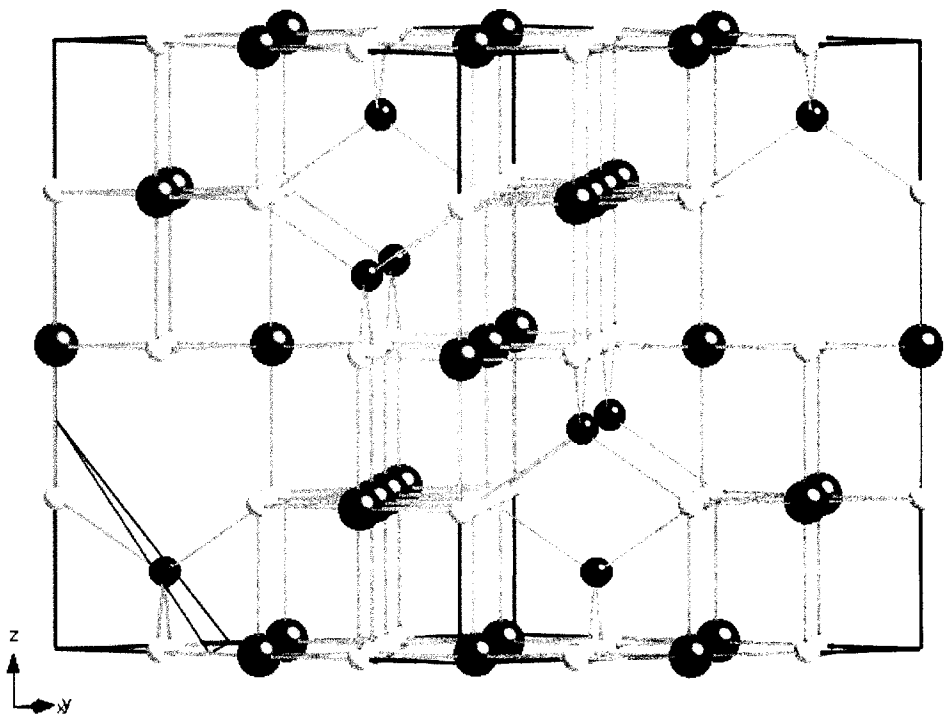

333

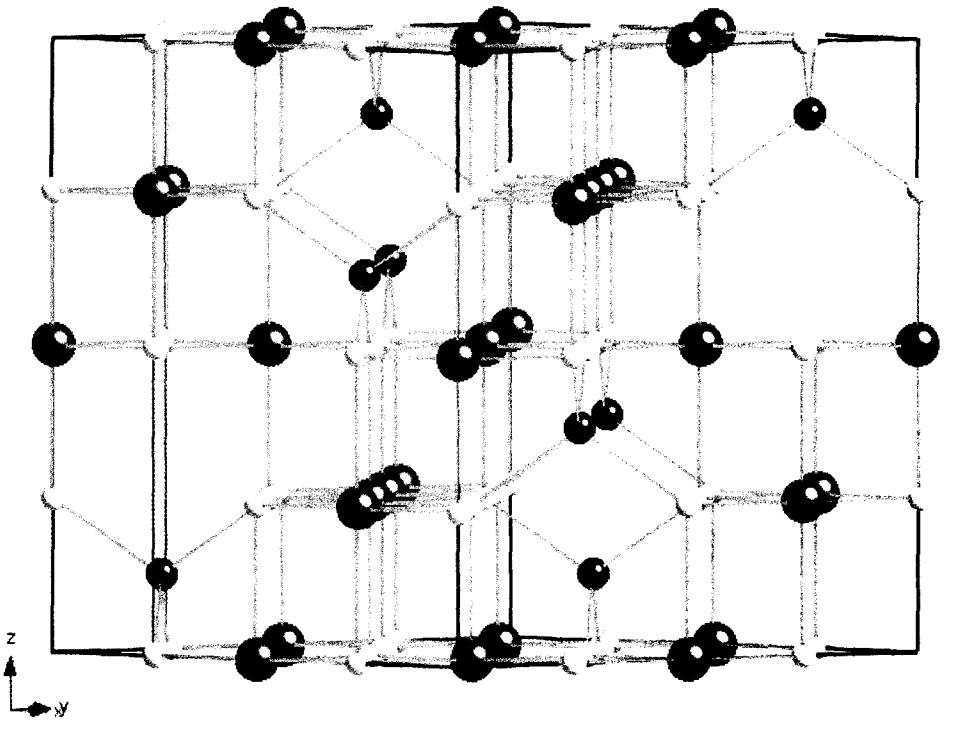

440

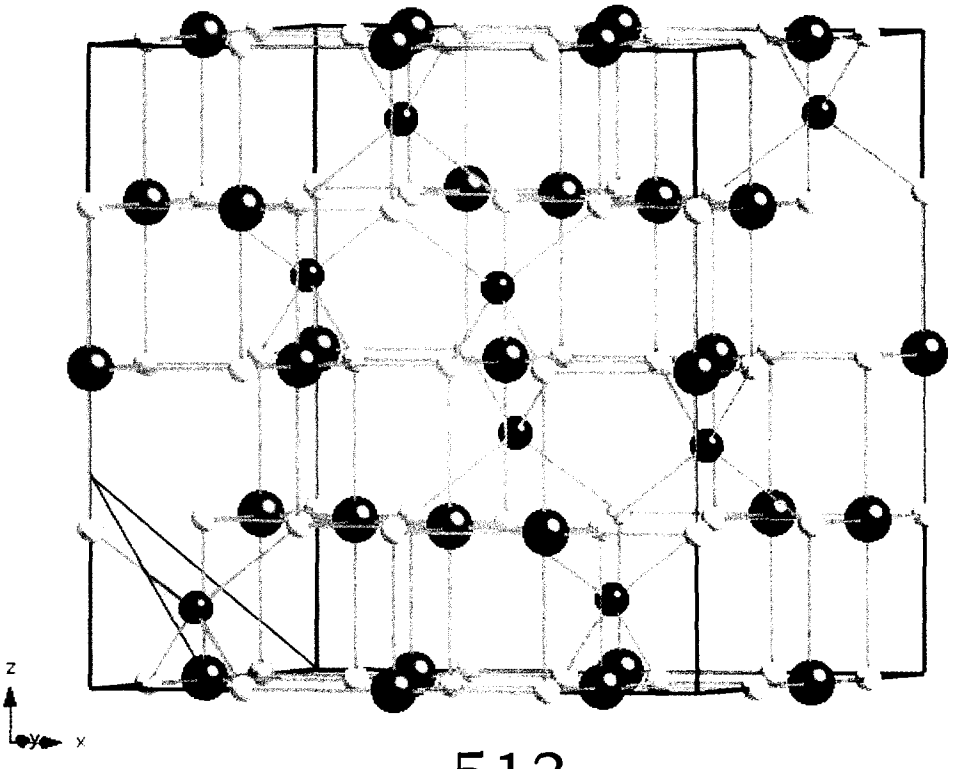

513

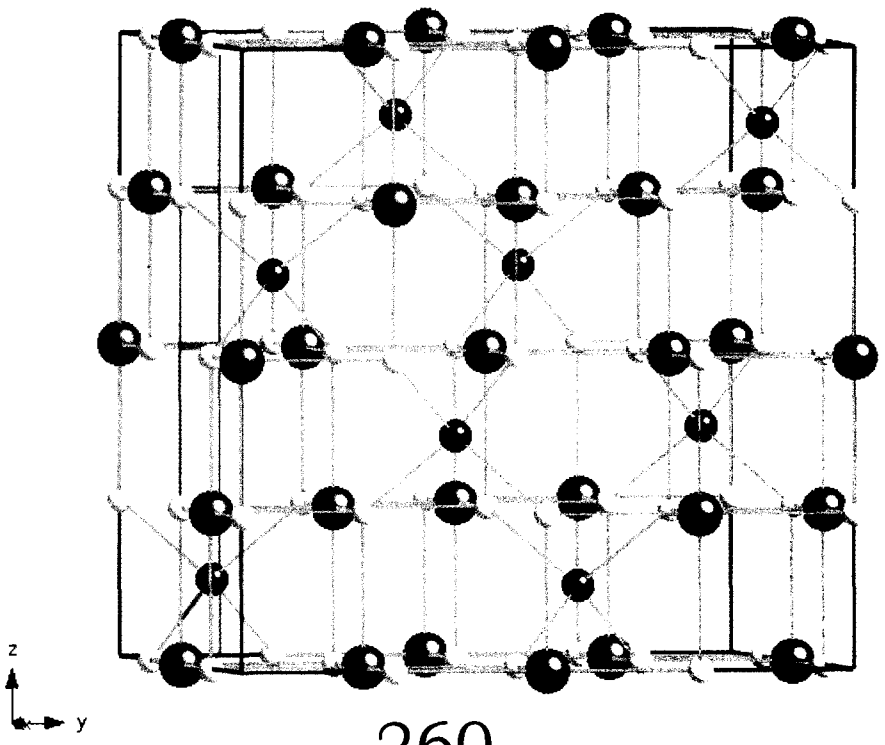

260

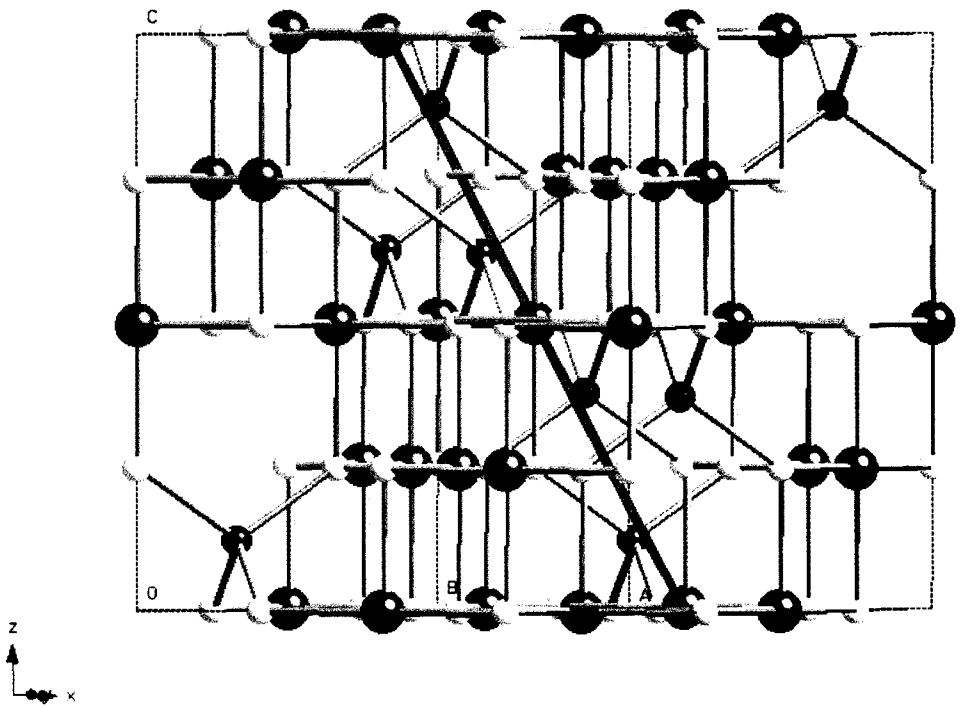

533

Appendix B

Reference Numbers for Novel Compounds

Formula	Reference Number
$Li_2FeSn_3S_8$	SEF222
$LiCuFeSn_3S_8$	SEF221
$Na_2FeSn_3S_8$	SEF126
$NaCuFeSn_3S_8$	SEF128
$CuMnSn_3S_8$	LMD1212B(II)
$Cu_2Sn_3S_8$	LMD1212C(III)
$CuFeSn_3S_8$	LMD1212D(IV)

Appendix C

Independent Research Proposal

Synthesis, Characterization and Application of Porous Materials Using Chevrel-type Clusters as Structural Building Blocks

Lisa Dysleski

July 23, 2002

Specific Aims

This research involves the synthesis of a new class of porous material using Chevrel-type clusters as molecular building blocks. The defining characteristic of the Chevrel-phase is the Mo_6S_8 core. These compounds are typically synthesized using high temperature, solid state techniques that produce condensed phases with intricate bonding between clusters. In this proposal, the solution phase chemistry of these clusters is investigated, including the use of templating techniques in order to form novel bonding patterns between clusters at lower temperatures. A variety of experimental parameters will be explored with the intent of producing previously unknown structures. In addition, a variety of physical characterization techniques, including powder x-ray diffraction, thermal analysis and x-ray photoelectron spectroscopy will be employed to characterize the structures. This chemistry is interesting in that it explores the relatively underdeveloped area of the synthesis of mesoporous sulfides. Although not many materials of this type are known, they will be useful for a wide variety of applications including hydrodesulfurization catalysis and lithium ion batteries.

Background

The synthesis of MCM-41 by scientists at Mobil Research and Development Corporation in 1992[1, 2] sparked a significant interest in the development of new micro- and mesoporous materials with novel structures and chemical properties. The applications of these types of materials include heterogeneous catalysis, ion exchange, optical and lithium ion batteries. The most common mesoporous materials are silicates, containing SiO_4^{4-} tetrahedral building blocks arranged in various conformations around a central porous structure, however this area has expanded to include many other building blocks as well.[3-8]

Despite the advances in the development of porous oxides, however, there has been a much less prolific development of porous materials containing sulfur and selenium.[9-12] This is mainly due to the difficulty associated with the use of analogous chemical precursors such as SiS_4^{4-} and the fact that many solids containing sulfur and selenium are prone to hydrolysis. The production of high surface area porous sulfides, however, would be useful for applications such as hydrodesulfurization catalysis. The massive, worldwide consumption of fossil fuels requires the removal of sulfur from petroleum feedstocks. Ni (or Co) impregnated MoS_2 has been developed as a hydrodesulfurization catalyst in the past,[13] however higher surface area materials are needed to increase the efficiency of this type of process.

One method of developing stable, non-oxide porous materials has been the use of molecular clusters such as the adamantane-like $Ge_4Q_{10}^{4-}$ (Q = S, Se), which, due to its overall tetrahedral symmetry, can be thought of as a molecular building block analogous to the SiO_4^{4-} unit. This cluster, shown in Figure 1, is composed of four GeQ_4^{4-} corner linked tetrahedra. In each case, three of the Q^{2-} anions act as bridging ligands between germanium atoms,

leaving one terminal Q^{2-} available as what Yaghi has termed a 'sticky site' that allows for the coordination of each cluster to other atoms outside of the cluster.[14] The use of these Ge–S building blocks in the synthesis of porous materials was first described by Yaghi in 1994.[14] In this report, a microporous material was made via slow diffusion of two aqueous solutions of $Mn(CH_3CO_2)_2$ and $Ge_4S_{10}[(CH_3)N]_4$ as described in Equation 1.

$$Mn(CH_3CO_2)_2(aq) + Ge_4S_{10}[(CH_3)_4N]_4(aq) \xrightarrow{\text{slow diffusion, 24h.}} MnGe_4S_{10}\bullet 2(CH_3)_4N(s) \quad (1)$$

The structure of this solid, shown in Figure 2, is composed of tetrahedral Mn(II) centers covalently linked to four germanium sulfide clusters forming a three-dimensionally porous material with channels occupied by tetramethylammonium cations. It is interesting to note that unlike the mesoporous oxides, which are formed through condensation reactions and involve edge and corner sharing linkages between molecular building blocks, there is no direct linkage between $Ge_4S_{10}^{4-}$ units in this structure. Instead, the blocks are held together by coordination through manganese centers.

In 1998, Kanatzidis also reported the synthesis of a mesostructured material using the $Ge_4S_{10}^{4-}$ anion as a structural building block.[15] This synthesis was accomplished using the ion-exchange reaction described in Equation 2.

$$4C_nH_{2n+1}N(CH_3)_3Br + Na_4Ge_4S_{10} \longrightarrow [C_nH_{2n+1}N(CH_3)_3]_4Ge_4S_{10} + 4NaBr \quad (2)$$

n = 12, 14,16, or 18

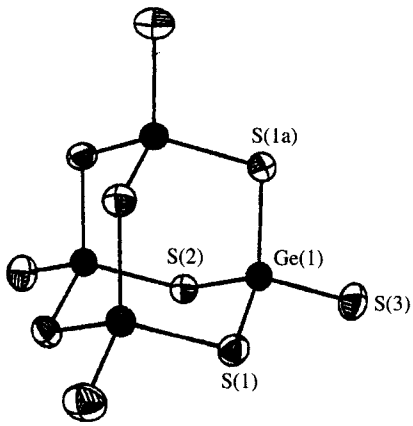

Figure 1 $Ge_4S_{10}^{4-}$ anion.[10]

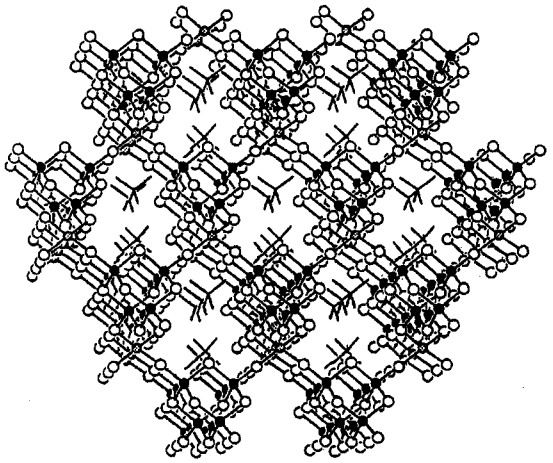

Figure 2 Structure of $MnGe_4S_{10}•2(CH_3)_4N$ along the [100] crystallographic direction. Framework is constructed of Mn(II) (gray spheres) tetrahedrally coordinated by $Ge_4S_{10}^{4-}$ anions. $(CH_3)_4N^+$ cations (represented by a line drawing without hydrogen atoms) are located in the pores.[10]

The structure, shown in Figure 3, contains individual $Ge_4S_{10}^{4-}$ clusters, hexagonally packed in a planar array, with surfactant molecules interdigitated in the interlayer space. This synthesis is similar to that reported by Yaghi in the use of germanium sulfide building blocks, however the new method did not use a transition metal cation to link the chalcogenide clusters. As a result, the clusters arranged in discrete units. In addition, the use of a much larger templating cation is the basis for forming a mesostructure. Using alkyltrimethylammonium cations, this synthesis is similar to the liquid crystal templating (LCT) technique originally proposed in the synthesis of MCM-41.

Also in 1998, Ozin and co-workers reported the synthesis of δ-GeS_2, the first example of a germanium sulfide phase with an expanded framework structure (i.e. not a dense phase).[16] This structure was achieved through a reaction of hydrochloric acid with $(NMe_4)_4[Ge_4S_{10}]$ at 50 °C and contains an interconnected framework of Ge_4S_{10} units, however this structure was not synthesized using a surfactant template and no pore sizes are reported for this structure.

There are other reports by the Ozin and Kanatzidis groups using a transition metal additive in conjunction with a longer chain alkylammonium cation in order to synthesize porous materials of this type.[17-19] The three-dimensional mesoporosity of these materials was confirmed by PXRD and TEM analysis although neither material was appropriate for complete structure determination. These materials formed worm-hole structures with pores ranging in size from ~30 Å to >40 Å depending on the length of the alkyl chain used on the cationic surfactant.[13]

Surprisingly, given the number and types of chalcogenide clusters known there are no other reports of the synthesis of structured, mesoporous materials using chalcogenide cluster precursors as molecular building blocks. One

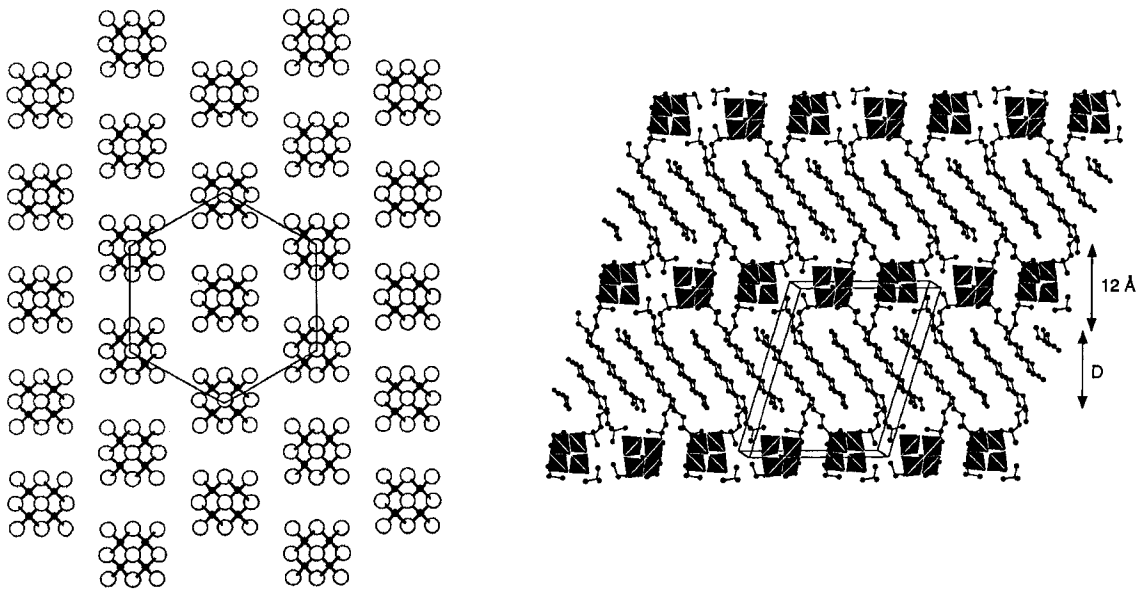

Figure 3 Structure of $C_{12}H_{25}N(CH_3)_3]_4Ge_4S_{10}$. (A) Hexagonal packing of the $Ge_4S_{10}^{4-}$anions (B) Overall structure showing interdigitation of C_{12} chains.[11]

interesting cluster type that will lend itself well to this type of synthetic technique, however, is the Chevrel cluster. Chevrel clusters, first described in 1971,[20] have the general formula $A_xMo_6S_8$ (where A is one of 40 different metals including Pb, Ln, Li, Cu). As can be seen in Figure 4, these clusters contain six octahedrally arranged molybdenum atoms surrounded by eight sulfur atoms that cap each triangular face of the octahedron. This can also be described as a Mo_6 octahedra inscribed in an S_8 cube. In addition, there are six terminal sulfur atoms located at each vertex of the octahedron. These terminal atoms, which can be compared to the 'sticky sites' of the $Ge_4S_{10}^{4-}$ anion are responsible for the interlinkage of clusters and the formation of different cluster arrangements in the condensed solids. In $PbMo_6S_8$, for example, each molybdenum vertex is coordinated directly to a capping sulfur atom on an adjacent cluster.

Although the Chevrel phases are specific to clusters containing molybdenum and sulfur (or selenium), there are many clusters with analogous structures in which other transition metals are substituted for molybdenum or a halide is substituted for sulfide (or selenium)[21-24]. The substitution of a halogen for sulfur allows for different chemical bonding between clusters. For example, in Mo_6Cl_{12}, four of the six vertex chlorides bridge adjacent clusters. The remaining two are terminal chlorides. This lack of bonding in the third dimension imparts a layered structure to the compound. A comparison of the structure of $PbMo_6S_8$ with that of Mo_6Cl_{12} can be seen in Figure 5. In addition, depending on the value of x in $A_xMo_6S_8$, the oxidation state of molybdenum in the cluster can vary from 2+ in to 2.67+. The variety of chemical compositions, intercluster bonding, and molybdenum oxidation state indicates that the Chevrel (or Chevrel-type) clusters are appropriate and interesting building blocks for proposed research of this type. The use of different cluster

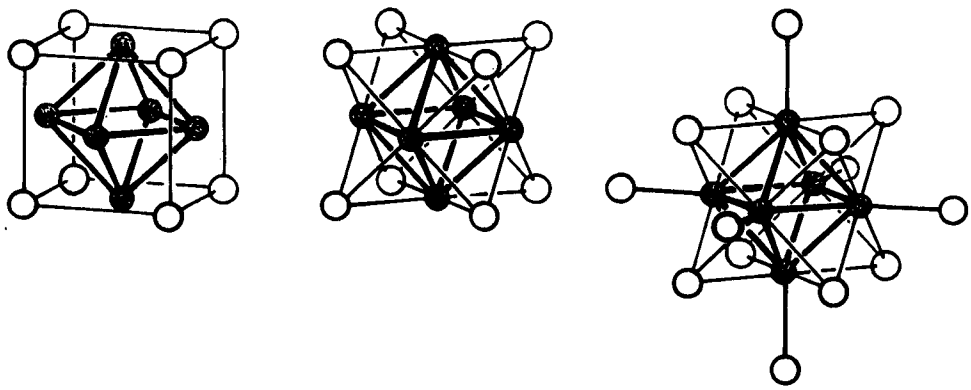

Figure 4 Different views of a Chevrel cluster. (A) Showing sulfur atoms at the corners of a cube bounding the molybdenum octahedra (B) Depiction of each sulfur as capping the triangular face of the molybdenum octahedra (C) Mo_6S_8 core with terminal sulfur atoms extending from each molybdenum vertex.[19]

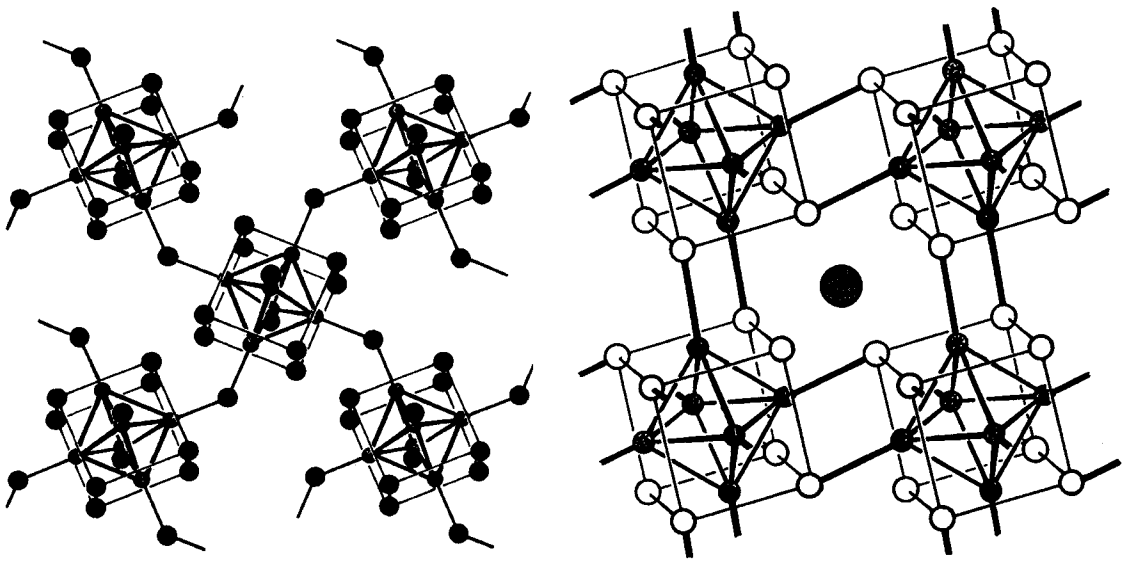

Figure 5 Comparison of the cluster bonding in (A) Mo_6Cl_{12} and (B) $PbMo_6S_8$. Red bonds indicate bonding between clusters.[19]

precursors or different reaction conditions (such as solvent, surfactant and reaction temperature) could all lead to new structures.

The goal of this research is to use the above mentioned qualities of the Chevrel-type clusters to synthesize new porous materials. This research is unique because although clusters have been used as molecular building blocks to prepare micro- and mesoporous materials previously, no research has been done using the Chevrel clusters. These clusters are especially appropriate for this type of chemistry in that intercluster bonding could produce interesting interconnectivities not seen in the Ge_4S_{10} research. In condensed phase Chevrel cluster chemistry, direct bonding between clusters is common. It is possible, therefore, that no metal additives would be necessary for this synthesis. More importantly, these synthetic methods and the resultant structures would represent the first rational, direct linkage of molybdenum chalcogenide clusters into porous arrays.

Research Design and Methods

I. Materials Synthesis

The elegance associated with the formation of porous solids using Chevrel clusters and the formation of novel structures will lie in the optimization of many experimental parameters such as solvent, surfactant, reaction temperature, other possible reactants (such as transition metal additives or reducing agents) and calcination temperature. Since this proposal suggests the formation of sulfur bridges or molybdenum sulfur bonds between clusters, the appropriate, soluble precursors must be selected along with the correct sulfiding agents. Due to the intricate intercluster bonding of the condensed Chevrel phases (such as $PbMo_6S_8$), these solids are not soluble in common reaction solvents. Therefore, the $Mo_6S_8^{2-}$ anion is not directly

accessible in solution. This insolubility requires the use of precursors other than completely sulfided clusters, such as $Mo_6Cl_{14}^{2-}$, that is soluble in common organic solvents such as ROH (R=Me, Et, Bu), THF, dichloromethane, and benzene. In addition, later phases of this research might investigate structure formation using other types of clusters that are water soluble such as a family of rhenium compounds developed by Holm ($Cs_5Re_6S_8X_7$ (X = Cl, Br), $Cs_6Re_6S_8I_8$ and $Cs_4Re_6Se_8I_6$).[18]

The first phase of synthesis will be directed towards the formation of microporous and mesoporous materials using $A_2[Mo_6Cl_8]Cl_6$ as a starting material to produce an interconnected network of clusters. The first experiments will be to investigate the ion exchange reaction between $(NH_4)_2[Mo_6Cl_8]Cl_6$ and R_4NCl (R = Me, Et) in ethanol as described in Equation 3.

$$(NH_4)_2[Mo_6Cl_8]Cl_6 + R_4NCl \longrightarrow [R_4N]_2[Mo_6Cl_8]Cl_6 + 2NH_4Cl \quad (3)$$

In this reaction, the tetraalkylammonium cation would act as a templating cation around which the cluster structure would form. The resultant structure will probably be microporous due to the relatively small size of this cation. In addition, since this is an ion exchange reaction, isolated clusters will be obtained. The reaction will be done at room temperature and crystals will be isolated through slow evaporation of the solution after filtration and washing to remove the NH_4Cl. In the presence of trimethylamine, chloride abstraction could produce a material with bridging chlorides, templated in this case by trimethylamine.

$$(NH_4)_2[Mo_6Cl_8]Cl_6 + x(CH_3)_3N \longrightarrow [(CH_3)_3N]_x[Mo_6Cl_8]Cl_4 + 2NH_4Cl \quad (4)$$

Since the overall goal is formation of interconnected molybdenum *sulfide* clusters, a sulfiding agent will have to be introduced into this scheme. McCarley and co-workers have shown that the reaction of Mo_6Cl_{12} with NaSH and NaOBu in refluxing *n*-BuOH will produce amorphous $Na_{2x}(Mo_6S_8)S_x \cdot yMeOH$. Therefore, the above reactions in the presence of NaSH or LiSH will form compounds with various degrees of thiolation. In these investigations, the appropriate experimental conditions will have to be determined through variation of time, temperature and a one versus a two step process. It is unknown at this point if the sulfiding agent must be present during cluster condensation or if it can be used after the solid has formed. In addition, the use of $H_2S(g)$ in solution during the formation of the porous solid or after the solid has been separated from the reaction mixture might produce the appropriate thiolated materials.

Of course, with the use of a longer chain surfactant, such as $C_nH_{2n+1}N(CH_3)_3Cl$ (where n = 12-18), precipitation of the solids will result in mesostructured compounds. Examples of proposed structures are given in Figures 6 and 7. In these figures, the templating cation has been removed for clarity. It is interesting to note that a variety of novel bonding schemes are possible. For example, in Figure 6, the clusters are connected via bridging ligands (sulfide or chloride), however in Figure 7, bonding between molybdenum atoms and capping sulfides on adjacent clusters forms edge-sharing polyhedra. Finally, in Figure 8, a structure with a larger pore size is proposed as the result of using a larger templating cation (i.e. with longer alkyl chains). Of course these are only a few of the possible structures that might result from the

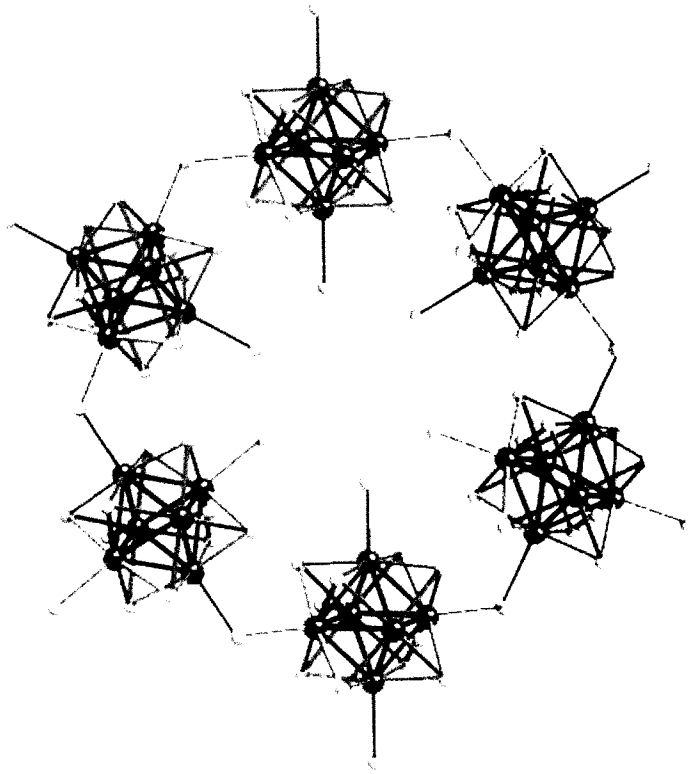

Figure 6 Proposed structure showing bridging ligands.

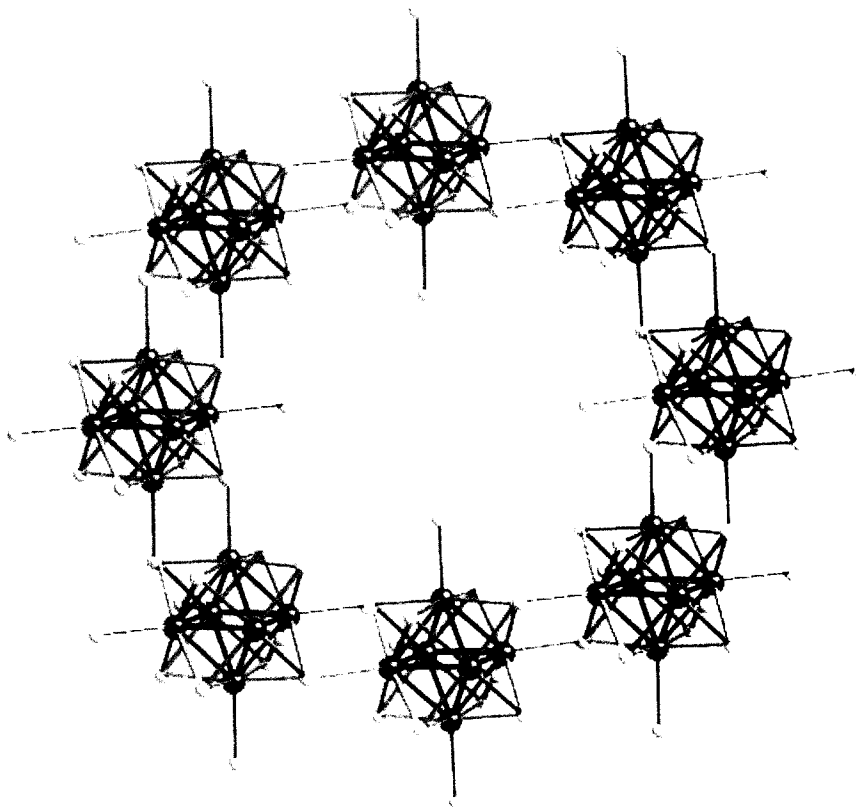

Figure 7 Proposed structure showing edge-sharing clusters.

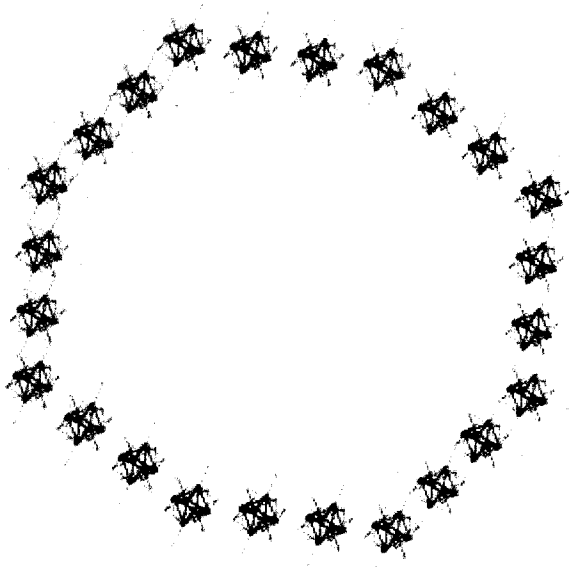

Figure 8 Depiction of mesopore built from Chevrel clusters.

reactions mentioned. It is possible that multiple bonding modes would be present in one structure (doubly bound clusters and bridged ones) and this would be the first example of such bonding in the literature concerning Chevrel phases.

We will also investigate the structural differences achievable with the use of different coordinating transition metal cations was done by Yaghi and Kanatzidis. The most appropriate cations would be chalcophilic cations such as Cu^{+}, Ag^{+}, Mn^{2+}, Pb^{2+}, Hg^{2+} etc. The synthetic methods will be similar to that described above, with a transition metal chloride salt added to the initial reaction mixture. These metals are commonly tetrahedrally coordinated which would introduce a tetrahedral geometry in addition to the octahedral geometry of the cluster. This combination of tetrahedral and octahedral building blocks could result in the formation of interesting structures such as the one synthesized by Yaghi.[14]

After the production of templated structures, which will contain surfactant molecules in the pores of the structure, calcination at various temperatures will be used to remove the surfactant molecules. These temperatures will probably range from ~ 200 °C to 500 °C depending on the surfactant and the decomposition temperature of the material. These materials will most likely be sensitive to oxygen, indicating that calcination under dynamic vacuum or inert atmosphere will be necessary. Again, an interesting set of experiments will be to test the effects of adding the sulfiding agents during the templating process versus during the calcination process.

Another area to be explored with these structures will be that of ion exchange with the cluster after precipitation. The use of NaSH will produce a material containing sodium cations in the channels of the structures. Using ion exchange reactions to insert transition metals such as cobalt, nickel or

platinum into the solid, these materials will be appropriate for testing as hydrodesulfurization catalysts. The possibilities of ion-exchange materials are endless and would depend mostly on size and orientation of the pores in the structures.

II. Materials Characterization

The most common technique that will be used to characterize micro- and mesoporous materials will be powder x-ray diffraction (PXRD) or low angle powder diffraction, depending on the size of the pores. Porous of materials are not usually highly crystalline and the identification of one or more reflections in a diffraction pattern will give insight into to the long-range order of the samples and the average pore size. With the smaller tetraalkylammonium cations, complete structure determination might be possible, however with the larger templating alkylammonium cations this is not likely. An analysis of the width of the diffraction peaks can be used to gain insight into the pore size distribution. Broader diffraction peaks indicate a larger distribution of pore sizes whereas sharper peaks indicate a smaller distribution. Powder diffraction will also distinguish between two-dimensional layered structures and three dimensional structures (with either ordered packing of channels or a relatively disordered formation of channels as seen in materials adopting a worm-hole structure). After calcination, it will be important to use x-ray diffraction to show if the porous structure is retained with surfactant loss or if there is a phase change to another product (the binary transition metal sulfide or a condensed Chevrel phase). Transmission electron microscopy (TEM) is also a technique used to visualize channels or pores in a solid. This will provide evidence for either a packed system of pores or the presence of a worm-hole structure.

In combination with structural analysis, thermal analysis, such as thermal gravimetric analysis (TGA) or differential scanning calorimetry (DSC) will be useful in determining at which temperature the materials begin to lose their surfactant molecules. This will also provide the decomposition temperatures of the materials. In the best case scenario, the loss of surfactant and decomposition will occur at very different temperatures (a difference of 200-300 °C) so that isolation of a material without surfactant is possible.

Finally, if complete structure determination is not possible, a technique such as x-ray photoelectron spectroscopy (XPS) will be used to determine the different types of chemical environments around each atom. This will provide insight into the bonding between clusters by indicating the number of different 'types' of atoms present in the structures. For example, capping sulfur atoms can be differentiated from bridging atoms, or atoms directly bound to a molybdenum atom on an adjacent cluster due to the difference in their binding energies. In addition, the use of quantitative XPS will provide information on the degree of thiolation of the clusters. By comparing the relative intensities of the sulfur and chlorine peaks, an average stoichiometry for the clusters can be obtained. It will also provide evidence for the presence or absence of surfactant in the pores based on the presence of a nitrogen signal in the spectra.

III. Application Testing

It is believed that these materials will make appropriate hydrodesulfurization catalysts because of the historical use of molybdenum disulfide as such a material. In order to test this hypothesis, a dynamic flow of an appropriate thiolated organic material such as thiophene, benzothiophene or dibenzothiophene in a hydrogen atmosphere will be run over the solid at an elevated temperature (250-300 °C). The products in the effluent will then be

identified by gas chromatography. A variety of transition metals will be ion exchanged into these solids and the effect of the various metal additives (such as Ni, Co, Pt) will be investigated. Due to the increased surface area of these materials, they are expected to exhibit increased catalytic activity. One potential problem with these materials is degradation of the porous structure over time at elevated temperatures. Using PXRD to monitor the structure before and after this catalytic testing will provide information about structure retention and will be important in evaluating this material as an effective catalyst.

In addition, these materials will have high ion conductivity due to the large pore size and relatively low coordinating ability of sulfur atoms on the clusters. This ion conductivity will be tested and compared to other solid state materials.

Significance of Completed Work

This research represents a new class of porous materials based on Chevrel type clusters as molecular building blocks. Not only will this work augment the rich chemistry of the micro and mesoporous oxides, it will introduce a new class of micro and mesoporous sulfides into a relatively underdeveloped area. The structure types that are attainable are unique and varied, in terms of known porous structures and in terms of known condensed phases. In addition, the increased surface area of these materials will greatly enhance their use in applications such as hydrodesulfurization catalysis. The versatility of cation stoichiometry also indicates other potential functions as well, including use as lithium ion battery electrodes or ion exchange materials.

References

1. Kresge, C.T., et al. *Nature* **1992,** *359,* 710-712.
2. Beck, J.S., et al. *J. Am. Chem. Soc.* **1992,** *114,* 10834-10843.
3. Zhao, D.; Luan, A.; Kevan, L. *Chem. Comm.* **1997,** 1009.
4. Xun, H.; Antonelli, D. *Angew. Chem. Int. Ed.* **2002,** *41,* 214-229.
5. Scott, B.J.; Wirnsberger, G.; Stucky, G.D. *Chem. Mat.* **2001,** *13,* 3140-3150.
6. Jimenez-Jimenez, J., et al. *Adv. Mat.* **1998,** *10,* 812-815.
7. Chang, J.-S., et al. *Chem. Comm.* **2001,** 859-860.
8. Farrusseng, D., et al. *Angew. Chem. Int. Ed. Engl.* **2001,** *40,* 4204-4207.
9. Braun, P.V.; Osenar, P.; Stupp, S.I. *Nature* **1996,** *380,* 325-328.
10. Sokolov, I.; Jiang, T.; Ozin, G.A. *Adv. Mat.* **1998,** *10,* 942-946.
11. Jiang, T.; Ozin, G.A. *J. Mat. Chem.* **1997,** *7,* 2213-2222.
12. Fröba, M.; Oberender, N. *Chem. Comm.* **1997,** 1729-1730.
13. Prins, R.; DeBeer, V.H.; Somorjai, G.A. *Catal. Rev. –Sci. Eng.* **1989,** *31,* 1.
14. Yaghi, O.M., et al. *J. Am. Chem. Soc.* **1994,** *116,* 807-808.
15. Bonhomme, F.; Kanatzidis, M.G. *Chem. Mat.* **1998,** *10,* 1153-1159.
16. MacLachlan, M.J., et al. *Angew. Chem. Int. Ed.* **1998,** *37,* 2076-2079.
17. MacLachlan, M.J., et al. *J. Am. Chem. Soc.* **1999,** *121,* 12005-12017.
18. MacLachlan, M.J. Coombs, N.; Ozin, G.A. *Nature,* **1999,** *397,* 681-684.
19. Wachhold, M., et al. *Adv. Mat.* **2000,** *12,* 85-91.
20. Chevrel, R.; Sergent, M.; Prigent, J. *J. Solid State Chem.* **1971,** *3,* 515.
21. Federov, V.E.; Mishchenko, A.V.; Fedin, V.P. *Russian Chemical Reviews* **1985,** *54,* 408-423.
22. Yaghi, O.M.; Scott, M.J.; Holm, R.H. *Inorg. Chem.* **1992,** *31,* 4778-4784.
23. Lee, S.C.; Holm, R.H. *Angew. Chem. Int. Ed. Engl.* **1990,** *29,* 840-856.

24. Long, J.R.; McCarty, L.S.; Holm, R.H. *J. Am. Chem. Soc.* **1996,** *118,* 4603-4616.

25. Müller, U. *Inorganic Structural Chemistry,* John Wiley & Sons: New York, 1993; 130.